

The Development of Point-of-Care Microfluidic Devices for the Detection of Infectious Diseases

Scott Macgill Karas
Barrington, IL

Bachelor of Science – Biochemistry, Ohio University, 2013
Master of Science – Synthetic Chemistry, University of Rhode Island, 2016

A Dissertation presented to the Graduate Faculty of the University of Virginia in
Candidacy for the Degree of Doctor of Philosophy

Department of Chemistry

University of Virginia

July 2022

Abstract

Point-of-care (POC) diagnostics is a discipline focused on using instrumentation or analytical techniques to detect and identify target analytes at or near a patient in need of treatment, whereby the patient is properly diagnosed and provided the necessary medical care. In the past few years, there has been an increased focus on the development and implementation of POC devices to rapidly detect infectious diseases. Microfluidics has assisted in bridging the technology gap to produce inexpensive, portable, and easy to use POC diagnostic devices.

An introduction into POC devices and microfluidics is described in **Chapter 1**, as well as the relevant literature surrounding their design and method of detection. Additionally, a thorough description of the types of paper-based immunoassays and their integration into microfluidic devices are presented. The work described in **Chapter 2** focused on the development of a novel centrifugally-driven orthogonal flow immunoassay (cOFI) disc with a long microfluidic channel which allows for a constant flow rate throughout the duration of the assay. Additionally, the work presented proof-of-concept to detect an infectious disease, *Yersinia pestis*, on disc. **Chapter 3** builds on the cOFI disc design to increase the assay's sensitivity by increasing the overall sample volume that can be analyzed; by leveraging 3D-printed technology, a large volume sample chamber was developed allowing up to 12 mL of sample to be handled on disc. Therefore, increasing the sensitivity ten times compared to the original disc design in **Chapter 2**. To further improve on the cOFI device, an automated cOFI system was presented in **Chapter 4** that could perform all of the assay steps and the image analysis of the membranes without requiring user input, simplifying the diagnostic

testing and meeting the requirements of a POC system. The work presented in **Chapter 5** was focused on the design and characterization of a multiplexed flow through assay (FTA). The FTA chip has the potential to detect up to six different target analytes on one membrane from a single sample, without requiring any off-chip sample preparation or external instrumentation.

Finally, **Chapter 6** highlights the potential applications and impacts the POC devices described in the previous chapters will have on medical diagnostics, as well as current challenges that need to overcome and future research that needs to be performed.

Acknowledgments

When I earned my degree in Biochemistry from Ohio University in 2013, it never crossed my mind that I would go on to earn my PhD in Chemistry, but now I am here finishing my degree and preparing to defend my dissertation. This day could not have happened without all the people in my life to help provide the necessary support, motivation, and encouragement to get me through both the highs and lows.

First, I want to thank the members of Prof. Landers' Lab. They all, both graduate and undergraduate students, helped me grow as a researcher and as a person. They put up with answering my ridiculous questions along with my non-stop singing and whistling. I want to thank you all for being great lab mates and even better friends. Thank you for mentoring me to be a better scientist, presenter, and writer. Next, I want to thank Prof. James Landers for accepting me into your research group and having faith in me to complete my PhD under the tight timeline set by the United States Air Force to complete my degree in three years. I appreciate your mentorship and guidance through my research. I would not be defending my dissertation without your support.

Second, I want to thank my amazing and loving parents: Robert and Dr. Debbie Karas. You have raised me to be the man I am today. I wouldn't be where I am now in my Air Force career if it wasn't for you. Growing up, my mom was constantly improving herself and earning advanced academic degrees. She went the non-traditional route of earning her Doctorate in Nursing Practice later in her career. Her determination and dedication to self-improvement helped motivate me to earn my PhD in Chemistry. My dad taught me to never quit and to never give up

no matter how hard life knocked me down. They both taught me the meaning of hard work and discipline. They told me that you have to earn everything in life and nothing is ever given to you. Thank you, mom and dad, for teaching me to be responsible, independent, and hardworking, I love you!

Finally, I want to thank my amazing, beautiful, and loving wife Dr. Dana Discenza. You have always been there for me through this crazy adventure of a PhD and have been my sound board during my highs and lows. You have put up with my crazy stress cleaning and non-stop singing at all hours of the day. You have continually pushed me and motivated me throughout my entire time at the University of Virginia. Thank you for sharing your knowledge and expertise you learned from your PhD in Chemistry to guide me through mine. I couldn't have asked for a better wife or better friend. I wouldn't be here at the University of Virginia or finishing my PhD if it wasn't for your full support and love. Dana, I love you! This chapter is closing in our life and I can't wait to see what life has in store for us next.

Table of Contents

Abstract.....	ii
Acknowledgments	iv
Table of Contents	vi
List of Figures	xi
List of Tables	xv
CHAPTER 1 – Introduction	16
1.1 – Point-of-Care Diagnostics and Microfluidics	16
1.2.1 – Lateral Flow Immunoassays.....	19
1.2.2 – Vertical Flow Immunoassays.....	26
1.3 – Detection and Identification of Infectious Diseases.....	30
1.4 – Research Goals and Concluding Remarks	33
1.6 – References	36
CHAPTER 2 – Detection of infectious Diseases with a Centrifugally-Driven Microfluidic Orthogonal Flow Immunoassay.....	39
2.1 – Introduction	39
2.2 Experimental Section	43
2.2.1 Fabrication of the Microfluidic OFI Disc.....	43
2.2.2 Flow Study – Buffer Solution Comparison.....	44
2.2.3 Proof-of-Concept: Orthogonal Flow Immunocapture Study..	45
2.2.4 Detection of Y. Pestis on Centrifugal Microfluidic Disc via Orthogonal Flow	46

2.2.5 Detection of Ebola Virus-Like Particle on Centrifugal Microfluidic Disc via Orthogonal Flow.....	47
2.2.6 Image processing and Data Analysis	48
2.3 Results and Discussion.....	48
2.3.1 Fabrication of the Microfluidic OFI Disc.....	48
2.3.2 Flow Study – Buffer Solution Comparison.....	52
2.3.2 Proof-of-Concept: Orthogonal Flow Immunocapture Study..	59
2.3.3 Detection of Y. Pestis F1 antigen	62
2.3.4 Detection of Ebola Virus-Like Particles	64
2.4 Conclusions	65
2.5 References	67
 CHAPTER 3 – Detection of Infectious Diseases with a 3D-Printed Large Volume Centrifugal Microfluidic Orthogonal Flow Immunoassay	70
3.1 Introduction	70
3.2 Experimental Section.....	73
3.2.1 Fabrication of the Microfluidic cOFI Disc.....	73
3.2.2 Fabrication of the 3D-Printed Large Volume Chamber	74
3.2.3 Proof-of-Concept: Immunocapture Study.....	75
3.2.4 Detection of Y. pestis F1 Antigen on the Centrifugal Microfluidic Orthogonal Flow Immunoassay Disc	76

3.2.5 Detection of Ebola Virus-Like Particles on the Centrifugal Microfluidic Orthogonal Flow Immunoassay Disc	77
3.2.6 Detection in Artificial Urine and Human Urine	78
3.2.7 Detection in Artificial Blood Plasma.....	79
3.2.8 Image Processing and Data Analysis.....	80
3.3 Results and Discussion.....	80
3.3.1 Fabrication of the Microfluidic cOFI Disc.....	80
3.3.2 3D-Printed Large Volume Chamber	83
3.3.3 Proof-of-Concept: Large Volume Immunocapture Study.....	87
3.3.4 Detection of Y. Pestis F1 antigen on Large Volume Centrifugal Orthogonal Flow Microfluidic Disc	89
3.3.5 Detection of Ebola Virus-Like Particles on Large Volume Centrifugal Orthogonal Flow Microfluidic Disc.....	91
3.3.6 Analysis of Human Samples on Large Volume Centrifugal Orthogonal Flow Microfluidic Disc	93
3.4 Conclusions	98
3.5 References	99
CHAPTER 4 – The Development of a Smartphone Point-of-Care Diagnostic Device a Centrifugal Microfluidic Orthogonal Flow Immunoassay	104
4.1 Introduction.....	104
4.2 Experimental Section	107

4.2.1 Fabrication of the Multiplexed cOFI Disc.....	107
4.2.2 Fabrication of the Multiplexed 3D-Printed Sample Chamber	108
4.2.3 Automated cOFI System, Image Processing and Data Analysis.....	108
4.2.4 Proof-of-Concept: Multiplexed Immunocapture Study.....	110
4.2.5 Detection of Y. pestis F1 Antigen on the Multiplexed cOFI Disc	111
4.3 Results and Discussion.....	113
4.3.1 Fabrication and Design of the Multiplexed cOFI Disc.....	113
4.3.2 Automated cOFI System, Image Processing and Data Analysis.....	115
4.3.3 Proof-of-Concept: Multiplexed cOFI Immunocapture Study	117
4.3.4 Detection of Y. Pestis F1 Antigen on Multiplexed cOFI Disc	120
4.4 Conclusions	124
4.5 References	126
CHAPTER 5 – The Design and Characterization of a Multiplexed Flow Through Assay for Rapid, Point-of-Need Diagnostics.....	128
5.1 Introduction.....	128
5.2 Experimental Section.....	131
5.2.1 Fabrication of the Flow Through Assay	131

5.2.3 Proof-of-Concept: Immunocapture Study.....	133
5.2.4 Detection of <i>Y. pestis</i> F1 Antigen on the Flow Through Assay Chip.....	134
5.2.5 Image Processing and Data Analysis.....	135
5.3 Results and Discussion.....	136
5.3.1 Fabrication and Design of the Flow Through Assay Chip ..	136
5.3.2 Proof-of-Concept: Immunocapture Study.....	137
5.3.3 Detection of <i>Y. pestis</i> F1 Antigen on the Flow Through Assay Chip.....	143
5.4 Conclusions	148
5.5 References	150
CHAPTER 6 – Final Remarks.....	152
6.1 Conclusions	152
6.2 Ongoing Studies, Persistent Challenges, and Future Work	155
6.2.1 Disc Design and Fabrication	155
6.2.1.1 Large Volume Sample Handling.....	156
6.2.2 On-Disc Immunocapture	156
6.2.3 Nitrocellulose Membrane Replacement	158
6.2.4 Hardware Improvements and Assay Automation	159
6.3 Summation.....	159
6.4 References	161

List of Figures

Figure 1-1: A centrifugal microfluidic disc with a fluid volume, identified in red, in a microfluidic channel.....	18
Figure 1-2: Example of how a traditional lateral flow immunoassay strip is designed and assembled.....	20
Figure 1-3: Scanning electron microscope micrograph of a nitrocellulose membrane layer with 0.2 μm pore size.	21
Figure 1-4: Antibody and its variants in various orientations on the surface when physisorbed.....	22
Figure 1-5: Hydrophobic and ionic interactions between antibody and gold nanoparticle surface.....	23
Figure 1-6: Examples of the two types of immunoassays that can be performed on an LFI.....	24
Figure 1-7: A centrifugally driven LFI disc with flow control.	25
Figure 1-8: Example of a Vertical Flow Immunoassay (VFI) Biosensor.....	27
Figure 1-9: Paper-based multiplexed vertical flow assay (VFA) and a mobile-phone reader.....	28
Figure 1-10: Schematic overview of the OFI disc and a photograph of a single domain on the OFI disc.....	29
Figure 1-11. Schematic of the VFI device to detect SARS-CoV-2 Antibodies.	32
Figure 1-12. Scheme of the VFI system and its operation principle.....	33
Figure 2-1: Schematic of 5-layer cOFI disc	41
Figure 2-3: Overview of the three cOFI disc versions.....	49

Figure 2-4: Schematic of the 7-Layer cOFI disc (Version 2) and method of assembly.....	50
Figure 2-5: Schematic of the 7-Layer cOFI disc (Version 3) and method of assembly.....	51
Figure 2-6: Schematic of the two OF disc designs: 5-layers versus 7-layers.	54
Figure 2-7: Comparison of average fluid drain times (n=3) between the short fluidic channel (3mm) and long fluidic channel (26 mm).....	56
Figure 2-8: Comparison of three different buffer solutions drained through the nitrocellulose membrane with the sample chamber near the CoR.	57
Figure 2-9: Comparison of three different buffer solutions through the nitrocellulose membrane with the sample chamber near the center of rotation.	57
Figure 2-10: Proof-of-concept of the 7-Layer OFI disc. A	60
Figure 2-11: Results showing the capability and the sensitivity of the OFI disc to detect the Y. Pestis F1 antigen (n=3), discs were spun at 1000 RPM.	62
Figure 2-12: Schematic of sandwich-type immunocapture on a cOFI device.	63
Figure 2-13: Results showing the detection of Ebola virus-like particle on the cOFI device (n=3), discs were spun at 1000 RPM.....	64
Figure 3-1: Concept of operations of the large volume centrifugal orthogonal flow immunoassay disc.....	73
Figure 3-2: Schematic of Version 1 of the large volume centrifugal orthogonal flow immunoassay disc.....	81

Figure 3-3: Schematic of version 2 of the large volume centrifugal orthogonal flow immunoassay disc.....	82
Figure 3-4: Schematic of the 4 mL capacity 3D-printed large volume chamber.	85
Figure 3-5: Schematic of the 3D-printed large volume chamber.....	86
Figure 3-6: Schematic of direct assay type immunocapture on a cOFI device. ..	87
Figure 3-7: Immunocapture Study Results.	88
Figure 3-8: Detection of <i>Y. pestis</i> F1 antigen in chase buffer.	90
Figure 3-9: Detection of Ebola Virus-Like Particles in chase buffer.	92
Figure 3-10: Detection in artificial urine.	94
Figure 3-11: Detection in human urine.	96
Figure 3-12: Detection in artificial blood plasma.	97
Figure 4-1: Overview of the Concept of Operations for the Automated cOFI System.	106
Figure 4-2: Schematic overview of the multiplexed cOFI disc	113
Figure 4-3: Workflow of the Automated cOFI System.....	115
Figure 4-4: Multiplexed cOFI - Immunocapture Study Results.	118
Figure 4-5: Multiplexed cOFI Detection of <i>Y. pestis</i> F1 antigen in chase buffer.	121
Figure 4-6: Large Volume cOFI Detection of <i>Y. pestis</i> F1 antigen in chase buffer.	123
Figure 5-1: Overview of the Flow Through Assay.....	130
Figure 5-2: Schematic overview of the Flow Through Assay.....	136
Figure 5-3: Antibody Volume Blotting Study.	138

Figure 5-4: Flow Rate Study – Whatman ProTran 0.2 μm	140
Figure 5-5: Flow Rate Study – Sartorius.....	141
Figure 5-6: Flow Through Assay Detection of <i>Y. pestis</i> F1 antigen in chase buffer - Sartorius.	143
Figure 5-7: Flow Through Assay Detection of <i>Y. pestis</i> F1 antigen in chase buffer – Whatman ProTran 0.2 μm	144
Figure 5-8: Flow Through Assay Detection of <i>Y. pestis</i> F1 antigen in chase buffer – Binding Study.	145

List of Tables

Table 2-1: The linear regression equations for each buffer at each rotational frequency	58
Table 2-2: 2-way ANOVA Tukey’s Multiple Comparisons Test: Comparing the statistical differences between the rotational frequencies.	59
Table 3-1: Composition of the artificial urine in 50 mL of deionized water.	79
Table 4-1: Multiplexed cOFI Immunocapture Study– One-Way ANOVA, Dunnett’s Multiple Comparison Test Results.....	120
Table 4-2: Multiplexed cOFI Detection of <i>Y. pestis</i> F1 antigen in chase buffer – One-Way ANOVA, Dunnett’s Multiple Comparison Test.....	122
Table 4-3: Large Volume cOFI Detection of <i>Y. pestis</i> F1 antigen in chase buffer – One-Way ANOVA, Dunnett’s Multiple Comparison Test.....	124
Table 5-1: Tukey’s Multiple Comparison’s Test.	139

CHAPTER 1 – Introduction

1.1 – Point-of-Care Diagnostics and Microfluidics

Microfluidics allows for the manipulation of small volumes of fluids (microliters to attoliters) in micron-sized channels.¹ The miniaturization of traditional analytical techniques (e.g., polymerase chain reaction (PCR), immunoassays, and DNA analysis) allow for conventional methods to perform sample analysis at the point-of-care (POC), rather than in a laboratory environment.^{2,3} In the early 1990s, the concept of micro total analysis systems (μ TAS), also known as lab-on-a-chip (LOC) or lab-on-a-disc (LoaD), was first introduced; LOC or LoaD is defined as a device that incorporates one or more laboratory instruments onto a 'chip'.^{3,4} The World Health Organization (WHO) has determined that a POC device, especially one that will be used in developing countries, needs to be ASSURED: affordable, sensitive, specific, user-friendly, rapid and robust, equipment free, and deliverable to end-users.⁵ As a result, POC microfluidic devices have become extremely popular over the last decade, especially since the SARS-CoV-2 outbreak in 2020.^{2,6-10}

When designing a new microfluidic POC device, there are many critical specifications to consider, including the mechanism used to drive fluid. There are two main methods of fluid movement on a microfluidic device, active and passive pumping.¹¹ Active pumping includes the use of external instrumentation (i.e., syringe pumps or pneumatic pumps) to drive fluid through the microfluidic channels.¹² The use of an external pump decreases the device's portability, increases cost, and adds additional complexity to the instrument. Conversely, fluid

can be moved passively, or without external power, via capillary forces, Euler forces, and osmotic forces, to name a few.¹²

Research and development of centrifugally-driven microfluidic devices has grown in popularity in the past decade due to their simplistic method of fluid flow and the limited amount of equipment required.^{2,12-15} The centrifugally-driven microfluidic discs described in **Chapters 2-5** pump fluids by taking advantage of the pseudo-gravitational forces generated by the rotation of the disc (**Figure 1-1**).¹⁶ The centrifugal force (F_{cen} , Equation 1) and pressure (P_{cen} , Equation 2) applied to a fluid column in a microfluidic channel can be easily characterized and controlled by changing the rotational frequency (ω), while keeping the following variables constant: fluid column length (\bar{r}) in relation to the center of rotation (CoR), fluid density (ρ), and the difference in height between the upper and lower menisci of the fluid column.

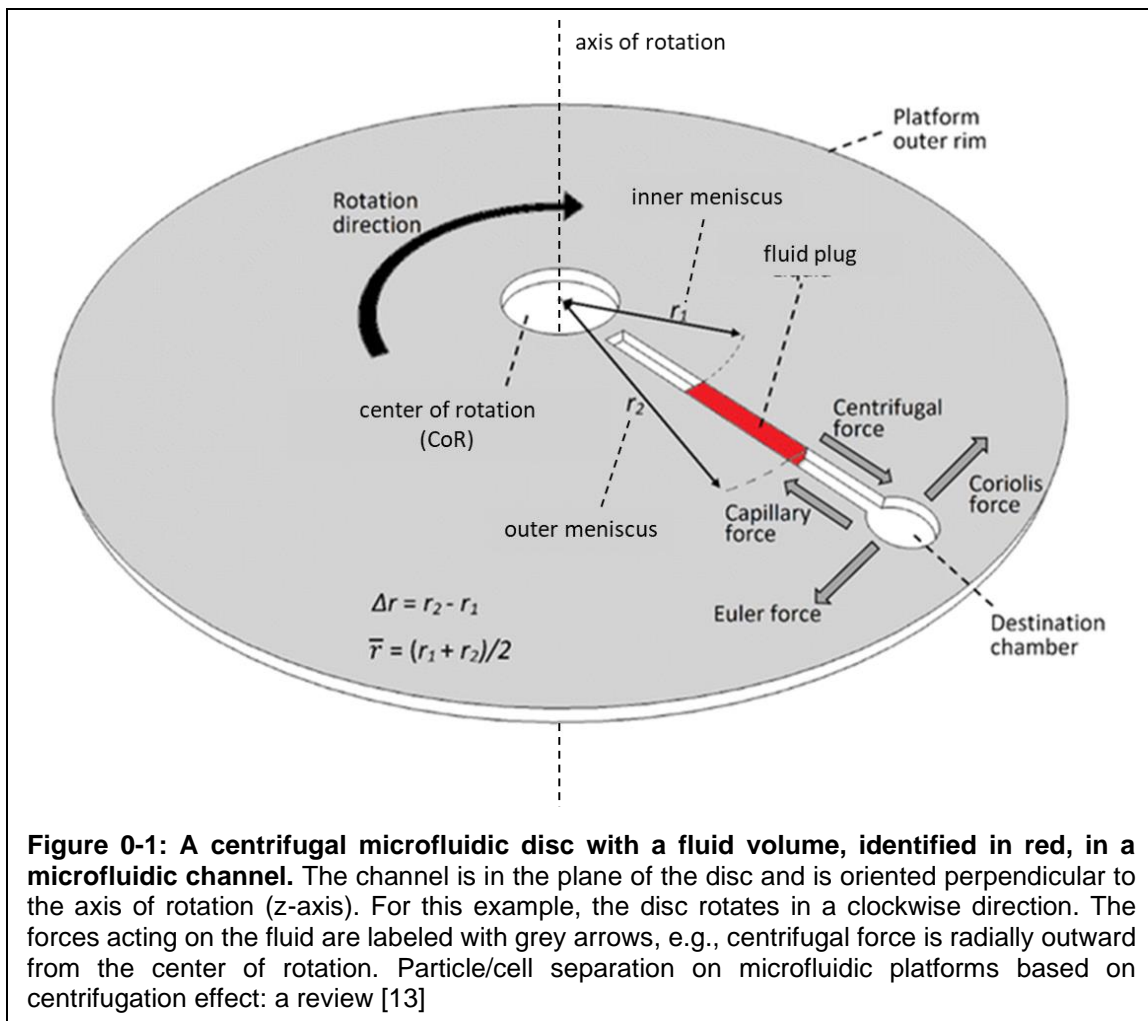
Equation 1:
$$F_{cen} = \rho\omega^2\bar{r}$$

Equation 2:
$$P_{cen} = \rho\omega^2\Delta r\bar{r}$$

The average fluid velocity (U) through the channel can be calculated through the following equation.

Equation 3:
$$U = \frac{D_h^2 P_{cen}}{32\mu L}$$

The variables affecting fluid velocity in a microfluidic channel include hydraulic diameter (D_h) of the channel or chamber, the fluid(s) viscosity (μ), and the length of the fluidic column (L) (**Figure 1-1**).¹⁶ In the following chapters, these variables will be further discussed and play an important role in the development of the centrifugally-driven microfluidic immunoassays.



1.2 – Immunoassays

An immunoassay is defined as a bioanalytical technique that uses antibodies, to detect small amounts of a target analyte (antigen) in a sample solution.^{17,18} The concept of an immunoassay was first introduced by Rosalyn Yalow and Solomon Berson in the 1950s.¹⁹ Since then, the development and application of immunoassays have grown exponentially due to the high sensitivity, specificity, and flexibility; those characteristics make them advantageous for the detection of various biomarkers found in human serum, as POC devices, in the food industry to test for bacteria or other toxins, to test for narcotics, and for a number of other biological and environmental applications.^{17,20}

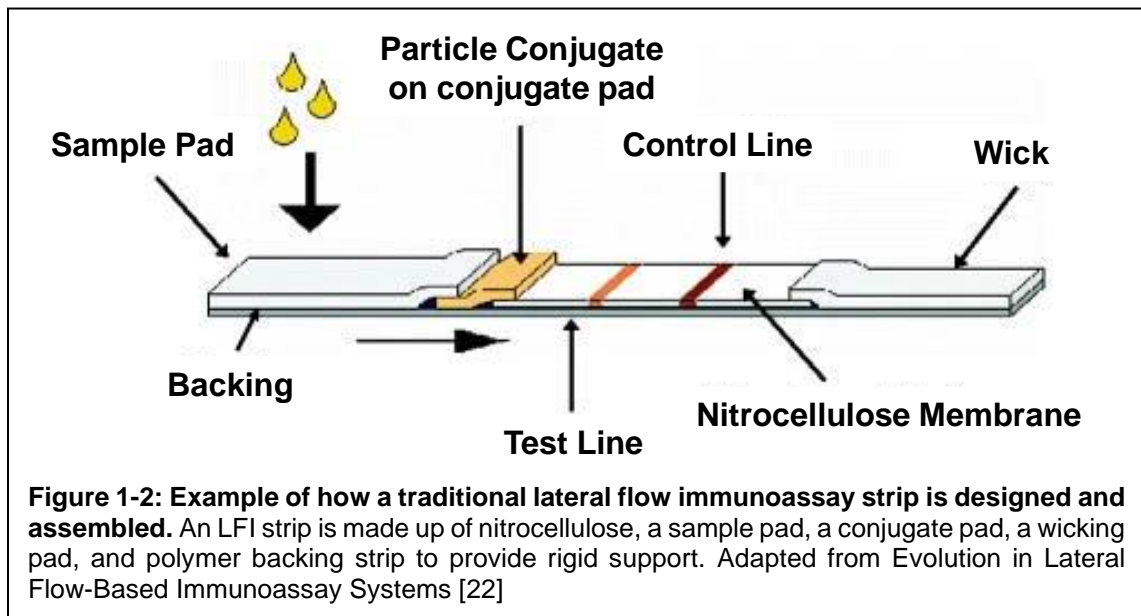
1.2.1 – Lateral Flow Immunoassays

The lateral flow immunoassay (LFI) is an example of a POC device that meets the ASSURED requirements.⁵ They are rapid (~15 min assay time), inexpensive to produce (\$0.10-\$3.00/test), reliable, and easy to use.²¹ Additionally, this type of assay is operated through capillary-driven forces due to the porous media used (e.g., nitrocellulose membrane). LFIs have been around since the 1970s and are arguably the most popular type of POC microfluidic devices, with the most commonly used LFI being the at-home pregnancy test.²² Within the last few years, LFIs have become extremely popular as home diagnostic kits to help diagnose early signs and symptoms of COVID-19.⁸

The traditional LFI is constructed of five major parts, to include various porous materials, with each part playing a vital role to achieve a sensitive and robust assay (**Figure 1-2**).²² Each piece overlaps each other and is placed onto a plastic backing card, for rigidity, with pressure sensitive adhesive (PSA). When an LFI strip is run, the sample solution is added to the sample pad whereby capillary forces cause the solution to wick through the sample pad to the conjugate pad, which contains immobilized detection particles, such as colloidal gold nanoparticles (AuNP), fluorescent particles, or latex nanoparticles.²³ These detection particles are conjugated to either an antibody or antigen, depending on the assay type, that are specific to the target analyte (**Figure 1-2**). When the solution wicks through the conjugate pad, the detection particles are re-suspended and bind to the target analyte as the sample wicks along the pad onto the nitrocellulose membrane. During manufacturing, the nitrocellulose membrane has capture antibodies, specific to the target analyte, immobilized in bands. The

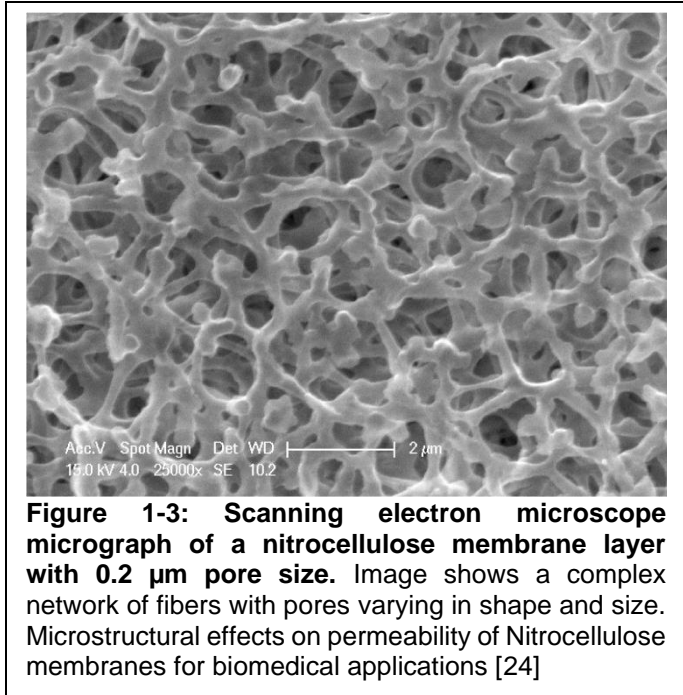
capture antibodies will bind to the target analyte while the excess sample solution continues to flow to the wicking pad. Once the sample reaches the wicking pad, the pad becomes completely saturated, flow on the LFI strip stops and the results of the assay are determined.

Nitrocellulose is inherently hydrophobic but is made more hydrophilic through the addition of surfactants during the manufacturing process.²¹ The



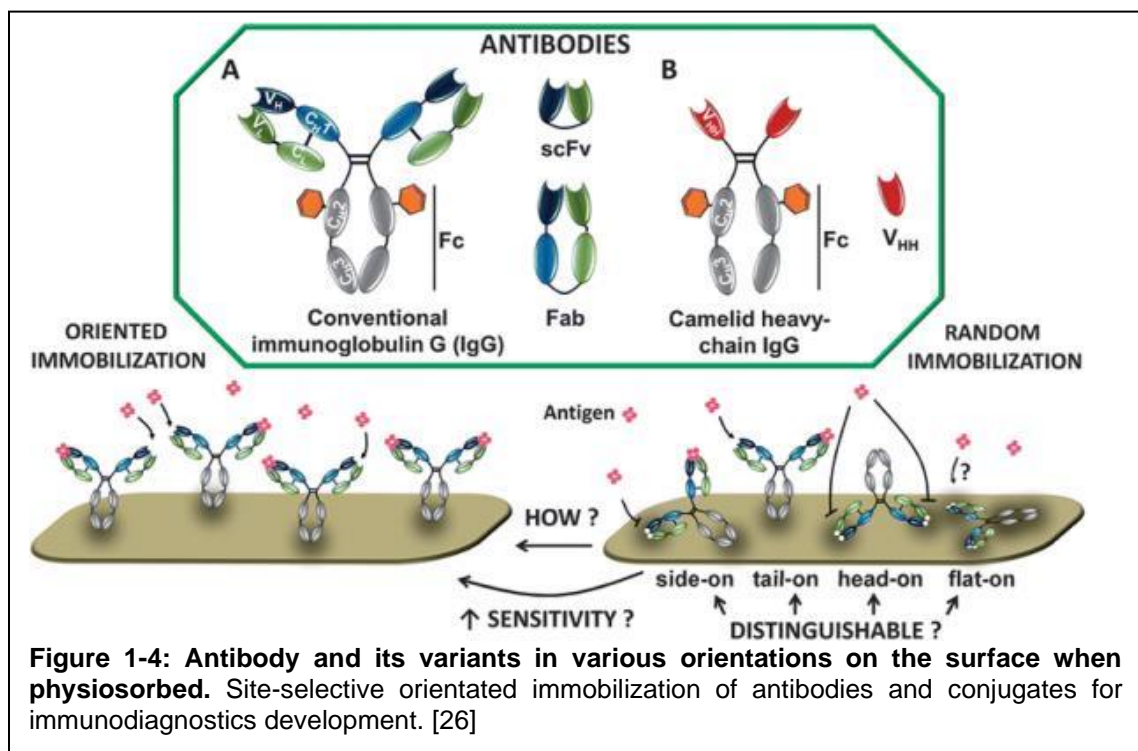
structure of nitrocellulose is similar to a sponge with an amorphous pore structure (**Figure 1-3**).^{22,24} The pore structure (i.e., pore diameter) can be controlled during the manufacturing process through either a slow or fast evaporation rate of the lacquer solution.²¹ After manufacturing, the average gaussian distribution of the pore size in the membrane is determined and given a numerical value (e.g., 0.2 μm pore diameter). Interestingly, a membrane's pore size can be altered based on the

solute concentration present in a sample resulting in either swelling or de-swelling of pores. For example, a solution containing sodium bicarbonate promotes membrane swelling, e.g., smaller pores, which results in slower fluid discharge but decreases the distance antibodies have to diffuse in order for them to interact and bind.¹³



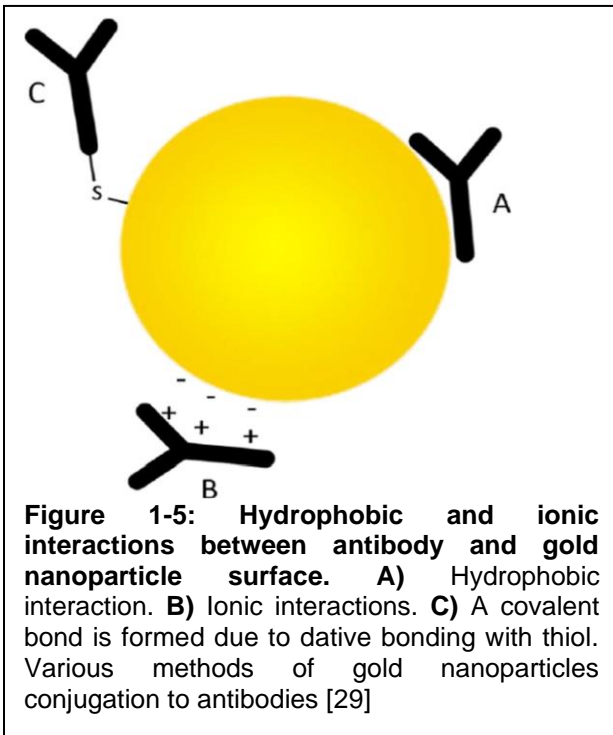
Furthermore, nitrocellulose has many biomedical applications due to high protein binding capacity, low cost, and ease of handling.²² With its high protein binding capacity, antibodies non-covalently bind to the surface of nitrocellulose through electrostatic interactions, hydrophobic interactions, and hydrogen bonds.^{21,22} The advantages to non-covalently binding to the surface of the membrane are the simplicity of application, speed of binding, and the increased density of antibodies on the surface.²⁵ The disadvantage to non-covalently binding or passively absorbing to the surface (e.g., nitrocellulose) is the orientation of the antibodies cannot be controlled (**Figure 1-4**).²⁶ The antibodies' orientation is random and depends on the dipole moments of the protein as well as the charge of the surface to which they are absorbed. It is important to note that the antibodies adsorb at any orientation and location on the surface of the nitrocellulose fibers,

e.g., underneath, on top, or all around the fiber (**Figure 1-3**). Unfortunately, the random orientation can result in decreased antigen binding activity due to the antigen binding regions (Fab fragments) being partially or completely blocked when the antibody binds to the surface.^{22,25} Fortunately, antibodies can be covalently bonded to a surface through primary amines or carboxyl groups distributed throughout the structure of antibody; covalently bonding the antibodies allows for them to be oriented with the Fab region to be exposed resulting in increased antigen binding activity and increased device sensitivity (**Figure 1-4**).^{25,26}



As previously stated, antibodies can be immobilized onto a nitrocellulose membrane through non-covalent interactions. Similarly, antibodies can also be conjugated to AuNP through non-covalent interactions: hydrophobic and ionic (**Figure 1-5**).²⁷⁻²⁹ The hydrophobic interactions occur between the surface of the

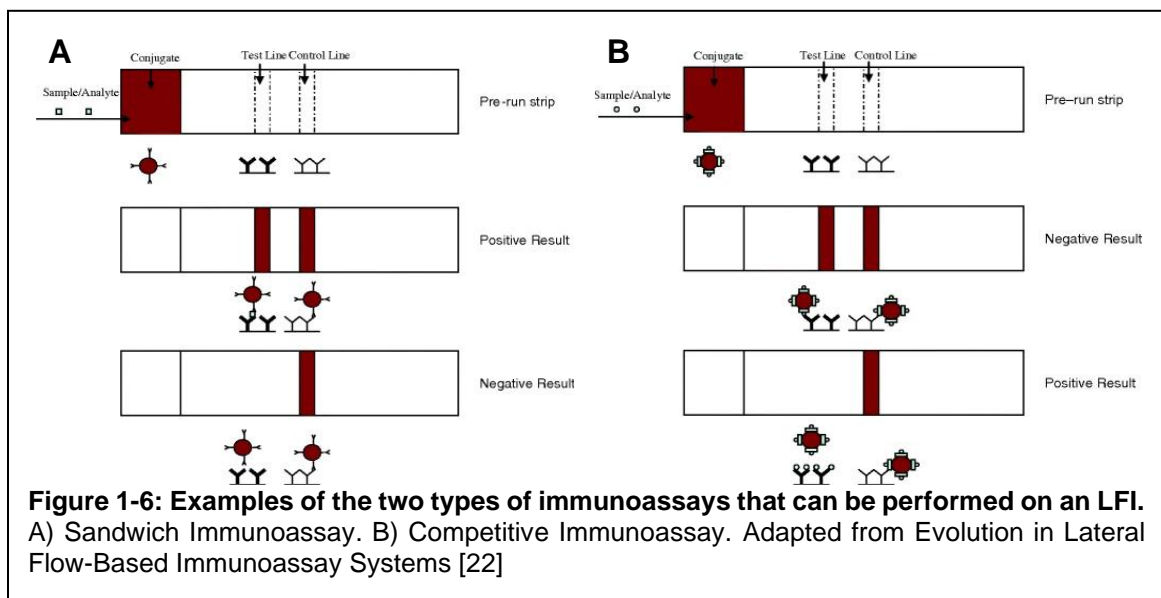
AuNP and the hydrophobic pockets found in the middle of an antibody via the hydrophobic side chains on the amino acids; the hydrophobic interactions require significant restructuring of the antibody which can result in decreased antigen binding activity.¹⁷ The disadvantages to the non-covalent binding method are a large concentration of antibodies are



required in order to bind to the AuNP, the antibodies are randomly oriented on the AuNP surface, and it is difficult to control the antigen binding activity of the antibody. Furthermore, the strength of the non-covalent bonds is dependent on the pH and salt concentration of the solution. Antibodies are typically conjugated to a AuNP at their isoelectric point (pI); further from the pI, the adsorption of the antibodies to the AuNP decreases and can potentially be replaced by another protein or other molecule present in the solution.²⁹

LFI strips can be designed to perform two assay types: sandwich assay (**Figure 1-6A**) and competitive assay (**Figure 1-6B**), with both types having a test and control lines.²² Sandwich assays are used mainly to detect large analytes that have multiple antibody binding sites (e.g., human chorionic gonadotropin). For a sandwich assay, a positive sample will present both the test and control lines, while

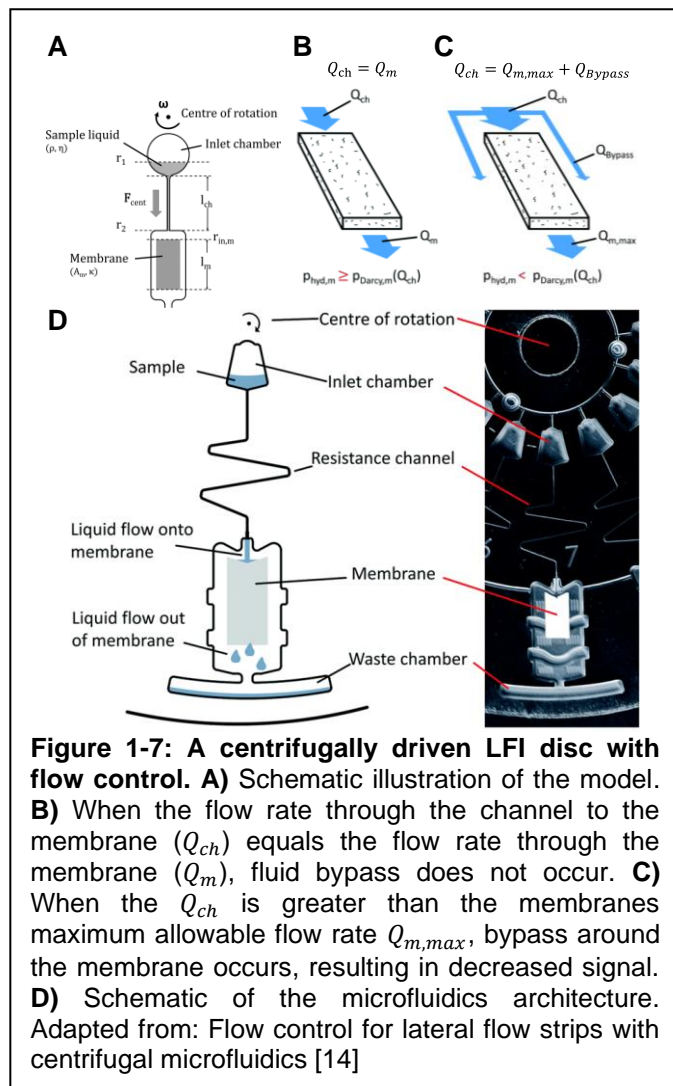
a negative sample will only display the control line. A competitive assay is most commonly used to test for small molecules because they are not big enough to bind to two antibodies at the same time; therefore, a positive sample will show only the test line while a negative sample will show both the test and control lines on the nitrocellulose membrane.²²



While the LFI strip has many advantages, there are drawbacks to this assay design: (1) inability to control flow rate, (2) cannot perform mixing on the device, (3) cannot handle large sample volumes, and (4) the inability to perform washing steps.¹⁴ To overcome these shortfalls, Kainz et al. developed a centrifugally driven device that allowed them to choose specific volumes, thereby allowing them to control fluid flow through an LFI (**Figure 1-7**).¹⁴ However, there is a major concern of sample loss due to the fluid flowing around the membrane; to account for this, they developed a model that would predict any fluid bypass around the LFI strip (**Figure 1-7A**). The model described that when a centrifugal force is applied to the fluidic column in the membrane, hydrostatic pressure is created ($p_{hyd,m}$), and the pressure generated is dependent on the length of the membrane (l_m) and has a

direct effect on the flow rate through the membrane (Q_m). As fluid is flowing through the membrane, a pressure drop ($P_{darcy,m}$) occurs along l_m . Ideally, all the sample would flow through the membrane without any bypass, but for that to occur, the flow rate through the channel to the membrane (Q_{ch}) must equal Q_m (**Figure 1-7B**). Sample bypass (Q_{Bypass}) occurs if the Q_{ch} is larger than the maximum flow rate through the membrane ($Q_{m,max}$) (**Figure 1-7C**). The Q_{ch} is dependent on the angular velocity of the disc, which generates the centrifugal forces applied to the sample fluid. Finally, the $Q_{m,max}$ is dependent on the membrane type, pore size, and manufacturing variations from lot to lot.

With these variables taken into consideration, Kainz *et al.* demonstrated a viable centrifugally driven LFI. They showed the ability to perform a sandwich immunoassay with colorimetric detection using AuNP and adjustable flow rate on-disc. Unfortunately, this disc was designed to promote fluid bypass, and the membrane was not fixed in place, which ultimately resulted in very large



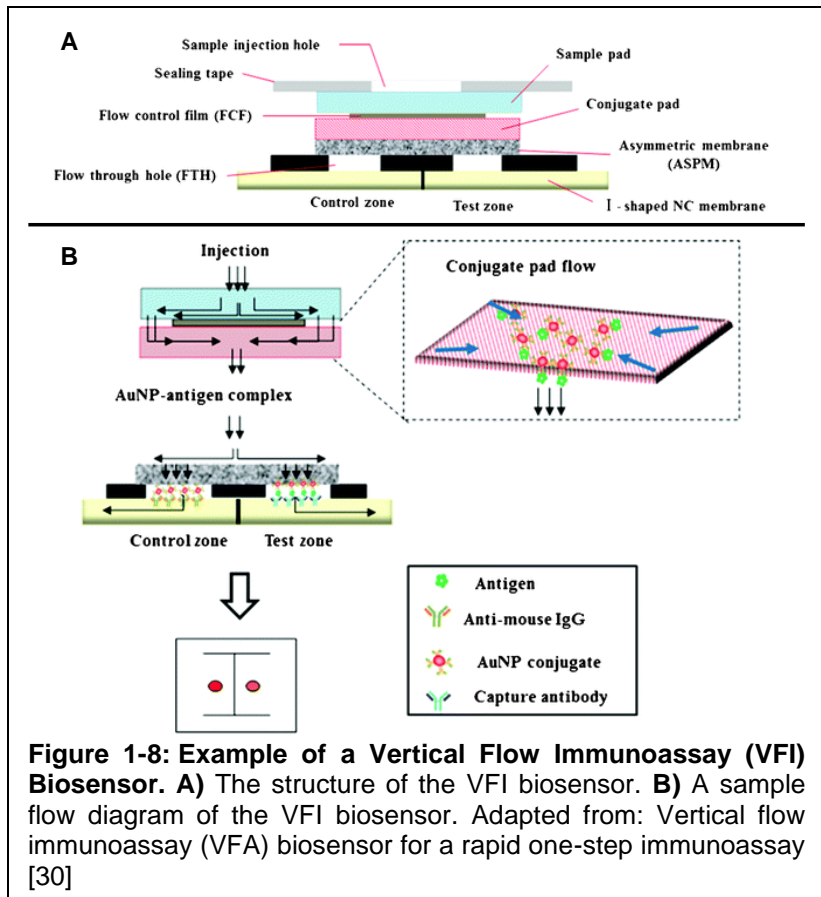
variations in the assay's results, i.e., either very strong or very weak signal. They did take into account the potential loss of hydraulic pressure and placed the membrane far from the CoR (**Figure 1-7D**). This approach was a step forward to assist in fluid flow control on LFI and assisted in the design of the orthogonal flow immunoassay discs described in subsequent chapters.

1.2.2 – Vertical Flow Immunoassays

Vertical flow immunoassays (VFI) were designed to overcome the previously described shortfalls of the LFI strip, but one of the main reasons was to increase the sensitivity and the ability to multiplex.³⁰ This section is meant to help contextualize the work that was performed in **Chapters 2-5** by describing relevant literature in regards to VFI, embedded membranes into microfluidic devices, and the use of these methods on-disc. To date, current publications have described applications of vertical and orthogonal flow through a membrane with different membrane placements as well as different methods of fluid movement: gravity-driven, pressure-driven, or centrifugally-driven.^{7,13,30–33}

In 2013, Oh *et al.* developed a one-step VFI biosensor to detect C-reactive protein (CRP) in human serum (**Figure 1-8**).³⁰ The biosensor was assembled by stacking the individual layers on top of each other: sample pad, flow control film, conjugate pad, and nitrocellulose membrane (**Figure 1-8A**). The capture antibodies were immobilized onto the membrane and the AuNP conjugate antibodies were suspended on the conjugate pad (**Figure 1-8B**). The sample

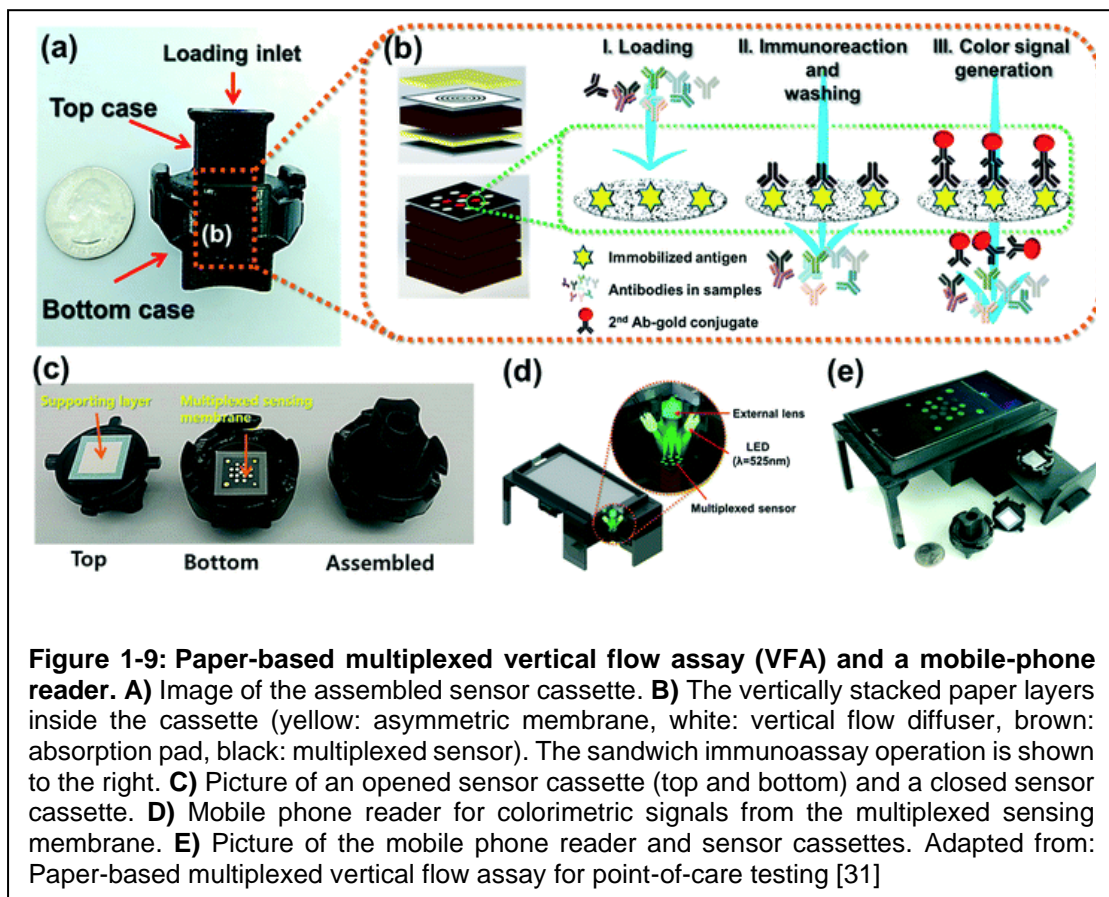
solution is added through the injection hole, and gravity-assisted flow facilitates the solution to wick into each layer, resulting in a visual colorimetric change on the device. They were able to detect between 10-0.01 $\mu\text{g/mL}$ of CRP in serum with a total



assay time of 2 minutes. In those studies, the sample flow rate was dependent on two variables: gravity and a hydrophobic film (flow control film); therefore, the user depended on the device materials to control the flow rate. Due to the small size of the sample holes, inconsistent results were observed. Finally, the device was not designed to handle large volumes, only 50 μL , but the use of a larger volume would permit an increase in the self-washing effectiveness and decrease the standard deviations.

In 2019 Joung *et al.* detected Lyme disease in humans using their multiplexed VFI POC device using 3D-printed technology and a smartphone to perform the image analysis (**Figure 1-9**).³¹ The device contained a diffuser to allow

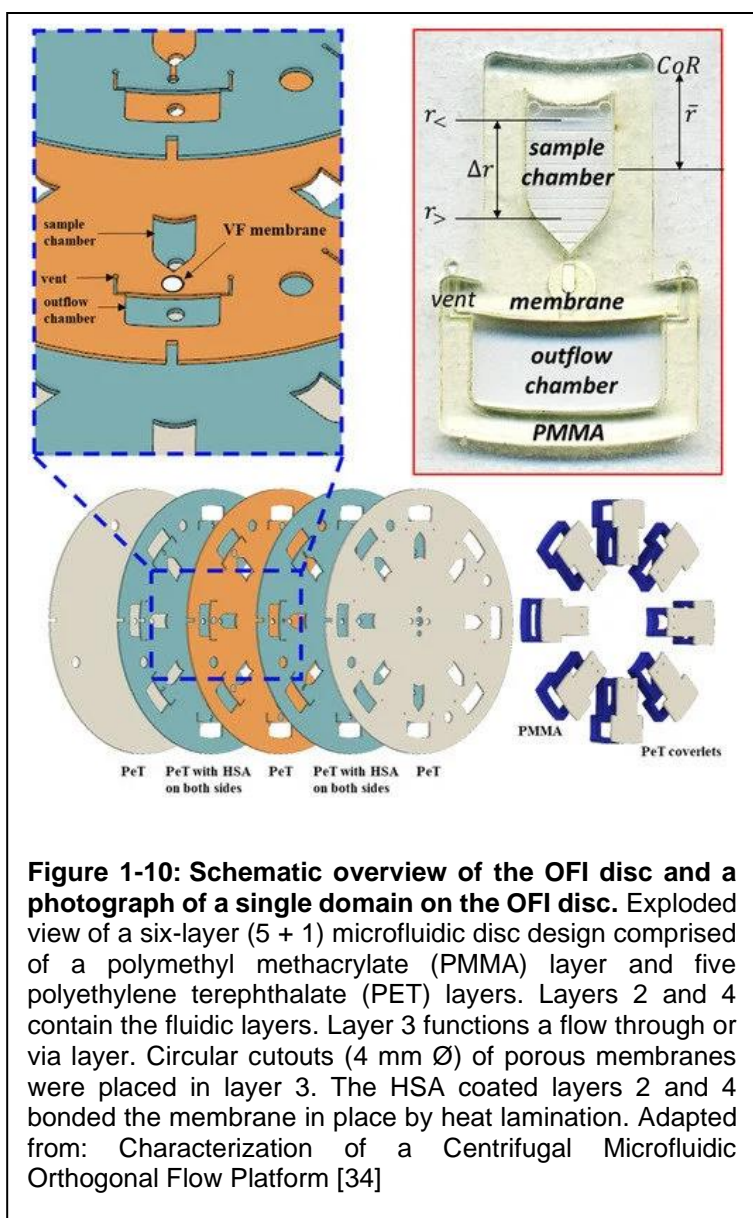
for even distribution of the sample onto the 13 different spots on the membrane (**Figure 1-9B**). The cassette was made of two 3D-printed pieces, the top contained the supporting layer and the bottom held the membrane; a platform was 3D-printed to hold the smartphone to perform automated image analysis (**Figure 1-9C & D**). Unfortunately, image analysis required disassembly of the cassette, which adds extra steps to the assay and, more importantly, exposes the user to potential contaminated samples (**Figure 1-9E**). Ultimately, the ideal POC immunoassay would be completely automated and enclosed to limit the number of assay steps as well as eliminate exposure to biological fluids.



In the Landers Lab, we focus on centrifugally driven microfluidics to develop devices that miniaturize many traditional techniques (e.g., enzyme-linked

immunosorbent assay, polymerase chain reaction), which ordinarily require additional instrumentation to move the fluid (i.e., pipetting or pumps) as well as mixing and washing steps. Shane *et al.* (2022) developed a novel centrifugally driven immunoassay which is synonymous with VFI, but fluid flow is driven orthogonally through the membrane with respect to the centrifugally generated force on the disc, creating an orthogonal flow immunoassay (OFI).¹³ This on-disc approach leveraged the rapid, inexpensive, print-cut-laminate (PCL) method of

disc fabrication with the ability to control the flow rate through an embedded membrane (Figure 1-10).³⁴ This POC OFI disc was capable of detecting eight target analytes from a single sample within the device's eight intrinsic domains. The authors characterized how the flow rate through the embedded membrane changes with the fluid type, membrane pore size, and the sample



volume. While the OFI was an innovative design and concept, the downside to this disc was the exponential decay of flow rate as Δr decreased due to the short microfluidic channel (**Figure 1-10**). Finally, the flow through the membrane was not true orthogonal flow, but a hybrid between that and lateral flow; this resulted in fluid bypass and nonuniform binding of the target analytes on the membrane. The nonuniform binding makes it difficult to perform consistent and simple image analysis. In **Chapter 2**, a 7-layer disc is described that mitigates the exponential decay of flow rate and eliminates any lateral flow along the membrane to produce true orthogonal flow.

1.3 – Detection and Identification of Infectious Diseases

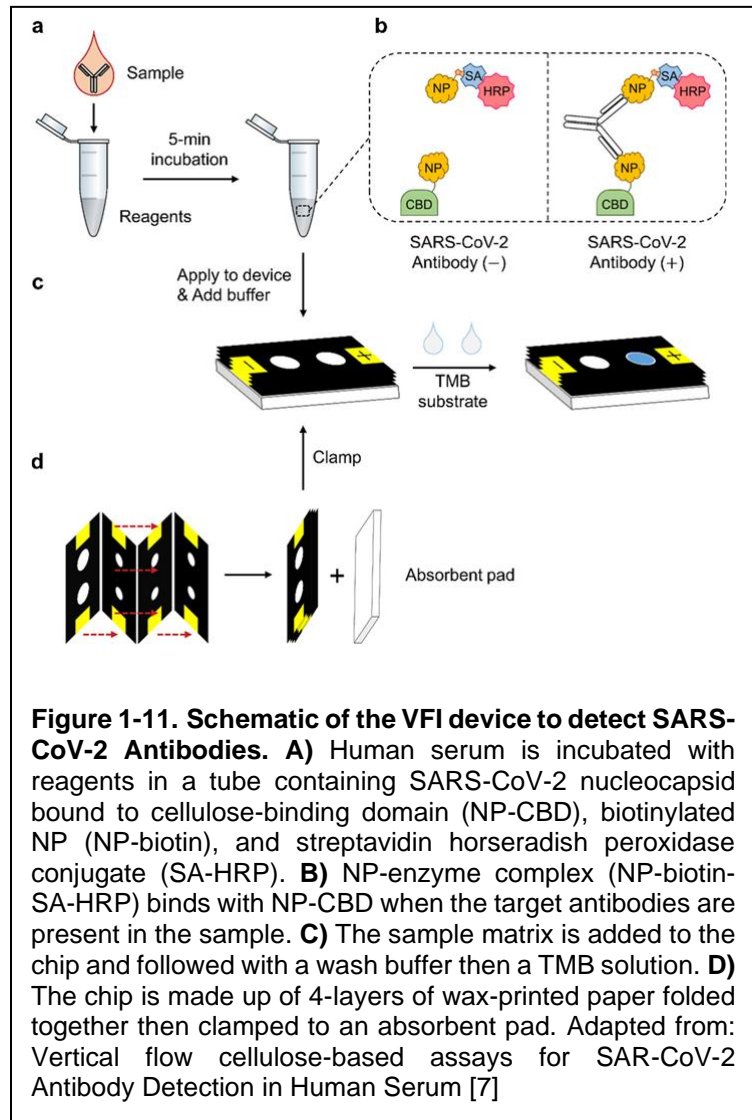
The early detection and identification of infectious diseases at the POC is important due to their potential fast incubation times as well as to prevent their spread. For example, *Yersinia pestis* (*Y. pestis*) has an incubation time of 1-6 days; similarly, Ebola has an incubation time of 5-9 days and is transmitted through either physical contact or bodily fluids.^{35,36} There are traditional methods (e.g., ELISA and PCR) available which are effective, but they are costly, time-consuming, laborious, and must be performed in a laboratory environment. POC diagnostics (e.g., microfluidic devices) can overcome those shortfalls because they are designed to be used at the point-of-need (PON); these devices diagnose a patient at the site of care in real-time while providing fast and accurate results.⁹ This is especially important in developing countries where there is little to no infrastructure available to diagnose and treat large populations of people.^{6,9,36} Infectious diseases are also a major threat to global health, as seen with COVID-19, and thus, they have the

potential to be used for biological warfare, biocrime, and bioterrorism.³⁶ The Centers for Disease Control and Prevention (CDC) has three categories to define bioterrorism agents, with Category A being the highest priority as they easily disseminate from person-to-person, cause high mortality rates, cause public panic, and require special action for public health awareness.³⁶

Since the spring of 2020, we have experienced what some may classify as a threat to our national security with the emergence of an unknown pathogen, COVID-19, which helped solidify the continuous development of ASSURED devices. Kim *et al.* developed and received emergency use authorization (EUA) by the US Food and Drug Administration (FDA) for a POC VFI that detects COVID-19 in human serum (**Figure 1-11**).⁷ Their chip design allowed for a rapid and inexpensive cellulose-based assay that was easy to produce using multiple layers (4 layers) of wax-printed paper, rather than a single layer, which was capable of producing a constant flow rate. In summary, they could analyze a 50 μL sample matrix (25 μL of human serum + 25 μL reagent solution) in 15 minutes while achieving a 5 nM LOD of SARS-CoV-2 antibodies in spiked human serum. The downsides to this device are two-fold: (1) blood needs to be drawn from the patient and spun down to obtain the serum, which may not be possible in remote or underdeveloped areas due to the additional equipment required to perform these steps; (2) the volume of serum analyzed is quite small and may not be enough to provide an accurate representation of the sample collected even though serum is already quite concentrated. In **Chapter 3**, we describe an OFI disc able to handle an array of bodily fluids, in various volumes, without the need for additional sample

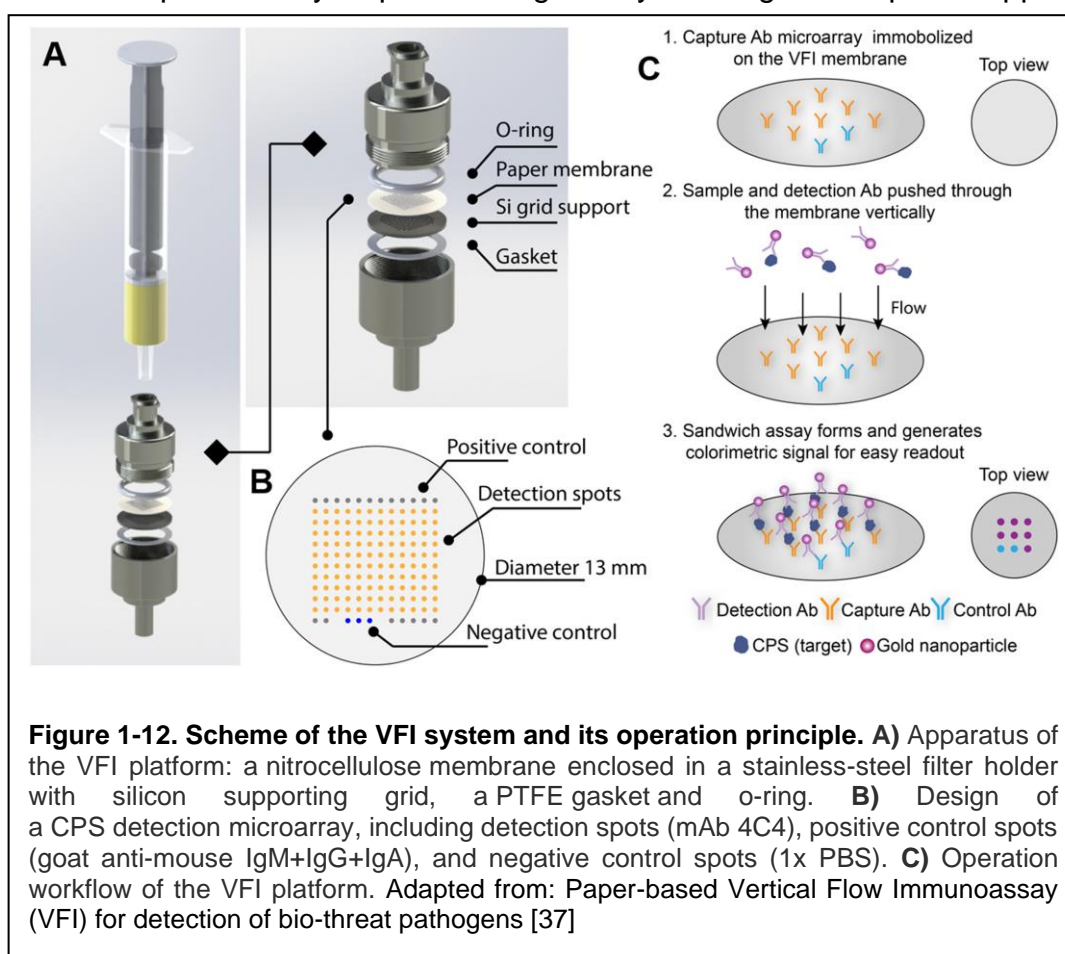
preparation off-disc.

To increase sensitivity, compared to a LFI, and to analyze large sample volumes, Chen et al. designed a syringe-driven multiplex VFI that can detect the *Burkholderia pseudomallei* surface capsular polysaccharide (CPS), a potential bio-threat agent (Figure 1-12).³⁷ Unlike the previously described VFIs, which mainly relied on gravity and wicking of the



sample through the membranes, this design pumped fluid through the membrane with a syringe. This has many advantages, including the ability to control flow rate, handle various sample types (i.e., blood, urine, saliva), and analyze large sample volumes. Additionally, they designed a silicon grid (Figure 1-12A) that allows for the detection of multiple target analytes; the multiplexed array allows for the membrane to contain both a positive and negative control (Figure 1-12B). The authors' described a LOD of 0.02 ng/mL CPS spiked in buffer by flowing 15 mL

through the nitrocellulose membrane. Unfortunately, to determine the test results and perform image analysis, the user needs to disassemble the device to access the membrane; this additional step unnecessarily exposes the technician to potential contaminated samples. The microfluidic devices described in **Chapters 3-4** allow for image analysis and assay results to be determined on-disc, then **Chapter 5** explains the development of a portable automated system that performs all of the required assay steps and image analysis using a smartphone application.



1.4 – Research Goals and Concluding Remarks

This dissertation focuses on the development and characterization of a POC OFI device that will achieve the unmet needs and capability gaps in the

medical diagnostics field. This includes the design of portable centrifugally driven OFIs that can detect the pathogen *Yersinia pestis* and other infectious diseases. Once this assay design is fully completed and integrated, this method of detection, using centrifugally driven fluidic pumping, will significantly impact the field of medical POC diagnostics. The future of these projects' hinges on microfluidic functionality, reliable reagents, and fluid flow through porous media. Knowing the limitations and advantages of these techniques provides the necessary insight into defining these research objectives. This introduction provides the outline of the subsequent chapters.

For the OFI project, the main research goal was to develop a centrifugally driven microfluidic immunoassay device that can analyze biological fluids (e.g., saliva, urine, blood plasma) for infectious diseases at the POC/PON. **Chapter 2** describes the disc design and characterization of fluid flow through the nitrocellulose membrane. Specifically, the focus was comparing the flow of different buffer solutions through the nitrocellulose membrane as well as how the flow rate changed as the sample volume decreased in the sample chamber. The hypothesis tested was that, by creating a long microfluidic channel, the hydraulic pressure would remain the same throughout the duration of the assay; therefore, the flow rate would remain constant. Additionally, by designing a 7-layer disc compared to a 5-layer disc, there would be true-orthogonal flow through the membrane and fluid bypass caused by lateral flow would be eliminated. Additionally, design of a uniform circle would make image analysis easy and reproducible.

Chapter 3 took the same disc design described in Chapter 2, but leveraged 3D-printed technology to increase the sample volume that the OFI disc could analyze. We hypothesized that, by increasing the sample volume on the disc, we could achieve greater sensitivity as well as overcome the macro-to-micro interface challenge which is a common hurdle found in microfluidics. Next, **Chapter 4** describes a research project of designing a flow-through assay that would eliminate the need for a centrifugally driven disc as well as any power equipment (e.g., compact motor or battery), while developing an immunoassay chip that could detect multiple target analytes.

Finally, the last research objective described in **Chapter 5** was to design a portable, automated system that could perform all the necessary assay steps (i.e., pre-wash, sample, post-wash) as well as the image analysis of the membrane with a smartphone application. In short, the following chapters present the key challenges and results from the development of the OFI devices as well as the development a small, portable multiplexed flow through assay chip. **Chapter 6** provides additional discussion of ongoing projects, their challenges, and their future directions.

1.6 – References

- (1) Whitesides, G. M. The Origins and the Future of Microfluidics. *Nature* **2006**, *442* (7101), 368–373. <https://doi.org/10.1038/nature05058>.
- (2) Everitt, M. L.; Tillery, A.; David, M. G.; Singh, N.; Borison, A.; White, I. M. A Critical Review of Point-of-Care Diagnostic Technologies to Combat Viral Pandemics. *Anal. Chim. Acta* **2021**, *1146*, 184–199. <https://doi.org/10.1016/J.ACA.2020.10.009>.
- (3) Fredrickson, C. K.; Fan, Z. H. Macro-to-Micro Interfaces for Microfluidic Devices. *Lab Chip* **2004**, *4*, 526–533. <https://doi.org/10.1039/b410720a>.
- (4) Reyes, D. R.; Iossifidis, D.; Auroux, P.-A.; Manz, A. Micro Total Analysis Systems. 1. Introduction, Theory, and Technology. *Anal. Biochem.* **2002**, *74*, 2623–2636. <https://doi.org/10.1021/ac0202435>.
- (5) Martinez, A. W.; Phillips, S. T.; Whitesides, G. M.; Carrilho, E. Diagnostics for the Developing World: Microfluidic Paper-Based Analytical Devices. *Anal. Chem.* **2010**, *82* (1), 26. <https://doi.org/10.1021/ac9013989>.
- (6) Jagannath, A.; Cong, H.; Hassan, J.; Gonzalez, G.; Gilchrist, M. D.; Zhang, N. Pathogen Detection on Microfluidic Platforms: Recent Advances, Challenges, and Prospects. *Biosens. Bioelectron. X* **2022**, *10*, 100134. <https://doi.org/10.1016/J.BIOSX.2022.100134>.
- (7) Kim, S.; Hao, Y.; Miller, E. A.; Tay, D. M. Y.; Yee, E.; Kongsuphol, P.; Jia, H.; Mcbee, M.; Preiser, P. R.; Sikes, H. D. Vertical Flow Cellulose-Based Assays for SARS-CoV-2 Antibody Detection in Human Serum. *ACS Sensors* **2021**, *6*, 1891–1898. <https://doi.org/10.1021/acssensors.1c00235>.
- (8) Liu, Y.; Zhan, L.; Qin, Z.; Sackrisson, J.; Bischof, J. C. Ultrasensitive and Highly Specific Lateral Flow Assays for Point-of-Care Diagnosis. *ACS Nano* **2021**, *15* (3), 3593–3611. https://doi.org/10.1021/ACSNANO.0C10035/SUPPL_FILE/NN0C10035_LIVESLIDES.MP4.
- (9) Wang, C.; Liu, M.; Wang, Z.; Li, S.; Deng, S.; He, N. Point-of-Care Diagnostics for Infectious Diseases: From Method to Devices. *Nano Today* **2021**, *37*. <https://doi.org/10.1016/j.nantod.2021.101092>.
- (10) Pandey, C. M.; Augustine, S.; Kumar, S.; Kumar, S.; Nara, S.; Srivastava, S.; Malhotra, B. D. Microfluidics Based Point-of-Care Diagnostics. *Biotechnol. J.* **2018**, *13* (1). <https://doi.org/10.1002/BIOT.201700047>.
- (11) Mark, D.; Haeberle, S.; Roth, G.; Stetten, F. Von; Zengerle, R. Microfluidic Lab-on-a-Chip Platforms: Requirements, Characteristics and Applications. *Chem. Soc. Rev.* **2010**, *39* (3), 1153–1182. <https://doi.org/10.1039/b820557b>.
- (12) Clime, L.; Daoud, - Jamal; Brassard, D.; Lidija Malic, -; Geissler, M.; Veres, - Teodor. Active Pumping and Control of Flows in Centrifugal Microfluidics. *Microfluid. Nanofluidics* **2019**, *23*, 29. <https://doi.org/10.1007/s10404-019-2198-x>.
- (13) Woolf, M.; Dignan, L.; Karas, S.; Lewis, H.; Hadley, K.; Nauman, A.; Gates-Hollingsworth, M.; AuCoin, D.; Green, H.; Geise, G.; et al. Characterization of a Centrifugal Microfluidic Orthogonal Flow Platform. *Micromachines* **2022**, *13* (3), 487. <https://doi.org/10.3390/MI13030487>.

- (14) Kainz, D. M.; Früh, S. M.; Hutzenlaub, T.; Zengerle, R.; Paust, N. Flow Control for Lateral Flow Strips with Centrifugal Microfluidics. *Lab Chip* **2019**, *19* (16), 2718–2727. <https://doi.org/10.1039/c9lc00308h>.
- (15) Maguire, I.; O'Kennedy, R.; Ducrée, J.; Ducrée, D.; Regan, F. A Review of Centrifugal Microfluidics in Environmental Monitoring. *Anal. Methods* **2018**, *10*, 1497–1515. <https://doi.org/10.1039/c8ay00361k>.
- (16) Al-Faqheri, W.; Hwai Gilbert Thio, T.; Ameen Qasaimeh, M.; Dietzel, A.; Madou, M.; Al-Halhouli, A. Particle/Cell Separation on Microfluidic Platforms Based on Centrifugation Effect: A Review. *Microfluid. Nanofluidics* **2017**, *21*, 102. <https://doi.org/10.1007/s10404-017-1933-4>.
- (17) Sataloff, R. T.; Johns, M. M.; Kost, K. M. *Immunoassays: Development, Applications, and Future Trends*; O'Kennedy, R., Murphy, C., Eds.; 2017.
- (18) Wild, D. Immunoassay for Beginners. *Immunoass. Handb.* **2013**, 7–10. <https://doi.org/10.1016/B978-0-08-097037-0.00002-6>.
- (19) Nistor, C.; Emnéus, J. Immunoassays: Potentials and Limitations. In *Biosensors and modern biospecific analytical techniques*; 2005; pp 375–399.
- (20) Dignan, L. M.; Woolf, M. S.; Ross, J. A.; Baehr, C.; Holstege, C. P.; Pravetoni, M.; Landers, J. P. A Membrane-Modulated Centrifugal Microdevice for Enzyme-Linked Immunosorbent Assay-Based Detection of Illicit and Misused Drugs. *Anal. Chem.* **2021**, *25*, 28. <https://doi.org/10.1021/acs.analchem.1c04102>.
- (21) Wong, R. C.; Tse, H. Y. *Lateral Flow Immunoassay*; Humana Press, 1981; Vol. 53.
- (22) O'Farrell, B. Evolution in Lateral Flow-Based Immunoassay Systems. In *Lateral Flow Immunoassay*; Humana Press, 2009; pp 1–33. https://doi.org/10.1007/978-1-59745-240-3_1.
- (23) Urusov, A. E.; Zherdev, A. V.; Dzantiev, B. B. Towards Lateral Flow Quantitative Assays: Detection Approaches. *Biosens. 2019, Vol. 9, Page 89* **2019**, *9* (3), 89. <https://doi.org/10.3390/BIOS9030089>.
- (24) Sun, S.; Feng, S.; Ji, C.; Shi, M.; He, X.; Xu, F.; Lu, T. J. Microstructural Effects on Permeability of Nitrocellulose Membranes for Biomedical Applications. *J. Memb. Sci.* **2020**, *595*, 117502. <https://doi.org/10.1016/J.MEMSCI.2019.117502>.
- (25) Hermanson, G. T. Antibody Modification and Conjugation. In *Bioconjugate Techniques*; 2013; pp 867–920. <https://doi.org/10.1016/b978-0-12-382239-0.00020-0>.
- (26) Shen, M.; Rusling, J. F.; Dixit, C. K. Site-Selective Orientated Immobilization of Antibodies and Conjugates for Immunodiagnosics Development. *Methods* **2016**, *116*, 95–111. <https://doi.org/10.1016/J.YMETH.2016.11.010>.
- (27) Yeh, Y.-C.; Creran, B.; Rotello, V. M. Gold Nanoparticles: Preparation, Properties, and Applications in Bionanotechnology. *Nanoscale* **2012**, *4* (6), 1871–1880. <https://doi.org/10.1039/c1nr11188d>.
- (28) Thobhani, S.; Attree, S.; Boyd, R.; Kumarswami, N.; Noble, J.; Szymanski, M.; Porter, R. A. Bioconjugation and Characterisation of Gold Colloid-

- Labelled Proteins. *J. Immunol. Methods* **2010**, *356* (1–2), 60–69. <https://doi.org/10.1016/J.JIM.2010.02.007>.
- (29) Jazayeri, M. H.; Amani, H.; Pourfatollah, A. A.; Pazoki-Toroudi, H.; Sedighimoghaddam, B. Various Methods of Gold Nanoparticles (GNPs) Conjugation to Antibodies. *Sens. Bio-Sensing Res.* **2016**, *9*, 17–22. <https://doi.org/10.1016/j.sbsr.2016.04.002>.
- (30) Oh, Y. K.; Joung, H. A.; Kim, S.; Kim, M. G. Vertical Flow Immunoassay (VFA) Biosensor for a Rapid One-Step Immunoassay. *Lab Chip* **2013**, *13* (5), 768–772. <https://doi.org/10.1039/c2lc41016h>.
- (31) Joung, H.-A.; Ballard, Z. S.; Ma, A.; Tseng, D. K.; Teshome, H.; Burakowski, S.; Garner, O. B.; Di, D.; Eg, C.; Ozcan, A. Paper-Based Multiplexed Vertical Flow Assay for Point-of-Care Testing. *Lab Chip* **2019**, *19*, 1027. <https://doi.org/10.1039/c9lc00011a>.
- (32) Devadhasan, J. P.; Gu, J.; Chen, P.; Smith, S.; Thomas, B.; Gates-Hollingsworth, M.; Hau, D.; Pandit, S.; AuCoin, D.; Zenhausern, F. Critical Comparison between Large and Mini Vertical Flow Immunoassay Platforms for *Yersinia Pestis* Detection. *Anal. Chem.* **2021**, *acs.analchem.0c05278*. <https://doi.org/10.1021/acs.analchem.0c05278>.
- (33) Clarke, O. J. R.; Goodall, B. L.; Hui, H. P.; Vats, N.; Brosseau, C. L. Development of a SERS-Based Rapid Vertical Flow Assay for Point-of-Care Diagnostics. *Anal. Chem.* **2017**, *89* (3), 1405–1410. <https://doi.org/10.1021/acs.analchem.6b04710>.
- (34) Thompson, B. L.; Ouyang, Y.; Duarte, G. R. M.; Carrilho, E.; Krauss, S.; Landers, J. P. Inexpensive, Rapid Prototyping of Microfluidic Devices Using Overhead Transparencies and a Laser Print, Cut, and Laminate Fabrication Method. *Nat. Protoc.* **2015**, *10* (6), 875–886. <https://doi.org/10.1038/nprot.2015.051>.
- (35) Breechin, N. J.; Fenech, M.; Houlihan, C. F. Ebola Virus Disease. *Br. Med. J.* **2014**, *349*. <https://doi.org/10.1136/bmj.g7348>.
- (36) Jansen, H. J.; Breeveld, F. J.; Stijnis, C.; Grobusch, M. P. Biological Warfare, Bioterrorism, and Biocrime. *Clin. Microbiol. Infect.* **2014**, *20* (6), 488–496. <https://doi.org/10.1111/1469-0691.12699>.
- (37) Chen, P.; Gates-Hollingsworth, M.; Pandit, S.; Park, A.; Montgomery, D.; AuCoin, D.; Gu, J.; Zenhausern, F. Paper-Based Vertical Flow Immunoassay (VFI) for Detection of Bio-Threat Pathogens. *Talanta* **2019**, *191* (August 2018), 81–88. <https://doi.org/10.1016/j.talanta.2018.08.043>.

CHAPTER 2 – Detection of infectious Diseases with a Centrifugally-Driven Microfluidic Orthogonal Flow Immunoassay

2.1 – Introduction

Biological warfare agents (BWAs) pose a great threat to global public health, national security, and the safety of deployed military personnel.^{1,2} *Yersinia pestis* (*Y. pestis*) is a naturally occurring bacterium which causes a disease colloquially referred to as ‘the plague’. From 2010 to 2015, the World Health Organization (WHO) reported 3,248 *Y. pestis* cases worldwide, resulting in 584 deaths.^{3,4} The bacterium has a rapid incubation period (3-7 days), resulting in an infectious disease that exhibits facile human-to-human transmissibility.⁵ Further, the Centers for Disease Control and Prevention (CDC) has identified the bacterium as a potentially potent agent of bioterrorism and biocrime.⁵

Deployable technology for the detection of BWAs was developed by the U.S. Army in the early 2000s; the Joint Biological Point Detection System (JBPDS) has the capacity to detect up to 10 different BWAs. While this system is effective, it is also costly (i.e., \$342,000/unit), cumbersome to transport, and requiring of highly trained personnel to perform the sample analysis.⁶⁻⁷ Cost-effective alternative methods exist, including enzyme-linked immunosorbent assays (ELISA) and polymerase chain reaction (PCR) assays, however, these approaches can be time-consuming, labor-intensive, and are preferably performed in a laboratory setting.⁷⁻⁸ Thus, there remains an insufficient development of practical, portable diagnostic methods for rapid detection and identification of BWAs in the field; as a result, there is an increased level of interest in the production of rapid diagnostic equipment.⁹

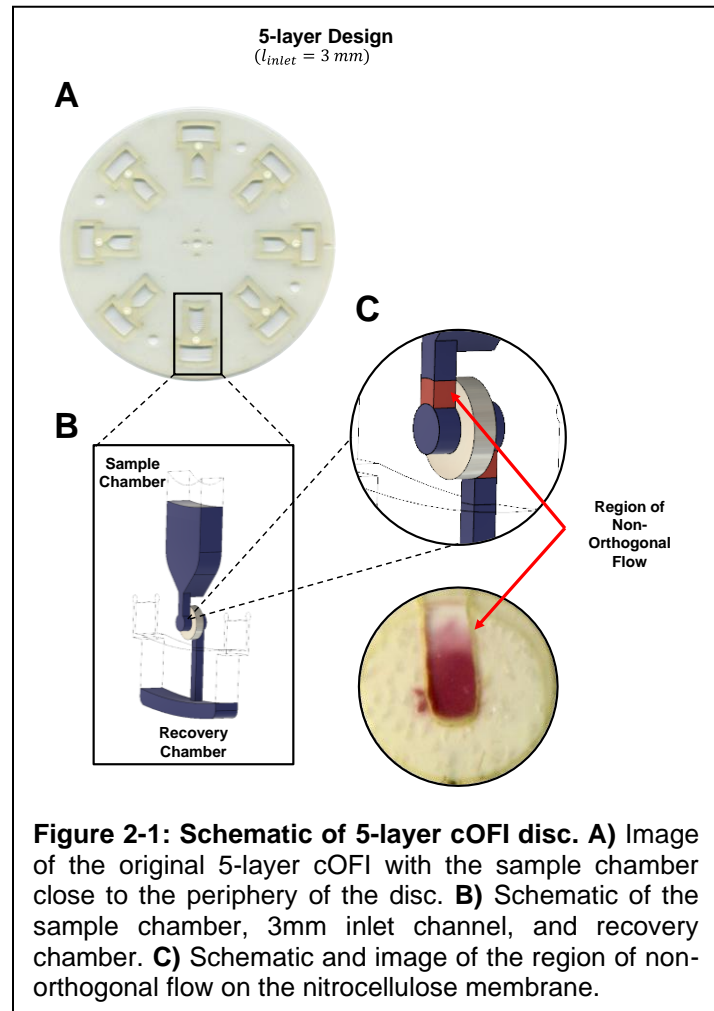
Alternatively, micro total analytical systems (μ TAS) have been increasingly

employed as point-of-need (PoN) solutions that can provide portable, rapid, and sensitive BWA detection.¹⁰⁻¹² In comparison to traditional analytical techniques, microfluidic devices require smaller sample input volumes, have shorter analysis time, reduce cost, and provide comparable or improved sensitivity when compared with conventional techniques.¹³ In particular, lateral flow immunoassays (LFIs) are paper-based PoN microfluidic devices that can provide rapid, cost-efficient detection of BWAs and biomarkers found in biofluids (i.e. blood, urine, saliva).⁸ However, reliance on capillary-driven fluid migration confers several key operational limitations: the inability to control flow rate and sample incubation time, and rapid saturation with fluid (i.e., once the absorbent pad is saturated, flow ceases).¹⁴ Oh *et al.* developed a gravity driven microfluidic device to overcome these limitations; a one-step vertical flow immunoassay (VFI) that mobilizes fluid vertically through a nitrocellulose (NC) membrane rather than laterally along the membrane surface.¹⁵ Using this approach, the group supplanted capillary action with gravity-driven flow, decreasing total analysis time 5-fold, from 10 minutes to 2 minutes.¹⁵ Chen *et al.* designed a syringe-based, pressure-driven microfluidic VFI device that has the ability to detect bio-threat agents.⁸ By flowing 15 mL of fluid through a NC membrane, they were able to increase sensitivity 10x from the conventional LFI method and detect down to 0.02 ng/mL of *Y. pestis* F1 antigen.⁸ Still, this VFI approach required extensive manual intervention, as it requires the user to disassemble the device, remove the NC membrane, and dry the membrane prior to visual examination. This pressure-driven system is effective for achieving extremely low sensitivities, but the mechanical aspects added time to the analysis

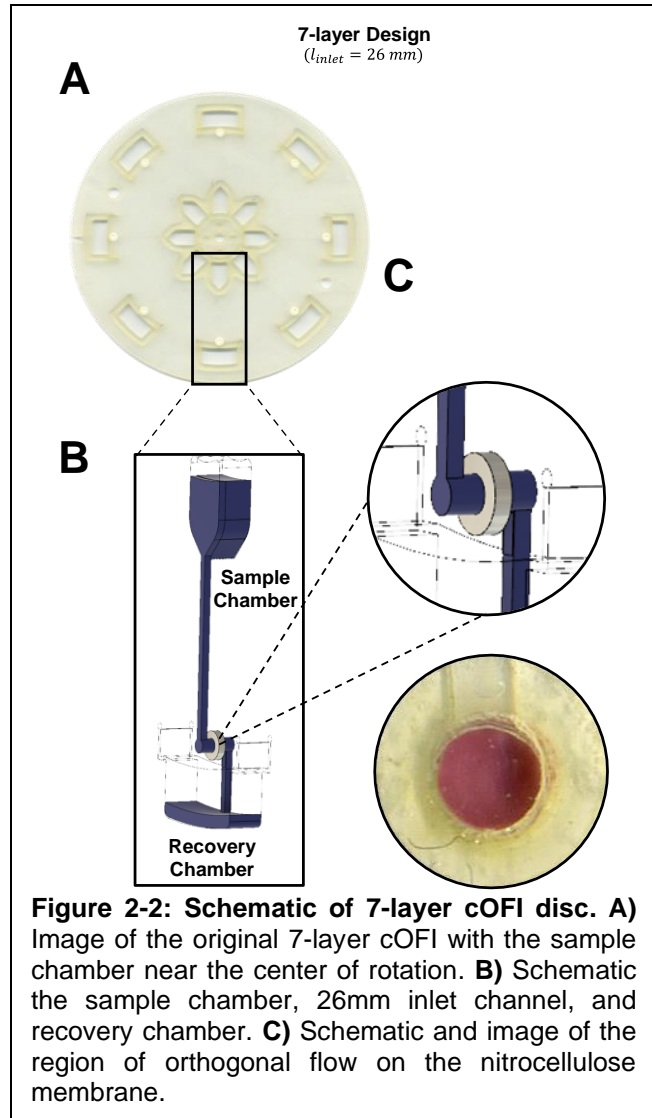
and created a potential BWA exposure risk for the user.

Woolf et al. developed a proof-of-concept centrifugally-driven microfluidic orthogonal flow immunoassay (OFI) to address these issues, with the goal of providing a rapid, cost-efficient colorimetric BWA detection system in a fully-enclosed, portable format (**Figure 2-1**).¹⁶ The microfluidic disc would provide a path to simple image analysis of the membranes without the need for device disassembly or user exposure and enables ease of assay automation. Despite these advantages, this OFI system utilized a 5-layer, print-cut-laminate (PCL) device with the sample chamber close to the periphery of the disc (**Figure 2-1A**),

which resulted in a nonlinear sample drain profile with distinct exponential decay character. Additionally, the membrane flow through port found in the original 5-layer disc design had a region of non-orthogonal flow that contributed to undesirable irregularities in color response, complicating downstream image analysis (**Fig. 2-1C**).



Here, we describe and characterize the next generation cOFI device, featuring a design that eliminates the exponential loss of hydraulic pressure during fluid flow and mitigates irregular color response as a result of non-orthogonal flow. The modified disc design incorporates several changes to impact fluidic control and streamline detection. First, the sample chamber was moved closer to the center of rotation (CoR) relative to the embedded membrane which provided a longer inlet channel (26 mm) compared to the original OFI disc (3mm) (**Figure 2-2**). Second, we modified the overall disc design to include 7 layers, rather than 5, which provided via ports that produced true orthogonal flow through the membrane, effectively eliminating any lateral flow (**Figure 2-2C**). Using *Y. Pestis* and Ebola virus-like particles as model organisms, we demonstrate the utility of these microfluidic changes by analytically characterizing fluid flow on a fully enclosed, portable, and cost-effective OFI device. In concert with our in-house engineered mechatronic system to drive fluid using rotational



forces with the developed microfluidic disc, we surmise that the modified OFI disc is capable of rapidly detecting and identifying various types of infectious diseases at the PoN.

2.2 Experimental Section

2.2.1 Fabrication of the Microfluidic OFI Disc

Microfluidic OFI devices were fabricated using the print-cut-laminate (PCL) method.¹⁷ Each device was comprised of seven polyethylene terephthalate (PET, 101.6 μm thickness, Film Source Inc., Maryland Heights, MO U.S.A.) sheets alternated with heat sensitive adhesive (HSA, 50.8 μm thickness, EL-7970-39, Adhesive Research Inc., Glen Rock, PA U.S.A) (**Figures 2-3, 2-4, and 2-5**). The disc architecture for each layer was designed using AutoCAD® 2019 (Autodesk Inc., San Rafael, CA, U.S.A.) and cut using a 50W CO₂ laser engraving system (VLS3.50, Universal Laser Systems®, Scottsdale, AZ, U.S.A.). Layers 1 and 7 acted as capping layers to fluidic layers 2 and 6, containing the microfluidic channels. Layers 3 and 5 operated as via layers containing circular orthogonal flow ports (2 mm diameter) to direct flow through layer 4, which contained 4 mm circular punches of the nitrocellulose (NC) membranes (0.2 μm pore size, Bio-Rad Laboratories Inc., Hercules, CA U.S.A.).¹⁶ To thermally bond the polymeric disc, layers were aligned and lamination bonded (185-195°C) (UltraLam 250B, Akiles Products Inc., Mira Loma, CA, U.S.A.) in three separate steps. First, disc layers 3-5 were aligned, NC membrane punches were inserted (layer 4), and bonded together when passed through an office laminator (2 passes). Second, layers 6 and 7 were aligned with and laminated to layers 3-5 (2 passes). Finally, layers 1

and 2 were aligned and laminated to the previously bonded layers (2 passes).

Horizontal lines were engraved (1 mm graduations) into the sample chamber PeT coverlets (**Figure 2-3A and B**) to monitor fluid drainage rates. Polymethyl methacrylate (PMMA, 1.5 mm McMaster-Carr, Elmhurst, IL U.S.A.) was used to increase sample and recovery chamber volumes (**Figure 2-3A and B**). PMMA accessory pieces and PeT coverlets were affixed to the OFI disc using pressure sensitive adhesive (PSA, 55.8 μm thickness, ARcare 7876, Adhesive Research Inc., Glen Rock, PA U.S.A). Completely assembled discs were placed in foil moisture barrier bags (Dri-shield™, Uline, Pleasant Prairie, WI, U.S.A.) with two 3-gram silica moisture absorbent packets (S-3904, Uline) overnight and pressed (15 lbs) to ensure PSA adhesion.

2.2.2 Flow Study – Buffer Solution Comparison

Phosphate buffered saline - tween (PBS-T, Thermo Fisher Scientific, Waltham, MA USA 02451) was prepared at 1X with pH = 7.5. Ebola chase buffer (1% 10G surfactant in Dulbecco's PBS at pH 7.2, Invitrogen, Waltham, MA USA 02451) was used without modification. *Y. pestis* chase buffer, or 50 mM carb- bicarbonate buffer at pH = 9.6, was prepared from sodium bicarbonate (Thermo Fischer Scientific, Waltham, MA USA 02451) and sodium carbonate (Thermo Fischer Scientific, Waltham, MA USA 02451). The respective buffer solution (200 μL) was pipetted into each sample chamber. The OFI disc was spun at a single rotational frequency ranging from 500-1500 RPM, with 250 RPM increments. The total drain time and drain intervals were measured using a highspeed stroboscopic video system (HSVS). The HSVS components included: MotionBLITZ EoSens® mini highspeed CMOS recording camera (Mikrotron-GmbH, Unterschleissheim,

Germany), MotionBLITZDirector software v.2 1.4.0.1, a TV Zoom lens G6x16 16-100 mm 1:1.9 1" macro (Mikrotron-GmbH), a Nova-Strobe PBL LED portable stroboscope (monarch Instrument, Amherst, NH, U.S.A.), and a custom-built mechatronic spin system that controls both the rotational spin frequency of the disc and the strobe rate. The mechatronic spin system was composed of a stepper motor (Sanmotion series, Sanyo denki, Moriguchi, Japan), a stepper motor driver (DRV8801, Texas Instruments, P.O. Box 655303, Dallas, Texas 75265), a photo-interrupting optical switch (TT Electronics/Optek Technology, Woking, U.K.), and an 8-core microcontroller (Propeller P8X32A-M44; Propeller Inc., Rockland, CA, U.S.A.).

2.2.3 Proof-of-Concept: Orthogonal Flow Immunocapture Study

In immunocapture studies, mouse whole molecule, IgG antibodies (m-IgG) (Jackson ImmunoResearch Laboratories Inc., West Grove, PA, U.S.A.) were manually spotted and immobilized onto 4 mm NC membrane punches prior to lamination (2.5 μ L, 5.5 mg/mL). The NC membrane was dried at 37°C for 1 hour in a convection oven (Binder 056FD – Convection Oven, P.O. Box 102, 78502 Tuttlingen, Germany). Negative controls and blanks consisted of NC membranes without immobilized m-IgG.

Two sample solutions of 4 nm colloidal gold nanoparticle conjugated goat anti-mouse IgG antibodies (AuNP; OD 2.0 at 520 nm, Jackson ImmunoResearch Laboratories, Inc., West Grove, PA, U.S.A.) were prepared with 1x PBS-T to make 1.82 nM and 0.91 nM AuNP solutions. Each AuNP solution (200 μ L) was pipetted into the sample chamber; three separate discs were prepared and spun at three different rotational frequencies (500 RPM, 1000 RPM, and 1500 RPM). The

negative control was a solution consisting of 1x PBS-T with AuNP.

2.2.4 Detection of *Y. Pestis* on Centrifugal Microfluidic Disc via Orthogonal Flow

Y. pestis reagents were prepared in the Diagnostics Discovery Laboratory (School of Medicine, University of Nevada, Reno, NV, U.S.A.) as per the protocol described by Hau et al.¹⁸ The OFI disc was assembled as described in Section 2.1 with a minor modification to the disc design and antibody blotting steps. In layer 7, a 2 mm access port was cut-out to allow for the NC membranes to be blotted, post-lamination, with 2.5 μ L of Yp11C7 0416 IgG1 (Yp-mAb) (YpF1 specific mAb, 5.85 mg/mL), then the discs were incubated at 37°C for 1 hour in a convection oven (Binder 056FD – Convection Oven, P.O. Box 102, 78502 Tuttlingen, Germany). Next, each membrane was blocked by pipetting 2.5 μ L of blocking buffer solution (0.25% PBS-Tween, 0.1% Bovine Serum Albumin) through the 2 mm access port in layer 7 and placed in the oven at 37°C for 1 hour. The access port, exposing NC membranes, was sealed by attaching a PET coverlet with PSA. Finally, the discs were placed in foil moisture barrier bags (Dri-shield™, Uline, Pleasant Prairie, WI, U.S.A.) with two 3-gram silica moisture absorbent packets (S-3904, Uline) for a minimum of 24 hours.

A pre-wash step (40 μ L) was performed using *Y. pestis* chase buffer pipetted into the sample chamber (1000 RPM, until the pre-wash solution was drained). Sample solutions (180 μ L) of the *Y. pestis* F1 antigen were prepared at 10-0.001 μ g/mL in chase buffer. Aliquots of each antigen dilution were mixed with 5 μ L of Yp3F2 gold conjugate (Yp-AuNP, OD 10.1 at 520 nm), and incubated in-tube at room temperature for 20 min. Negative controls consisted of 180 μ L of

chase buffer and 5 μ L of Yp-AuNP; blank controls consisted entirely of 185 μ L chase buffer. Sample solutions were loaded into the sample chambers and centrifugally pumped through the membrane at 1000 RPM until the sample chambers were completely drained (20 minutes). Finally, a post-wash step (40 μ L chase buffer, 1000 rpm, 100 s) was completed to remove any excess sample solution from the membrane.

2.2.5 Detection of Ebola Virus-Like Particle on Centrifugal Microfluidic Disc via Orthogonal Flow

Ebola reagents were prepared in the Diagnostics Discovery Laboratory (School of Medicine, University of Nevada, Reno, NV, U.S.A.) as per the protocol described by DeMers et al.¹⁹ The OFI disc was assembled with the same modification to the disc design and antibody blotting steps as described in Section 2.4. In layer 7, the NC membranes to be blotted, post-lamination, with 2.5 μ L of 1HK7 IgG2b (Eb-mAb) (Ebola virus-like particle specific mAb, 10.2 mg/mL), then the discs were incubated at 37°C for 1 hour in a convection oven (Binder 056FD – Convection Oven, P.O. Box 102, 78502 Tuttlingen, Germany). Next, each membrane was blocked by pipetting 2.5 μ L of blocking buffer solution (0.25% PBS-Tween, 0.1% Bovine Serum Albumin) through the 2 mm access port in layer 7 and placed in the oven at 37°C for 1 hour. The access port, exposing NC membranes, was sealed by attaching a PET coverlet with PSA. Finally, the discs were placed in foil moisture barrier bags (Dri-shield™, Uline, Pleasant Prairie, WI, U.S.A.) with two 3-gram silica moisture absorbent packets (S-3904, Uline) for a minimum of 24 hours.

A pre-wash step (40 μ L) was performed using Ebola chase buffer pipetted

into the sample chamber (1000 RPM, until the pre-wash solution was drained). Sample solutions (180 μ L) of the Ebola virus-like particles (EBOV) were prepared at 10-0.0001 μ g/mL in chase buffer. Aliquots of each antigen dilution were mixed with 5 μ L of 1HK11 gold conjugate (Eb-AuNP, OD 10.5 at 520 nm), and incubated in-tube at room temperature for 20 min. Negative controls consisted of 180 μ L of chase buffer and 5 μ L of Eb-AuNP; blank controls consisted entirely of 185 μ L chase buffer. Sample solutions were loaded into the sample chambers and centrifugally pumped through the membrane at 1000 RPM until the sample chambers were completely drained (20 minutes). Finally, a post-wash step (40 μ L chase buffer, 1000 rpm, 100 s) was completed to remove any excess sample solution from the membrane.

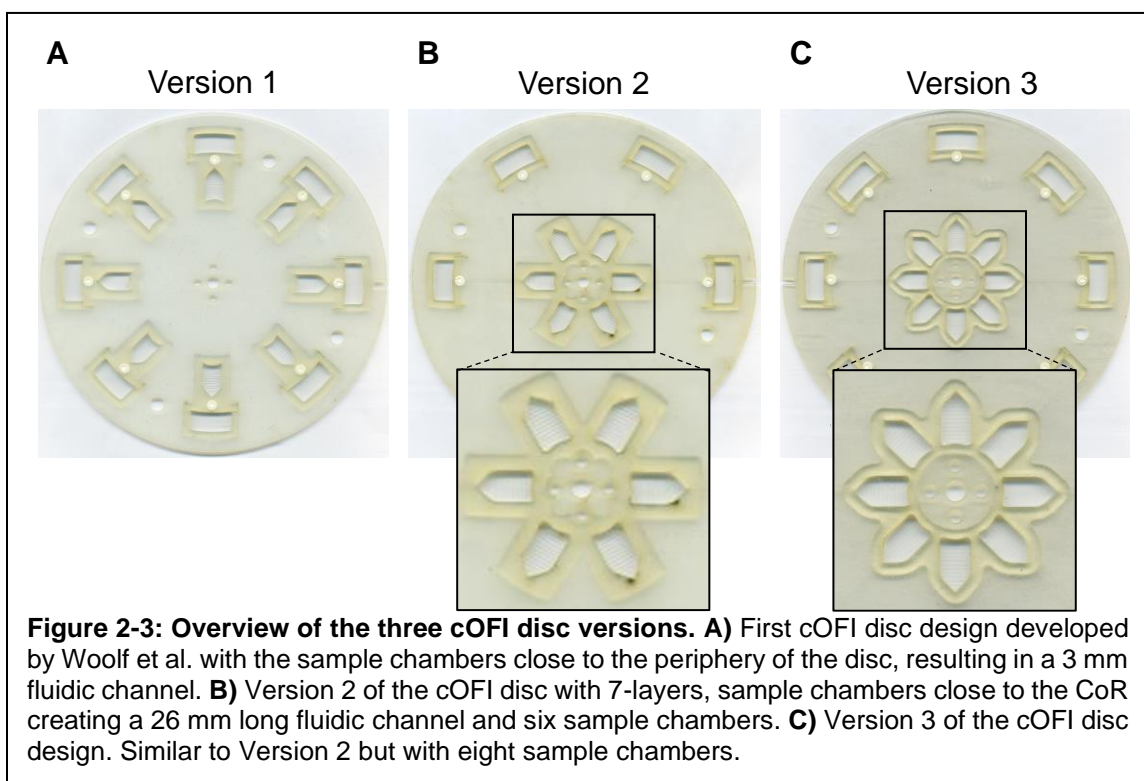
2.2.6 Image processing and Data Analysis

Each OFI disc was digitally imaged (1200 dpi, TIF format), before and after each assay, using a Perfection V100 desktop scanner (Epson, Suwa, Nagano, Japan). Circular regions of interest (ROIs, 50-pixel diameter) from the NC membranes were selected using the Microsoft Windows 64-bit Fiji distribution of ImageJ v.1.52p (<https://imagej.net/Fiji/Downloads>), as described in Woolf et al.²⁰ The ROI for each NC membrane was converted in ImageJ to weighted 8-bit grayscale and subsequently analyzed to measure mean grayscale value (GV). Fiji ImageJ measures the GV from 0-255, where 0 is completely black and 255 is entirely white.

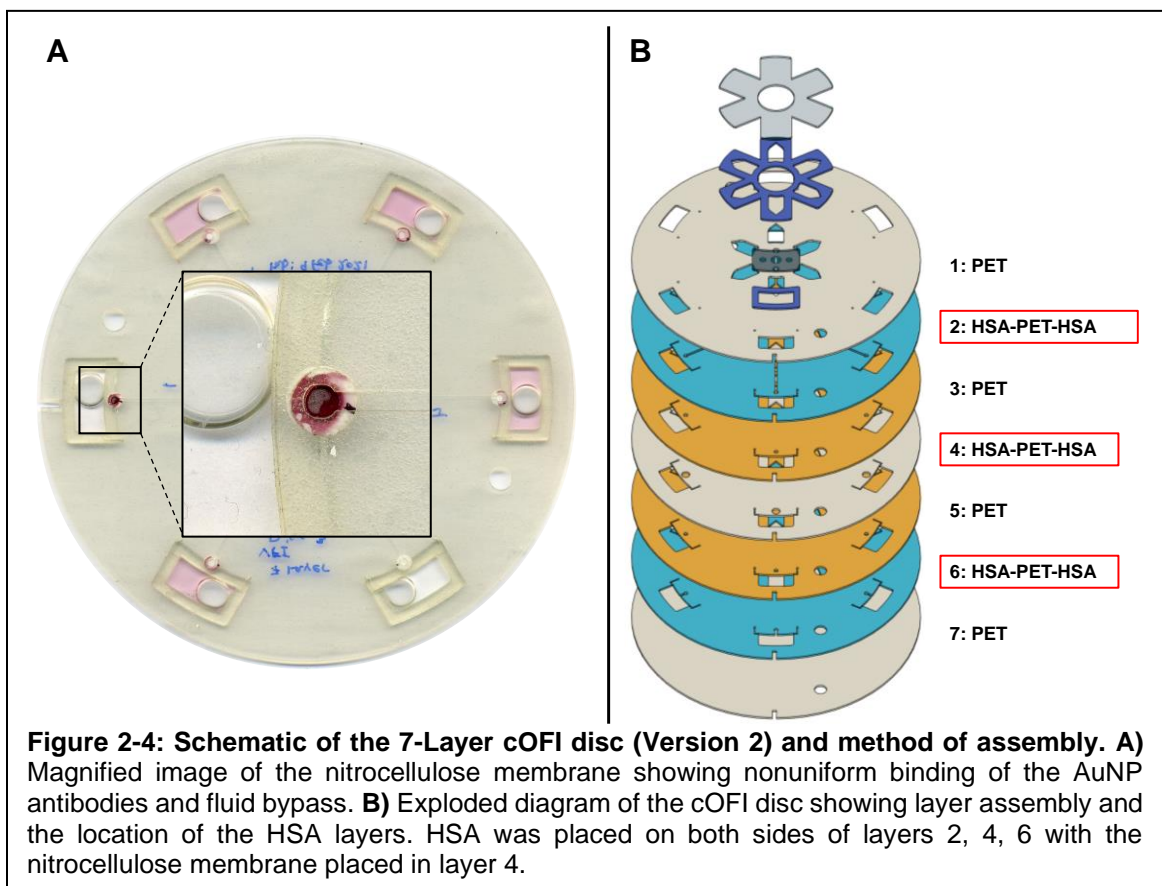
2.3 Results and Discussion

2.3.1 Fabrication of the Microfluidic OFI Disc

The fabrication of the cOFI disc went through three iterations (**Figure 2-3**). cOFI version 1 was the original design developed by Woolf et al with a the 3 mm fluidic channel to the membrane (**Figure 2-3A**).¹⁶ Version 2 moved the sample chambers closer to the CoR, as stated previously, to create a 26 mm fluidic channel and added two additional PET layers to eliminate regions of non-orthogonal flow (**Figure 2B**). Additionally, the sample number of sample chambers were decreased from eight to six due to concerns that there would not be enough PSA to bond the PMMA sample chamber to the disc to prevent leaking between each chamber. Version 3 went back to the original number of sample chambers, eight, to optimize the number of target analytes on-disc while keeping the 7-layer design (**Figure 2-3C**).

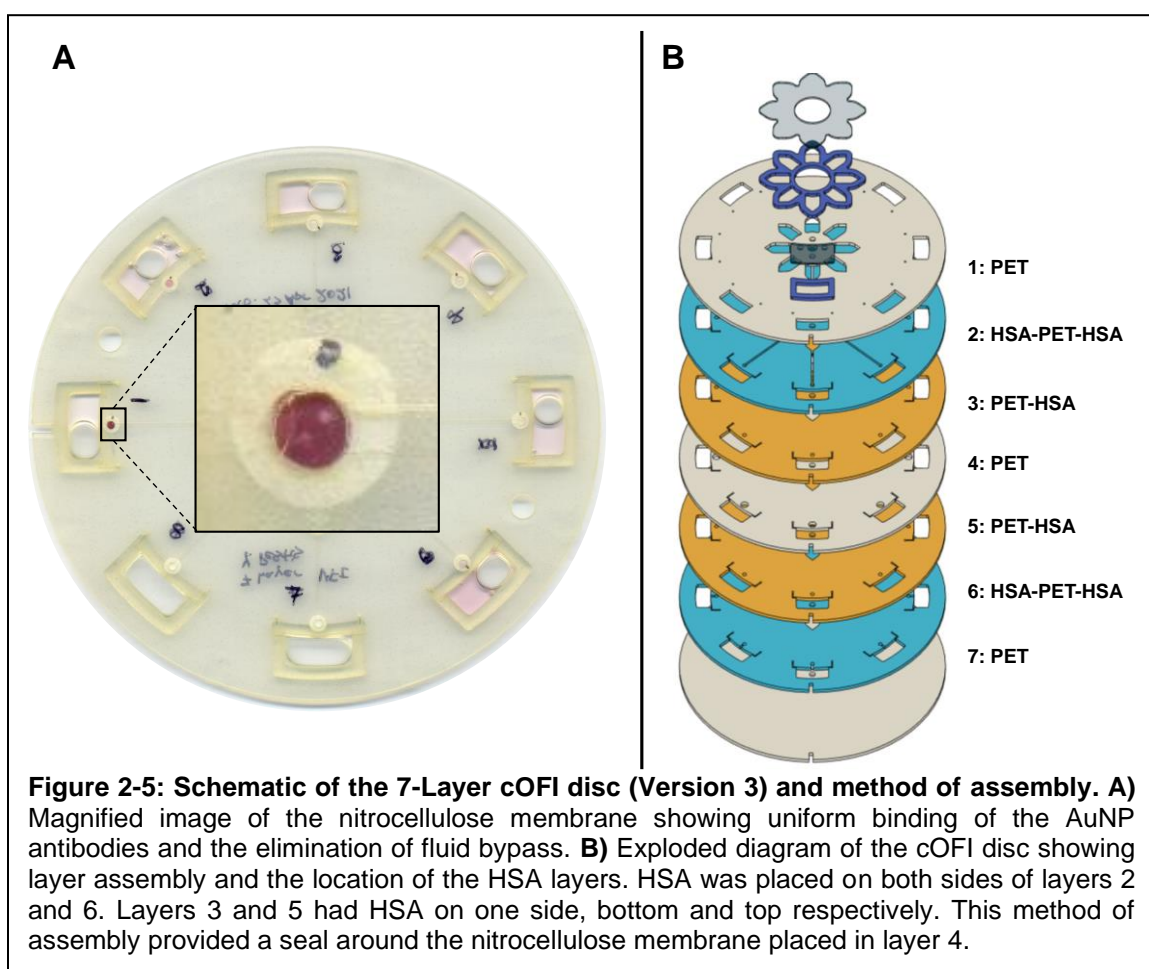


In order to eliminate the regions of non-orthogonal flow, cOFI version 2 contains two additional PET layers to act as via layers. The addition of two PET layers required careful consideration of the placement of the HSA. **Figure 2-4** shows the initial placement of the HSA on both sides (top and bottom) of PET layers 2, 4, and 6. **Figure 2-4A** shows the initial placement of the HSA on both sides (top and bottom) of PET layers 2, 4, and 6. By placing the HSA in layer 4, the PET layers did not provide a proper seal around the membrane, as shown in **Figure 2-4A**, resulting in non-uniform distribution of the AuNP antibodies to regions outside the via ports (layers 3 and 5) which is an example of fluid bypass around the membrane. Fluid bypass can produce fluctuations in flow rate due to the change in resistance either through or around the membrane. The main concern with fluid bypass is the potential for



loss in signal due to the target analyte not interacting or binding to the capture antibodies on the membrane.

In order to eliminate fluid bypass, a seal needed to be formed around the membrane in layer 4; layers 3 and 5 were cut to have a single HSA layer on the bottom and top, respectively (**Figure 2-5**). Note, the HSA on layers 2 and 6 remained unchanged. The single-sided HSA were able to seal the membrane which eliminated fluid bypass and resulted in uniform binding through the via ports in layers 3 and 5 (**Figure 2-5A**). As described in Section 2.1, proper bonding of the PET layers was ensured by laminating the disc in three separate stages. Layers



3-5 were laminated first, then layers 6-7 were laminated to 3-5, and finally layers 1-2 were laminated to 3-7.

2.3.2 Flow Study – Buffer Solution Comparison

This iteration of the cOFI disc features a long inlet channel design to permit a constant flow rate that could be maintained throughout the assay's duration, regardless of sample fluid type (e.g., urine, saliva, blood serum).²¹ The data presented here shows that the total drainage time decreased as the rotational frequency increased. The average fluid flow rate (U) through a microfluidic channel can be defined by **Equation 1**: hydraulic diameter of the channel (D_h), fluid density (ρ), angular velocity (ω), change in the difference between the top and bottom of the fluidic plug (Δr), the average distance the fluid plug is from the CoR (\bar{r}), the fluid viscosity (μ), and length of the channel (L).^{16,22,23}

$$(1) \quad U = \frac{D_h^2 \rho \omega^2 \Delta r \bar{r}}{32 \mu L}$$

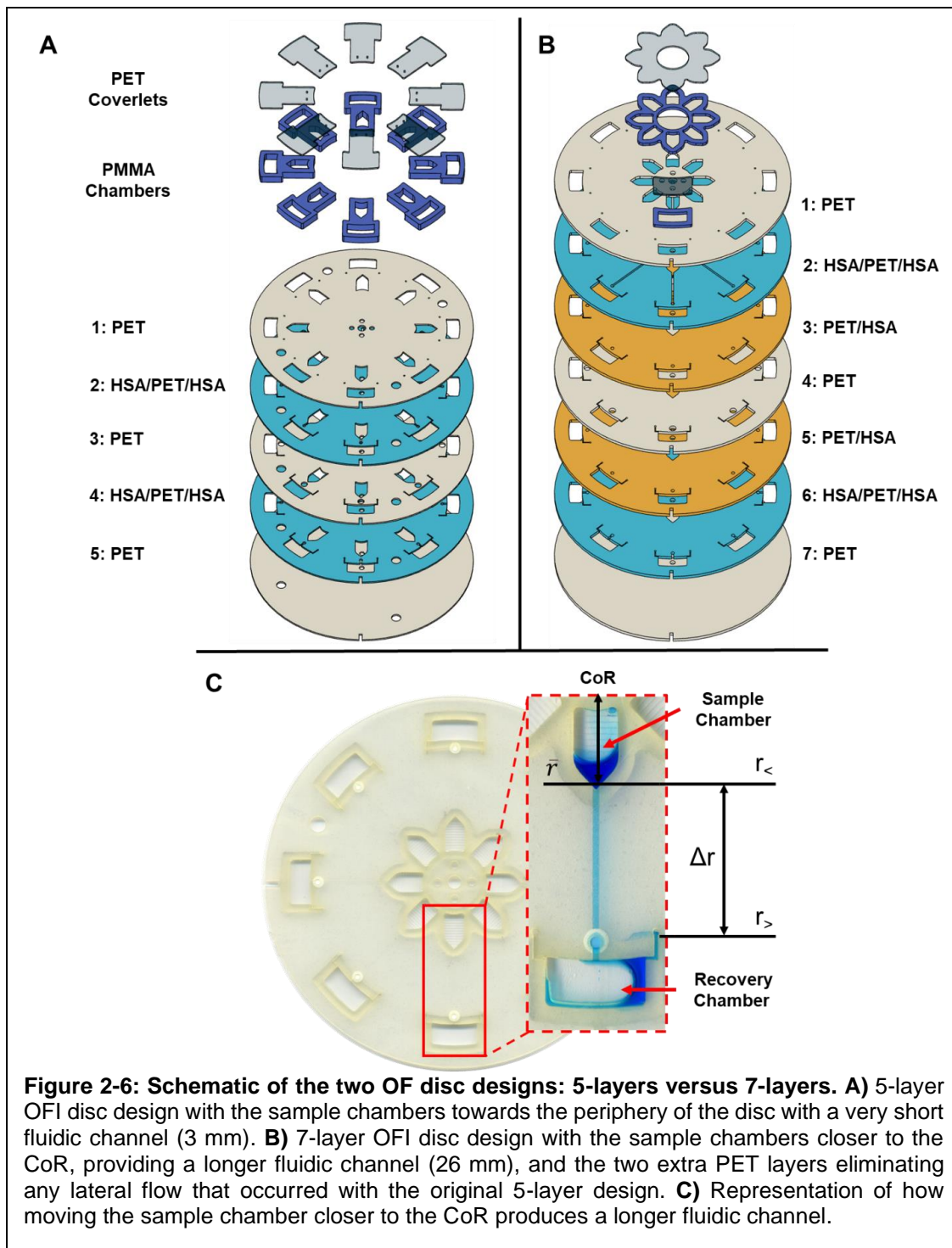
The microfluidic channel on the cOFI disc is 26 mm long, producing a 26 mm fluidic plug; as a result, both Δr and \bar{r} remain unchanged as the fluid volume in the sample chamber decreases (**Figure 2-6**). Additionally, both the channel geometries (D_h and L) and fluid properties (ρ and μ) play an important role in the average flow rate through the cOFI disc's channels, but these parameters also remain unchanged. We can then assume that flow rate is directly proportional to Δr , \bar{r} , and L (**Equation 2**).

$$(2) \quad \Delta U \propto \frac{\Delta r \bar{r}}{L}$$

When comparing the fractional change in flow rates between a short fluidic plug ($L = 3$ mm) and long fluidic plug ($L = 26$ mm), there is a smaller fractional change over time with the long fluidic plug; therefore, producing a more constant flow rate over time and throughout the duration of the assay. Ultimately, the long fluidic channel isolates angular velocity as the sole parameter that can be changed allowing for precise fluid control on the cOFI disc.

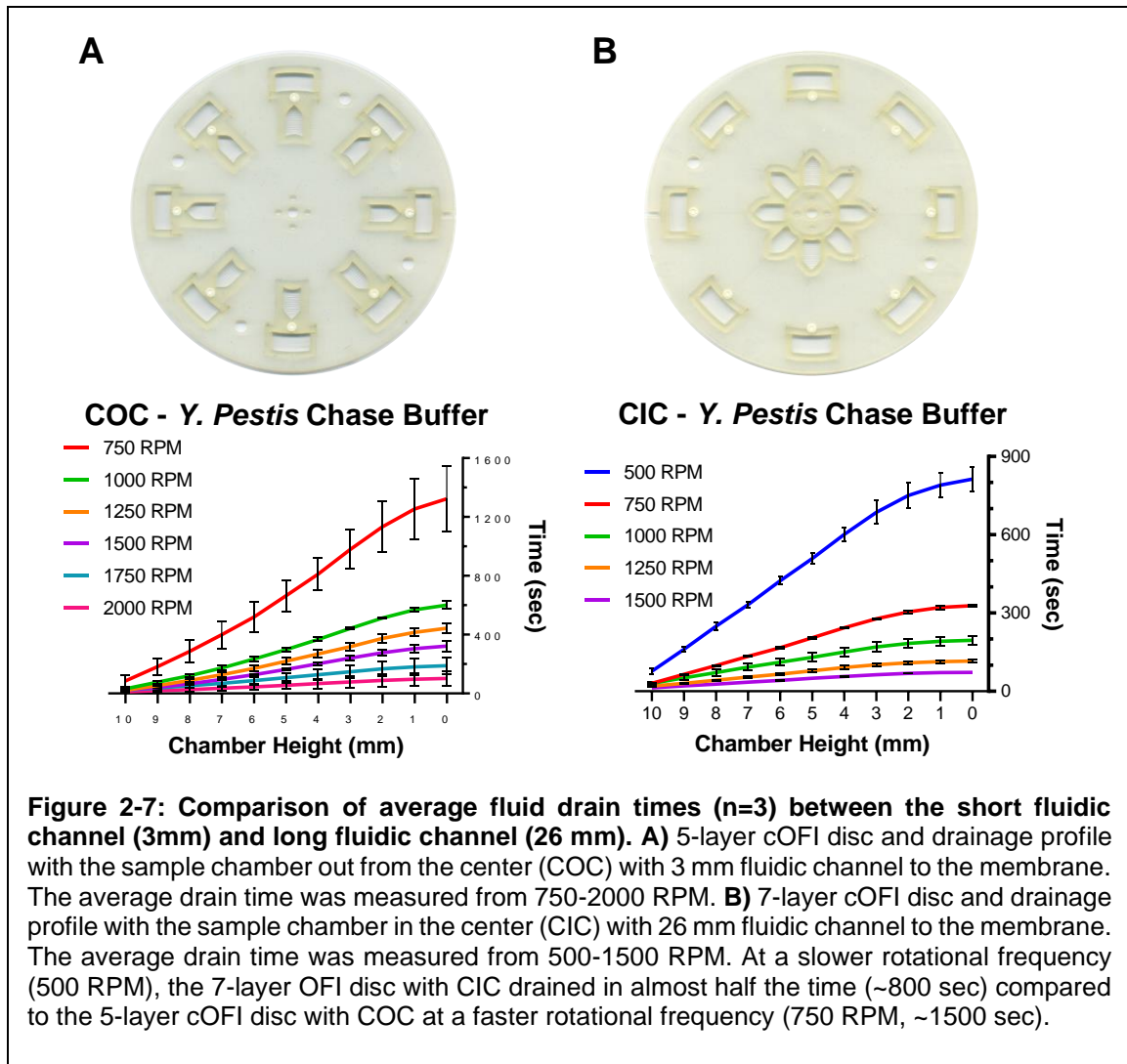
Previously published research by Woolf et al. describes a 5-layer OFI design (**Figure 2-6A**) with the sample chamber furthest away from the CoR with a short microfluidic channel (3 mm). This design resulted in an exponential decay of the fluid column height (L) in relation to the elapsed time; simply, as the fluid drained from the sample chamber, the hydraulic pressure driving fluid flow decreased, resulting in a slower flow rate, longer drainage time, and longer assay time.¹⁶ Furthermore, **Equation 3** describes how the volumetric flow rate (Q) is proportional to the volume of the fluid (V) per unit of time (t); therefore, Q is proportional to the mean fluid velocity (\bar{v}) and cross sectional area (A) of the fluidic channel.²⁴

$$(3) \quad Q = \frac{V}{t} = \frac{A(\text{Distance})}{t} = \bar{v}A$$

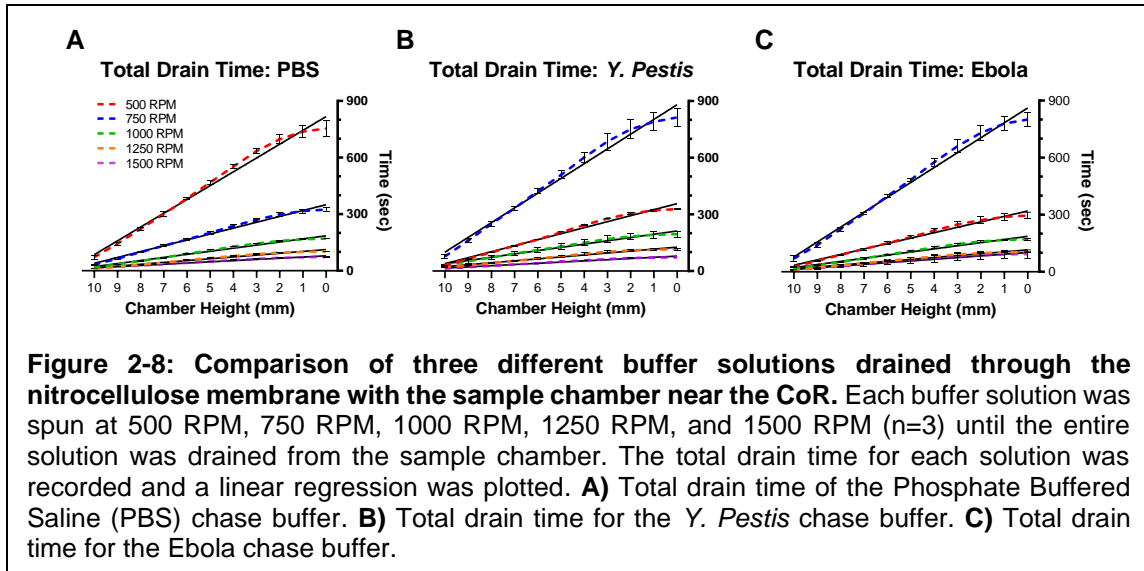


We hypothesized that a longer inlet channel (26 mm), from the sample chamber to the NC membrane, could maintain more stable hydraulic pressure as the sample fluid volume decreased. To implement this architectural change, the

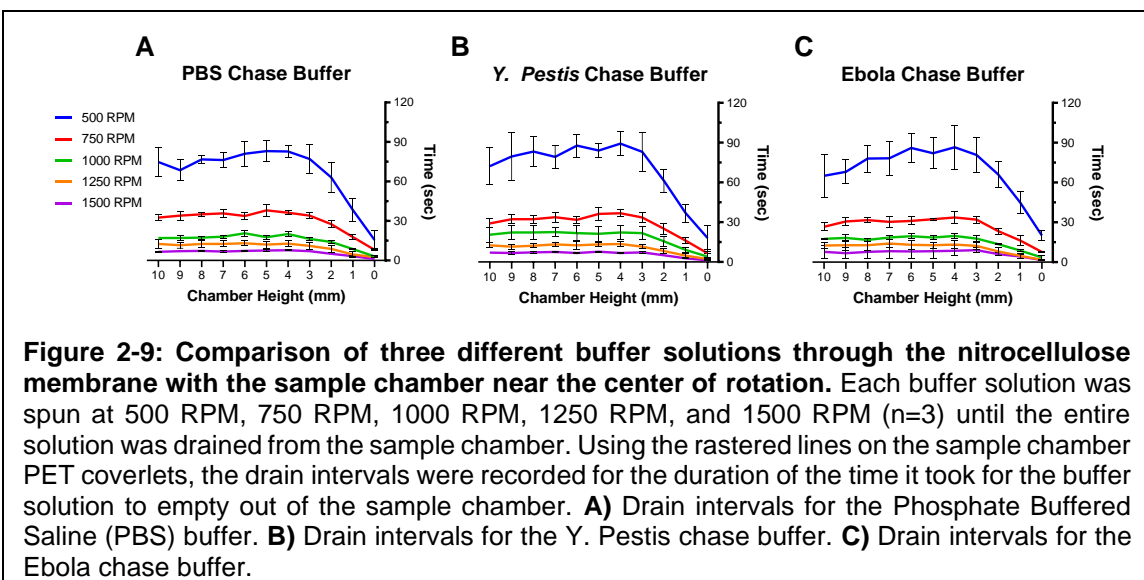
sample chamber was positioned closer to the CoR, while the embedded membrane and OF port remained closer to the periphery (**Figure 2-6C**). The longer inlet channel creates a 2.64 μL fluidic column, designed to maintain the hydraulic pressure until the fluidic column is drained. It is important to note that the 2.64 μL of fluid present in the inlet channel is insignificant when considering the total sample volume, as it makes up less than 1% of the total sample being pumped through the membrane. With the length of the channel (L) remaining constant (see **Equation 1**), the rotational frequency (angular velocity (ω)) variable can be controlled. This provides the user with the ability to control disc fluid velocity and total assay time by simply altering the rotational frequency. As anticipated, elongation of the inlet channel from 3 mm (**Figure 2-7A**) to 26 mm (**Figure 2-7B**) upstream of the membrane resulted in a linear drainage profile when the column height is plotted against the elapsed time (**Figure 2-7**). Stated another way, as the fluid volume drains from the sample chamber, there is little to no change in the flow rate throughout the duration of the assay as shown in **Figure 2-7**. When the two average drain times were compared at the same rotational frequency, the longer fluidic channel resulted in fivefold reduction in drain time.



Previous research has described how fiber morphology in NC membranes (i.e., swelling or de-swelling of the pores) can be changed by the salt concentration and ionic strength of a solution; therefore, effecting the sample flow rate through NC membranes.^{16,25-27} Hence, we evaluated the overall drain time (**Figure 2-8**) and the drain intervals (**Figure 2-9**) for three different types of buffer solutions – PBS-T buffer, *Y. pestis* chase buffer, and Ebola chase buffer – at five different rotational frequencies (500-1500 RPM, 250 RPM intervals). Overall, there was a nominal difference observed between the total drain times of the buffers at the five rotational frequencies (**Figure 2-8**). All correlation coefficients for these data were



> 0.98, indicating that a strong, linear relationship exists between total elapsed time and sample chamber filling height. Fitted regression models and correlation coefficients are reported in **Table 2-1**. Simply put, as the fluid volume decreased in the sample chamber, the hydraulic pressure and flow rate remained constant. A two-way ANOVA ($\alpha = 0.05$) was performed to compare the effect that rotational frequency and buffer solution type have on fluid drainage time. Analysis revealed there was no statistically significant interaction between the effects of rotational frequency and buffer solution ($F(8, 30) = 2.167, p = 0.059$). However, rotational



PBS Buffer				
500 RPM	750 RPM	1000 RPM	1250 RPM	1500 RPM
$Y = -73X + 817$	$Y = -31X + 350$	$Y = -16X + 185$	$Y = -9.7X + 112$	$Y = -6.4X + 79$
$R^2 = 0.99$	$R^2 = 0.99$	$R^2 = 0.98$	$R^2 = 0.98$	$R^2 = 0.98$
Y. Pestis Buffer				
500 RPM	750 RPM	1000 RPM	1250 RPM	1500 RPM
$Y = -78X + 881$	$Y = -32X + 357$	$Y = -17X + 212$	$Y = -10X + 126$	$Y = -6.3X + 79$
$R^2 = 0.99$	$R^2 = 0.99$	$R^2 = 0.98$	$R^2 = 0.98$	$R^2 = 0.98$
Ebola Buffer				
500 RPM	750 RPM	1000 RPM	1250 RPM	1500 RPM
$Y = -78X + 861$	$Y = -29X + 320$	$Y = -16X + 186$	$Y = -9.9X + 115$	$Y = -8.9X + 101$
$R^2 = 0.99$	$R^2 = 0.99$	$R^2 = 0.98$	$R^2 = 0.98$	$R^2 = 0.98$

Table 2-1: The linear regression equations for each buffer at each rotational frequency showing the drain times are linear as the fluid volume decreases in the sample chamber and the flow rates remain constant.

frequency did have a significant effect on fluid drainage time ($p < 0.0001$). Additionally, a statistically significant effect was observed between the buffer solution and fluid drainage time, ($p = 0.0118$). With regard to which parameter provided the greatest percentage of total variation on the fluid drainage time, rotational frequency exhibited the largest total variation percentage (98.9%). Basically, the change in drain time was greatly influenced by the rotational frequency and not the fluid type. Using a Tukey's multiple comparisons test, it was determined there was no significant difference between 1250 RPM vs 1500 RPM with a mean difference in drain time of 28.22 sec (**Table 2-2**), while comparing the slower rotational frequencies resulted in a significant difference in mean drains times. Overall, for all three buffer solutions, the salt content and ionic strength did not present an adverse effect functionally on the flow rate throughout the drainage cycle as previously hypothesized in Woolf et al.¹⁶

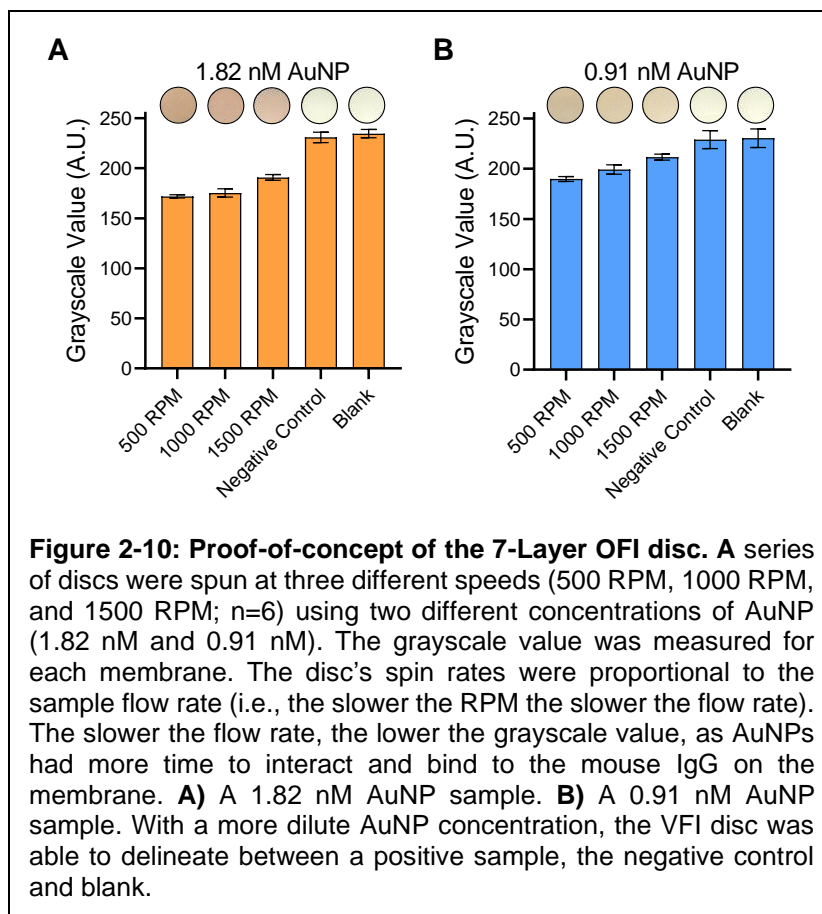
Rotational Frequency (RPM)	Mean Difference	95.00% CI of Diff.	Significant	P-Value
500 vs. 750	473	436.5 to 509.5	Yes	<0.0001
500 vs. 1000	598.6	562.0 to 635.1	Yes	<0.0001
500 vs. 1250	681.7	645.1 to 718.2	Yes	<0.0001
500 vs. 1500	709.9	673.3 to 746.4	Yes	<0.0001
750 vs. 1000	125.6	89.01 to 162.1	Yes	<0.0001
750 vs. 1250	208.7	172.1 to 245.2	Yes	<0.0001
750 vs. 1500	236.9	200.3 to 273.4	Yes	<0.0001
1000 vs. 1250	83.11	46.57 to 119.7	Yes	<0.0001
1000 vs. 1500	111.3	74.79 to 147.9	Yes	<0.0001
1250 vs. 1500	28.22	-8.321 to 64.77	No	0.1976

Table 2-2: 2-way ANOVA Tukey's Multiple Comparisons Test: Comparing the statistical differences between the rotational frequencies.

2.3.2 Proof-of-Concept: Orthogonal Flow Immunocapture Study

Having characterized flow behavior through the NC membrane, we explored the effect that rotational frequency has on the ability to form the AuNP-m-IgG complex and, ultimately, endow the assay with ample signal intensity for detection. Previously, Devadhasan et al. reported successful binding with flow rates from 0.1 to 1 mL/min using a syringe pump; however, we were concerned that the flow rate through the cOFI would be too fast with centrifugal pumping to permit effective binding of the AuNP to the m-IgG.²⁵ To evaluate this, two sample solutions varying in AuNP concentration - 1.82 nM and 0.91 nM - were prepared using PBS-T buffer. It is important to note that the greyscale values (GVs) reported in **Figure 2-10** are inversely related to the amount of AuNPs bound to the m-IgG blotted membranes, i.e., the more AuNPs bound to the membrane, the lower the GV. The 1.82 nM AuNP samples were spun at the three rotational frequencies: 500 RPM (GV = 172 ± 2), 1000 RPM (GV = 175 ± 4), and 1500 RPM (GV = 191 ± 3). This resulted in positive responses that were readily distinguishable from the negative control (GV = 231 ± 5) and blank (GV = 235 ± 4) samples (**Figure 2-10A**).

Additionally, the 0.91 nM AuNP samples were spun at the same rotational frequencies: 500 RPM (GV = 190 ± 2), 1000 RPM (GV = 199 ± 5), 1500 RPM (GV = 212 ± 3). This also resulted in positive responses that were easily distinguishable from



the negative control (GV = 229 ± 9) and blank (GV = 230 ± 9) samples (**Figure 2-10B**). An unpaired t-test to compare the means between the 1.82 nM AuNP GVs for 500 RPM and 1500 RPM were statistically different ($\alpha = 0.05$, $p < 0.0001$); the 0.91 nM AuNP GVs for 500 RPM and 1500 RPM were also statistically different ($\alpha = 0.05$, $p < 0.0001$). Therefore, the data shows spinning at a slower rotational frequency (i.e., 500 RPM) resulted in a lower GV, and thus was more valuable in discerning a positive compared to the blank, compared to faster rotational frequencies (i.e., 1500 RPM).

The sensitivity of the OFI and binding of the AuNP (analyte) to the m-IgG is dependent on three factors: flow rate, diffusion, and membrane pore size. The

small pore size, 0.2 μm , used on this device allows for a short diffusion distance for the analyte to interact with the m-IgG i.e., a greater binding interaction time for the AuNP to bind to the m-IgG, even at high flow rates. These three factors can be better explained by the *Péclet* number (Pe) which describes the relationship between the flow rate (U) through the NC membrane (L_s) and the diffusion rate of the analyte (D) to the wall of the pores (pore radius, d^2) in the NC membrane **(Equation 4)**.^{28–30}

$$(4) \quad Pe = \frac{\text{convection rate}}{\text{diffusion rate}} = \frac{U/L_s}{D/d^2}$$

We consider the OFI device to be a non-diffusion-limited immunoassay which is defined by a $Pe < 1$ and an antigen capture efficiency $>90\%$.²⁸ Referring back to **Figure 2-8**, a higher rotational frequency resulted in a faster flow rate through the membrane and this correlates with the data we see in the antibody binding study **(Figure 2-10A & B)**. The faster the flow rate, the weaker the signal present on the NC membrane as a result of limited interaction time between the analyte and the capture antibody located on the pore wall; therefore, it can be confirmed that a higher flow rate directly effects the sensitivity of the device. Our reported cOFI device reaches average maximum and minimum flow rates of 0.17 mL/min and 0.016 mL/min with speeds of 1500 RPM and 500 RPM, respectively; flow rates equal to or slower than those reported by Devadhasan et al. using pneumatically-driven flow.²⁵

2.3.3 Detection of *Y. Pestis* F1 antigen

Having demonstrated fluidic control through the OFI device and proof of on-disc immunocapture, we next sought to demonstrate how our disc could be applied in the real world to detect the F1 antigen expressed by *Y. pestis*. We begin this work by diluting the *Y. pestis* F1 antigen into aqueous sample solutions from 10-0.001 $\mu\text{g/mL}$ for on disc detection. **Figure 2-11** shows the resultant mean GV (n=3)

for each of the sample dilutions flowed through the sample architecture. It is

important to note, that unlike the results presented in section 3.2, this experimental setup comprised a full sandwich-type immunoassay (**Figure 2-12**). Across the three highest concentrations (10 to 0.1 $\mu\text{g/mL}$) the GV became more intense as the F1 antigen concentration was decreased (GV = 140 ± 15 , 43 ± 18 , and 26 ± 1 , respectively). At 10 $\mu\text{g/mL}$, a GV of 142 was 81% less intense than that observed at 0.1 $\mu\text{g/mL}$ (GV = 26 ± 1).

We attribute this loss in signal at the highest concentrations to the “hook effect”.^{15,31} In these instances, the F1 antigen is so abundant that both the Yp-AuNP and the Yp-mAb binding

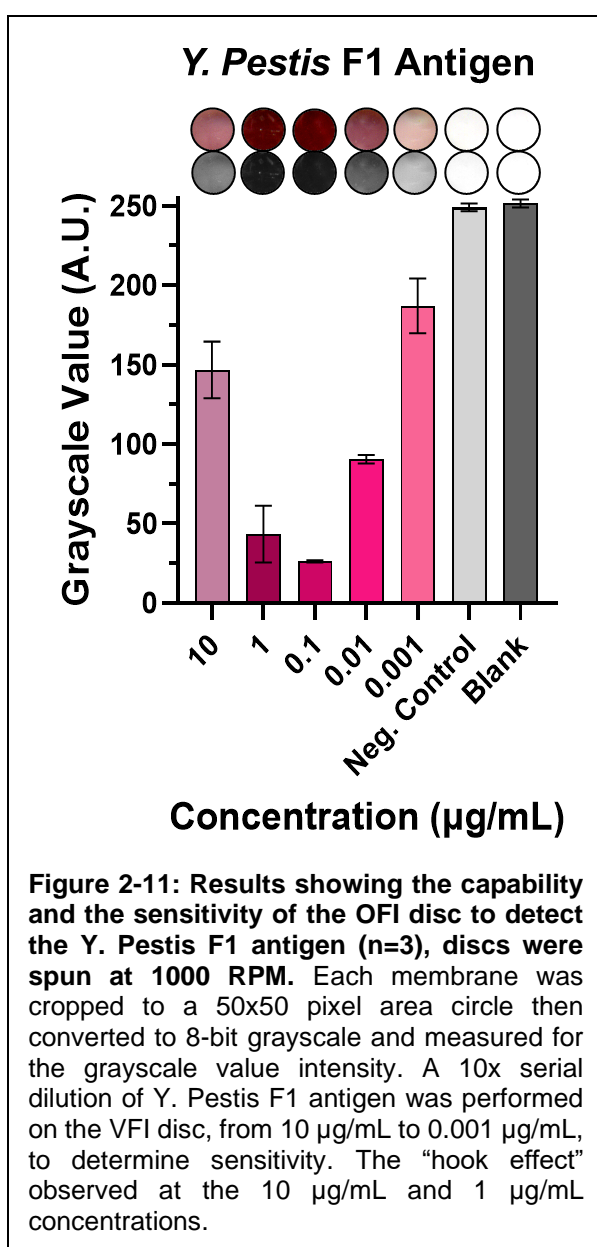
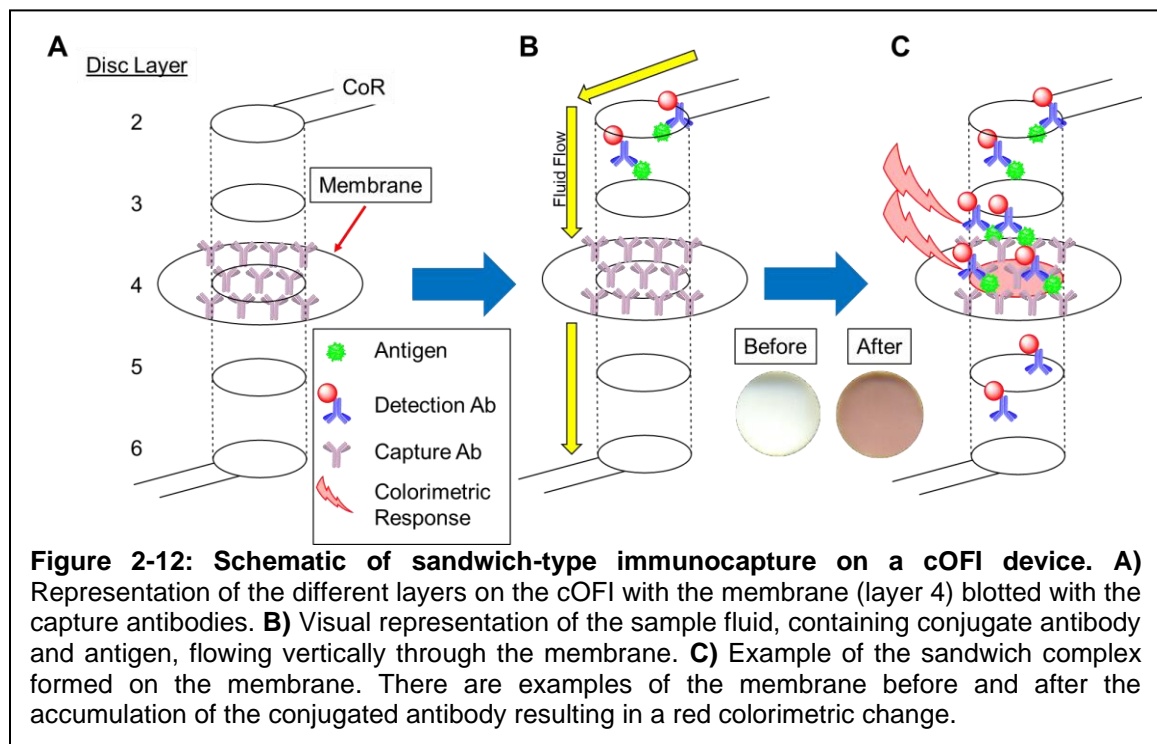


Figure 2-11: Results showing the capability and the sensitivity of the OFI disc to detect the *Y. Pestis* F1 antigen (n=3), discs were spun at 1000 RPM. Each membrane was cropped to a 50x50 pixel area circle then converted to 8-bit grayscale and measured for the grayscale value intensity. A 10x serial dilution of *Y. Pestis* F1 antigen was performed on the VFI disc, from 10 $\mu\text{g/mL}$ to 0.001 $\mu\text{g/mL}$, to determine sensitivity. The “hook effect” observed at the 10 $\mu\text{g/mL}$ and 1 $\mu\text{g/mL}$ concentrations.

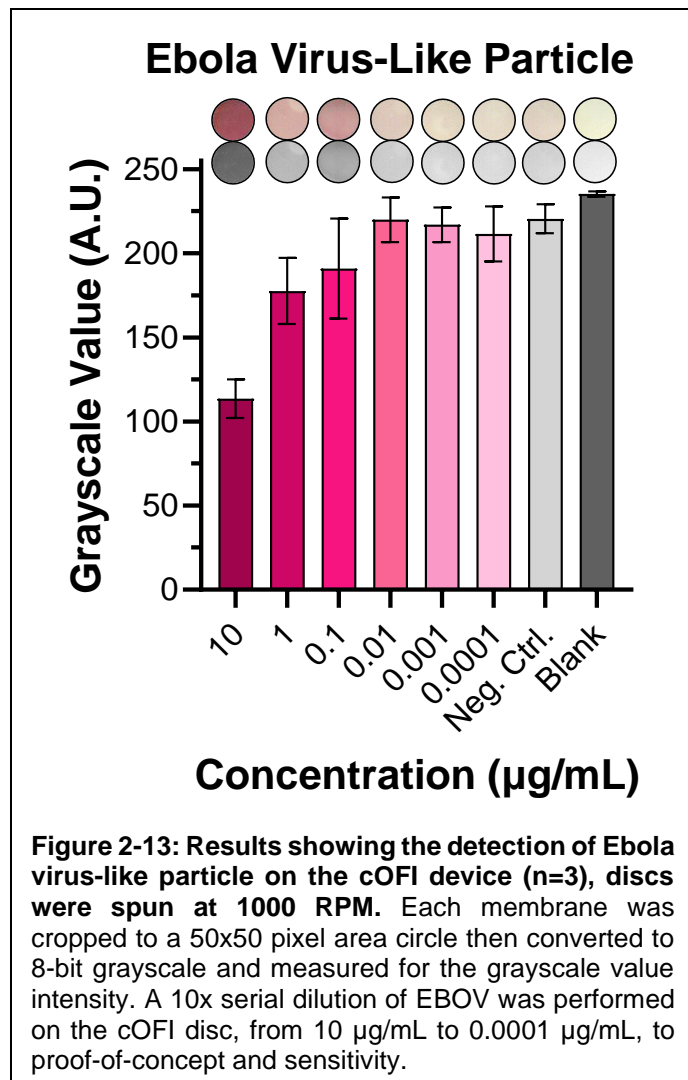
sites are occupied by the F1 antigen. Thus, with no unoccupied binding sites, the antibodies are unable to form the sandwich complex for chromogenesis from the accumulation of the AuNP on the NC membrane.^{32–34} The sample concentration of 0.001 $\mu\text{g/mL}$ ($\text{GV} = 187 \pm 17$) showed a GV that was readily distinguishable from the negative control ($\text{GV} = 248 \pm 2$) and blank ($\text{GV} = 252 \pm 2$) samples.

The cOFI device detected target antigen as low as 1 ng/mL; thus, to detect at lower concentrations, a larger sample volume would be required for flow through the NC membrane.⁸ As a proof of principle, Devadhasan et al, has shown the ability to detect 0.025 ng/mL by flowing 5 mL of sample through a NC membrane.²⁵ By modifying the architecture from the original 5-layer OFI disc, we were able to demonstrate a fully enclosed analytical device to rapidly detect *Y. pestis* F1 antigen on disc within approximately 30 minutes, paving the way for a fully automated and portable PoN device.



2.3.4 Detection of Ebola Virus-Like Particles

Next, we wanted to demonstrate immunocapture using another pathogen, Ebola. We began by diluting the EBOV into aqueous sample solutions from 10-0.0001 $\mu\text{g}/\text{mL}$ for on-disc detection. **Figure 2-13** shows the resultant mean GV ($n=3$) for each of the sample dilutions flowed through the sample architecture. The experimental setup was similar to section 3.3 and comprised of a full sandwich-type immunoassay (**Figure 2-12**). Across the three highest concentrations (10 to 0.1 $\mu\text{g}/\text{mL}$) the GV became less intense as the EBOV concentration was decreased (GV = 114 ± 12 , 178 ± 20 , and 191 ± 30 , respectively), but eventually plateaued. When comparing the membranes of 10-0.1 $\mu\text{g}/\text{mL}$ samples, there is visual difference from the negative control (GV = 221 ± 9) and blank (GV = 235 ± 2). A one-way ANOVA ($\alpha = 0.05$) determined there was no statistical difference between samples 1-0.0001 $\mu\text{g}/\text{mL}$ and negative control (respectively $p = 0.07, 0.36, 0.99, 0.99, \text{ and } 0.99$). Therefore, these results determine that the current limitations of the cOFI device



are not a result of the method of detection (i.g., orthogonal flow or sandwich assay), but the limitations on how specific the antibodies are to the target analyte. The antibodies used in this were shown to not be very specific and resulted in non-specific binding occurring on the NC membrane, seen as a slight reduction in GV in negative control sample (**Figure 2-13**). In future assay development, reagents need to be designed and produced in a way that will minimize or eliminate false-positives while still being able to bind to the target in a complex matrix. False-positives and non-specific binding can be minimized, or completely eliminated, by increasing the volume of wash buffer incorporated into the assay, which can be done by increasing the reagent volumes present on the cOFI device. Ultimately, we have shown a proof-of-concept cOFI device that can detect two infectious diseases by simply blotting the NC membranes with different capture antibodies.

2.4 Conclusions

We presented a 7-layer, centrifugally driven OFI device that employs colorimetric analysis for detection, and demonstrated linear drainage profiles throughout assay duration. With this device design, we were able to eliminate the region of lateral flow that was described in previously published work, instead, achieving complete orthogonal flow with the addition of 2 more polymeric layers. Further, this device produced 2 mm circular detection spots to enable simplified image segmentation and downstream analysis. Using the new device, we demonstrated differences in signal intensity as a result of changes to rotational frequency; these parameters will need to be considered for alternative applications and antigen-antibody pairs. With our assay, we were able to detect as low as 1

ng/mL of *Y. pestis* and 10 µg/mL with EBOV antigens. We plan to achieve lower detection sensitivities by increasing the sample volumes on disc. Future work will include implementation of a 3D-printed large volume sample chamber onto the cOFI disc in order to handle the increased volume of fluid.

2.5 References

- (1) Emanuel, Peter A; Hankla, L. W. *Recommendations on the Use of Diagnostic Devices in Far-Forward Military Operations*; 2016.
- (2) CDC: Bioterrorism Agents & Diseases - Emergency Preparedness & Response <https://emergency.cdc.gov/agent/agentlist-category.asp#catdef> (accessed Jan 10, 2021).
- (3) Regula-, I. H.; Organ-, T.; Office, T. R.; Asia, S.; Office, R. *Human Plague in 2002 and 2003.*; 2004; Vol. 79.
- (4) Plague <https://www.who.int/news-room/fact-sheets/detail/plague>.
- (5) Jansen, H. J.; Breeveld, F. J.; Stijnis, C.; Grobusch, M. P. Biological Warfare, Bioterrorism, and Biocrime. *Clin. Microbiol. Infect.* **2014**, *20* (6), 488–496. <https://doi.org/10.1111/1469-0691.12699>.
- (6) Joint Biological Point Detection System (JBPDS) <https://www.globalsecurity.org/military/library/budget/fy2000/dote/other/00jbpd.html> (accessed Nov 2, 2020).
- (7) Saito, M.; Uchida, N.; Furutani, S.; Murahashi, M.; Espulgar, W.; Nagatani, N.; Nagai, H.; Inoue, Y.; Ikeuchi, T.; Kondo, S.; et al. Field-Deployable Rapid Multiple Biosensing System for Detection of Chemical and Biological Warfare Agents. *Microsystems Nanoeng.* **2018**, *4*. <https://doi.org/10.1038/micronano.2017.83>.
- (8) Chen, P.; Gates-Hollingsworth, M.; Pandit, S.; Park, A.; Montgomery, D.; AuCoin, D.; Gu, J.; Zenhausern, F. Paper-Based Vertical Flow Immunoassay (VFI) for Detection of Bio-Threat Pathogens. *Talanta* **2019**, *191* (August 2018), 81–88. <https://doi.org/10.1016/j.talanta.2018.08.043>.
- (9) Li, F.; You, M.; Li, S.; Hu, J.; Liu, C.; Gong, Y.; Yang, H.; Xu, F. Paper-Based Point-of-Care Immunoassays: Recent Advances and Emerging Trends. *Biotechnol. Adv.* **2019**, *39*. <https://doi.org/10.1016/j.biotechadv.2019.107442>.
- (10) Manz, A.; Graber, N.; Widmer, H. M. Miniaturized Total Chemical Analysis Systems: A Novel Concept for Chemical Sensing. *Sensors Actuators B Chem.* **1990**, *1* (1–6), 244–248. [https://doi.org/10.1016/0925-4005\(90\)80209-l](https://doi.org/10.1016/0925-4005(90)80209-l).
- (11) Gong, M. M.; Sinton, D. Turning the Page: Advancing Paper-Based Microfluidics for Broad Diagnostic Application. *Chem. Rev.* **2017**, *117*, 8447–8480. <https://doi.org/10.1021/acs.chemrev.7b00024>.
- (12) Reyes, D. R.; Iossifidis, D.; Auroux, P.-A.; Manz, A. Micro Total Analysis Systems. 1. Introduction, Theory, and Technology. *Anal. Biochem.* **2002**, *74*, 2623–2636. <https://doi.org/10.1021/ac0202435>.
- (13) Whitesides, G. M. The Origins and the Future of Microfluidics. *Nature* **2006**, *442* (7101), 368–373. <https://doi.org/10.1038/nature05058>.
- (14) Gong, M. M.; Sinton, D. Turning the Page: Advancing Paper-Based Microfluidics for Broad Diagnostic Application. *Chemical Reviews*. American Chemical Society June 28, 2017, pp 8447–8480. <https://doi.org/10.1021/acs.chemrev.7b00024>.
- (15) Oh, Y. K.; Joung, H. A.; Kim, S.; Kim, M. G. Vertical Flow Immunoassay (VFA) Biosensor for a Rapid One-Step Immunoassay. *Lab Chip* **2013**, *13*

- (5), 768–772. <https://doi.org/10.1039/c2lc41016h>.
- (16) Woolf, M.; Dignan, L.; Karas, S.; Lewis, H.; Hadley, K.; Nauman, A.; Gates-Hollingsworth, M.; AuCoin, D.; Green, H.; Geise, G.; et al. Characterization of a Centrifugal Microfluidic Orthogonal Flow Platform. *Micromachines* **2022**, *13* (3), 487. <https://doi.org/10.3390/M13030487>.
- (17) Thompson, B. L.; Ouyang, Y.; Duarte, G. R. M.; Carrilho, E.; Krauss, S.; Landers, J. P. Inexpensive, Rapid Prototyping of Microfluidic Devices Using Overhead Transparencies and a Laser Print, Cut, and Laminate Fabrication Method. *Nat. Protoc.* **2015**, *10* (6), 875–886. <https://doi.org/10.1038/nprot.2015.051>.
- (18) Hau, D.; Wade, B.; Lovejoy, C.; Pandit, S. G.; Reed, D. E.; DeMers, H. L.; Green, H. R.; Hannah, E. E.; McLarty, M. E.; Creek, C. J.; et al. Development of a Dual Antigen Lateral Flow Immunoassay for Detecting *Yersinia Pestis*. *PLoS Negl. Trop. Dis.* **2022**, *16* (3), e0010287. <https://doi.org/10.1371/JOURNAL.PNTD.0010287>.
- (19) Demers, H. L.; He, S.; Pandit Id, S. G.; Hannah Id, E. E.; Zhang, Z.; Yan, F.; Greenid, H. R.; Reyes, D. F.; Huid, D.; Mclartyid, M. E.; et al. Development of an Antigen Detection Assay for Early Point-of-Care Diagnosis of Zaire Ebolavirus. *PLoS Negl. Trop. Dis.* **2020**, *14* (11). <https://doi.org/10.1371/journal.pntd.0008817>.
- (20) Woolf, M. S.; Dignan, L. M.; Scott, A. T.; Landers, J. P. Digital Postprocessing and Image Segmentation for Objective Analysis of Colorimetric Reactions. *Nat. Protoc.* **2020**, *16*, 218–238. <https://doi.org/10.1038/s41596-020-00413-0>.
- (21) Kainz, D. M.; Früh, S. M.; Hutzenlaub, T.; Zengerle, R.; Paust, N. Flow Control for Lateral Flow Strips with Centrifugal Microfluidics. *Lab Chip* **2019**, *19* (16), 2718–2727. <https://doi.org/10.1039/c9lc00308h>.
- (22) Gorkin, R.; Park, J.; Siegrist, J.; Amasia, M.; Lee, B. S.; Park, J. M.; Kim, J.; Kim, H.; Madou, M.; Cho, Y. K. Centrifugal Microfluidics for Biomedical Applications. *Lab Chip* **2010**, *10* (14), 1758–1773. <https://doi.org/10.1039/b924109d>.
- (23) Al-Faqheri, W.; Hwai Gilbert Thio, T.; Ameen Qasaimeh, M.; Dietzel, A.; Madou, M.; Al-Halhouli, A. Particle/Cell Separation on Microfluidic Platforms Based on Centrifugation Effect: A Review. *Microfluid. Nanofluidics* **2017**, *21*, 102. <https://doi.org/10.1007/s10404-017-1933-4>.
- (24) Madou, M.; Zoval, J.; Jia, G.; Kido, H.; Kim, J.; Kim, N. Lab on a CD. *Annu. Rev. Biomed. Eng.* **2006**, *8*, 601–628. <https://doi.org/10.1146/annurev.bioeng.8.061505.095758>.
- (25) Devadhasan, J. P.; Gu, J.; Chen, P.; Smith, S.; Thomas, B.; Gates-Hollingsworth, M.; Hau, D.; Pandit, S.; AuCoin, D.; Zenhausern, F. Critical Comparison between Large and Mini Vertical Flow Immunoassay Platforms for *Yersinia Pestis* Detection. *Anal. Chem.* **2021**, *acs.analchem.0c05278*. <https://doi.org/10.1021/acs.analchem.0c05278>.
- (26) Geise, G. M.; Freeman, B. D.; Paul, D. R. Sodium Chloride Diffusion in Sulfonated Polymers for Membrane Applications. *J. Memb. Sci.* **2013**, *427*, 186–196. <https://doi.org/10.1016/j.memsci.2012.09.029>.

- (27) Moore, W. R. The Swelling of Nitrocellulose in Binary Mixtures. *Frith, Trans. Faraday SOC* **1923**, 42 (6), 543.
- (28) Squires, T. M.; Messinger, R. J.; Manalis, S. R. Making It Stick: Convection, Reaction and Diffusion in Surface-Based Biosensors. *Nat. Biotechnol.* **2008**, 26 (4). <https://doi.org/10.1038/nbt1388>.
- (29) Zimmermann, M.; Delamarche, E.; Wolf, M.; Hunziker, P. Modeling and Optimization of High-Sensitivity, Low-Volume Microfluidic-Based Surface Immunoassays. *Biomed. Microdevices* **2005**, 7 (2), 99–110.
- (30) Schlappi, T. S.; Mccalla, S. E.; Schoepp, N. G.; Ismagilov, R. F. Flow-through Capture and in Situ Amplification Can Enable Rapid Detection of a Few Single Molecules of Nucleic Acids from Several Milliliters of Solution. *Anal. Chem.* **2016**, 88, 7647–7653. <https://doi.org/10.1021/acs.analchem.6b01485>.
- (31) Tiplady, S. Lateral Flow and Consumer Diagnostics. *Immunoass. Handb.* **2013**, 533–536. <https://doi.org/10.1016/B978-0-08-097037-0.00036-1>.
- (32) Serrano, R. A. Introduction: Surface Plasmons. In *Modified Au-Based Nanomaterials Studied by Surface Plasmon*; Springer International Publishing, 2015; pp 1–27. <https://doi.org/10.1007/978-3-319-19402-8>.
- (33) Products, M. S.; Science, C.; Products, N.; Nanofibers, C.; Nanostructures, G.; Mesoporous, G.; Nanoparticles, G.; Nanoparticles, S.; Dots, Q.; Advantage, Q.; et al. Gold Nanoparticles: Properties and Applications Optical & Electronics Properties of Gold Nanoparticles. *Sigma Aldrich* **2016**, 8–12.
- (34) Bohren, C. F. Absorption and Scattering of Light by Small Particles. *Absorpt. Scatt. Light by small Part.* **1983**. <https://doi.org/10.1088/0031-9112/35/3/025>.

CHAPTER 3 – Detection of Infectious Diseases with a 3D-Printed Large Volume Centrifugal Microfluidic Orthogonal Flow Immunoassay

3.1 Introduction

Miniaturized total analysis systems (μ TAS), also known as lab-on-a-chip (LOC) or lab-on-a-disc (LoaD), were first developed in the 1950s with the ability to move nanoliter and picoliter volumes of fluid.¹ The evolution of LOC designs continued to grow, especially over the last 20 years, and can be divided into five categories based on the method of fluid flow: capillary, pressure driven, centrifugal, electrokinetic, and acoustic.^{1,2} These microfluidic platforms provide analytical instrumentation with the potential for portability, improved sensitivity, cost-effective manufacturing, and reduced analysis times.^{1,3} With this framework of characteristics, LOC or LoaD devices have become very desirable for point-of-care (POC) diagnostics.

Microfluidic POC devices allow for a simple, rapid, and portable method to analyze biological samples (e.g., urine, saliva, blood).⁴⁻⁶ Devices based on lateral flow immunoassay (LFI) have existed for decades, with the pregnancy test (for chorionic gonadotropin) among the greatest success stories in bioanalysis.^{4,7} Through capillary driven force, fluid flows through the matrix of the LFI strip (e.g., nitrocellulose membrane) from the sample pad to wicking pad.⁸⁻¹⁰ The positive attributes of LFI include ease of use, rapid assay time, and inexpensive manufacturing, but the inherent disadvantage is the limited sample volume that the device can accept, the inability to control flow rate, and lack of multiplexing capability.^{8,9,11}

Existing literature has presented a different approach, called a vertical flow immunoassay (VFI), which has the potential to compliment or supplant the

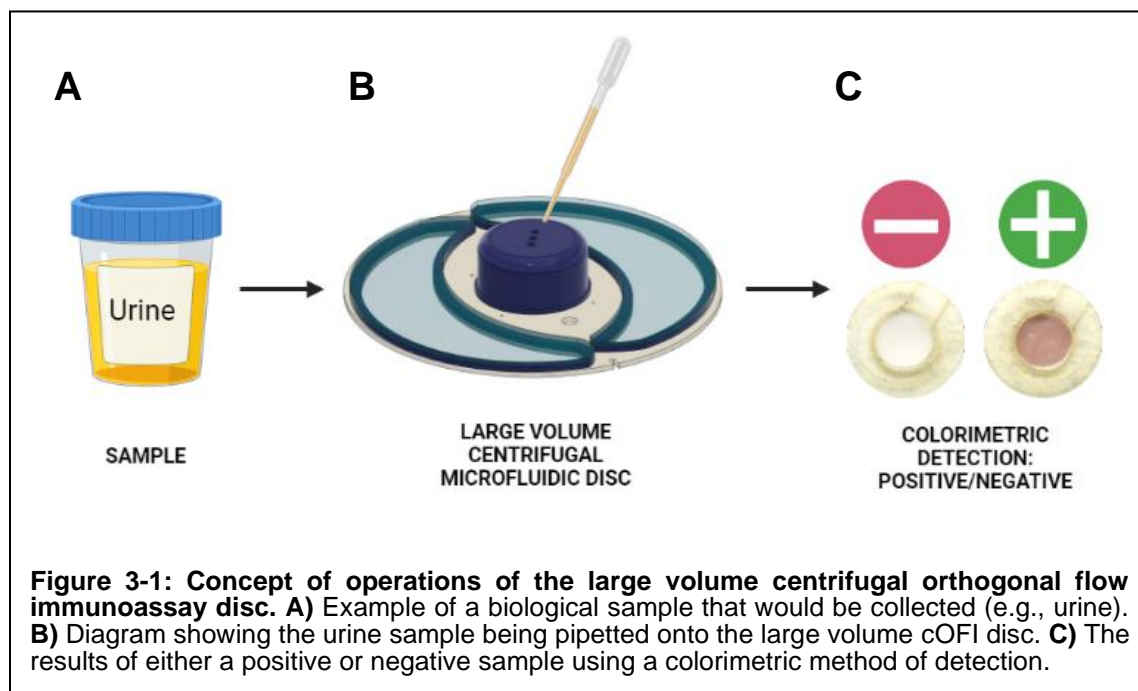
standard LFI. In contrast to LFI, where fluid moves parallel to the membrane surface, fluid movement with VFI flows vertically through the membrane, driven by either gravity or pressure.^{9,10,12,13} LFI has been reported to be at least five times less sensitive compared to a VFI, when detecting the same target analyte.¹⁰ The VFI approach to fluid movement and detection provides a number of advantages over LFI, including a faster assay time, analysis of larger sample volumes, and the ability to multiplex on the membrane.^{9,12,13} For example, Devadhasan *et al.* have designed a multiplexed VFI capable of testing large volume samples (15 mL) for *Yersinia pestis* (*Y. pestis*), the infectious agent responsible for plague in the 14th century.¹⁴ Using pressure-driven fluid flow (e.g., syringe pump), they demonstrated a limit of detection (LOD) of 0.025 ng/mL for the *Y. pestis* F1 antigen, substantially more sensitive than a traditional LFI where an LOD of 4 ng/mL was obtained.^{14,15} Relative to VFI or LFI, more sensitive analytical techniques like enzyme-linked immunosorbent assay (ELISA) and quantitative polymerase chain reactions (PCR) do exist, but these suffer from long analysis time, high cost, the requirement for highly trained personnel, making these techniques less suitable for POC deployment.^{16–18}

The VFI approach described by Devadhasan *et al.* is both rapid and sensitive; however, in order to obtain the assay results, the disc must be disassembled and the nitrocellulose membrane removed in order to be imaged for analysis; this puts the user at an unnecessary risk of exposure to contaminated samples. To address these issues, we described a portable, centrifugal microfluidic orthogonal flow immunoassay (cOFI) in **Chapter 2** with the

overarching goal to provide a fully-enclosed, cost-effective and rapid POC device. The cOFI disc pumps fluid through the membrane through centrifugal forces, and provides a simple detection method exploiting image analysis on the device, without requiring disassembly. Despite these advantages, the cOFI disc described in **Chapter 2** was limited to sample volumes of 200 μL /chamber (8 chambers) and detected as low as 1 ng/mL of the F1 antigen. In order to detect lower concentrations with this cOFI system, it was clear that sample volume capacity of the microfluidic disc had to be increased.¹⁴

Here, for the first time, we describe a large volume cOFI device, featuring a 3D-printed sample chamber that holds up to 12 mL of sample (**Figure 3-1**). 3D-printing technology not only allows for greater sample volumes but also maintains a longer inlet channel which is required to maintain hydraulic pressure through the duration of the assay. Additionally, the structural integrity of the sample chamber is significantly stronger and can handle the large amount of centrifugal force applied while spinning the disc (313 x gravity), unlike previous cOFI designs that used polymethyl methacrylate (PMMA, 1.5 mm thick) for sample chambers.¹⁹ A 7-layer design was used, as described in **Chapter 2.**, with the nitrocellulose membrane in the middle layer, sandwiched between two via layers which provide orthogonal flow. To show proof-of-concept and sensitivity, *Y. pestis* F1 antigen and Ebola virus-like particles (EBOV), both category A biological threat agents as defined by the Center for Disease Control and Prevention (CDC), were used as model organisms.²⁰ With 3D-printed technology and a custom mechatronic system

to centrifugally pump fluid, we present a rapid, cost effective POC microfluidic device that can detect low concentrations of infectious diseases.



3.2 Experimental Section

3.2.1 Fabrication of the Microfluidic cOFI Disc

Microfluidic cOFI devices were fabricated using the print-cut-laminate (PCL) method.²¹ Each device was comprised of seven polyethylene terephthalate (PET, 101.6 μm thickness, Film Source Inc., Maryland Heights, MO U.S.A.) sheets alternated with heat sensitive adhesive (HSA, 50.8 μm thickness, EL-7970-39, Adhesive Research Inc., Glen Rock, PA U.S.A). The disc architecture for each layer was designed using AutoCAD® 2020 (Autodesk Inc., San Rafael, CA, U.S.A.) and cut using a 50W CO₂ laser engraving system (VLS3.50, Universal Laser Systems®, Scottsdale, AZ, U.S.A.). Layers 1 and 7 were the external capping layers, while layers 2 and 6 contained the microfluidic channels. Layers 3 and 5 were via layers containing circular orthogonal flow ports (2 mm diameter)

that directed flow to and through layer 4, which contained 4 mm circular punches of the nitrocellulose (NC) membranes (0.2 μm pore size, Whatman ProTran BA 83, Marlborough, MA U.S.A.). To activate the HSA, the disc layers were aligned and lamination bonded (185-195°C) (UltraLam 250B, Akiles Products Inc., Mira Loma, CA, U.S.A.) in three separate steps. First, disc layers 3-5 were aligned, NC membrane punches were inserted into layer 4, and bonded together when passed through an office laminator (2 passes). Second, layers 6 and 7 were aligned with and laminated to layers 3-5 (2 passes). Finally, layers 1 and 2 were aligned and laminated to the previously bonded layers (2 passes). The three separate lamination steps were performed to allow the HSA to properly bond each of the PET layers together.

Polymethyl methacrylate (PMMA, 1.5 mm McMaster-Carr, Elmhurst, IL U.S.A.) was used to increase sample recovery chamber volumes. PMMA pieces and PET coverlets were affixed to the cOFI disc using pressure sensitive adhesive (PSA, 55.8 μm thickness, ARcare 7876, Adhesive Research Inc., Glen Rock, PA U.S.A.). Layer 7 contains a 2 mm access port to allow for the NC membranes to be blotted with desired capture antibodies post-lamination then capped with PET using PSA. Completely assembled discs were placed in foil moisture barrier bags (Dri-shield™, Uline, Pleasant Prairie, WI, U.S.A.) with two 3-gram silica moisture absorbent packets (S-3904, Uline) overnight and pressed (15 lbs.) to ensure PSA adhesion.

3.2.2 Fabrication of the 3D-Printed Large Volume Chamber

The 3D-printed large volume sample chamber was designed using Autodesk Fusion 360 (Autodesk Inc., San Rafael, CA, U.S.A.) then printed on a

FormLabs 3B stereolithography 3D-printer (FormLabs Inc., Somerville, MA, U.S.A.) with clear v4 resin (Formlabs Inc., Somerville, MA, U.S.A.) (**Figure 3-4 and 3-5**).²² The inside of each sample chamber was blocked with 500 μ L of blocking buffer solution (0.25% phosphate buffered saline-tween, PBS-T; 0.1% Bovine Serum Albumin) then placed in a convection oven (Binder 056FD – Convection Oven, P.O. Box 102, 78502 Tuttlingen, Germany) at 37°C for 1 hour. The large volume chamber was manually aligned and attached to the cOFI disc using PSA (**Figure 3-2 and 3-3**).

3.2.3 Proof-of-Concept: Immunocapture Study

In this study, 2.5 μ L of mouse whole molecule, IgG antibodies (mIgG) (5.5 mg/mL, Jackson ImmunoResearch Laboratories Inc., West Grove, PA, U.S.A.) were manually spotted and immobilized onto 4 mm NC membranes through the 2 mm access port in layer 7 (2.5 μ L, 5.5 mg/mL). The NC membranes were dried at 37°C for 1 hour in a convection oven (Binder 056FD – Convection Oven, P.O. Box 102, 78502 Tuttlingen, Germany). mIgG was not immobilized on the membranes for the negative and blank controls. Each membrane was subsequently blocked with a blocking buffer solution (2.5 μ L/membrane) then dried in the convection oven at 37°C for 1 hour. The discs were placed in foil moisture barrier bags (Dri-shield™, Uline, Pleasant Prairie, WI, U.S.A.) with two 3-gram silica moisture absorbent packets (S-3904, Uline) for a minimum of 24 hours.

A custom-built mechatronic spin system was used to control the rotational spin frequency of the disc. The mechatronic spin system was composed of a stepper motor (Sanmotion series, Sanyo denki, Moriguchi, Japan), stepper motor driver (DRV8801, Texas Instruments, P.O. Box 655303, Dallas, Texas 75265), and

an 8-core microcontroller (Propeller P8X32A-M44; Propeller Inc., Rockland, CA, U.S.A). A pre-wash step (400 μ L) was performed using 1x PBS-T, pH = 7.5 (Thermo Fisher Scientific, Waltham, MA USA 02451) pipetted into the sample chamber (2000 RPM, until the pre-wash solution drained). Sample solutions were prepared using 4 nm colloidal gold nanoparticle conjugated goat anti-mouse IgG antibodies (m-AuNP; Optical Density (OD) = 2.0 at 520 nm, Jackson ImmunoResearch Laboratories, Inc., West Grove, PA, U.S.A.), diluted (dilution: 200x-450x) with PBS-T, and incubated in-tube at room temperature for 20 min. Negative controls consisted of PBS-T buffer (6 mL) and m-AuNP (30 μ L), 200x dilution; blank controls consisted of only PBS-T buffer (6 mL). Each sample solution (6 mL) was pipetted into the sample chamber and centrifugally pumped through the membrane at 2000 RPM until the sample chamber drained completely (45 minutes). A final post-wash step (500 μ L PBS-T buffer, 2000 rpm, 500 sec) was performed to remove any excess sample from the membrane.

3.2.4 Detection of *Y. pestis* F1 Antigen on the Centrifugal Microfluidic Orthogonal Flow Immunoassay Disc

Y. pestis reagents were prepared in the Diagnostics Discovery Laboratory (School of Medicine, University of Nevada, Reno, NV, U.S.A.) as per the protocol in Hau et al.²³ The large volume cOFI disc was assembled as described in Section 2.1. The membranes were blotted post-lamination with 2.5 μ L of Yp11C7 0416 IgG1 (Yp-mAb) (*Y. pestis* F1 antigen specific mAb, 5.85 mg/mL), then the discs were incubated at 37°C for 1 hour in a convection oven (Binder 056FD – Convection Oven, P.O. Box 102, 78502 Tuttlingen, Germany). Next, each

membrane was blocked with blocking buffer solution (2.5 μL) through the 2 mm access port in layer 7 then placed in the oven at 37°C for 1 hour.

A pre-wash step (400 μL) was performed using *Y. pestis* chase buffer, or 50 mM carb-bicarbonate buffer at pH = 9.6, prepared from sodium bicarbonate (Thermo Fisher Scientific, Waltham, MA USA 02451) and sodium carbonate (Thermo Fisher Scientific, Waltham, MA USA 02451), pipetted into the sample chamber (2000 RPM, until the pre-wash solution was drained). Sample solutions (6 mL) of the *Y. pestis* F1 antigen were prepared at 10-0.01 ng/mL in chase buffer. Aliquots of each antigen dilution were mixed with 10 μL of Yp3F2 gold conjugate (Yp-AuNP, OD 10.1 at 520 nm), and incubated in-tube at room temperature for 20 min. Negative controls consisted of 6 mL of chase buffer and 10 μL of Yp-AuNP; blank controls consisted of 6 mL chase buffer. Sample solutions were loaded into the sample chambers and centrifugally pumped through the membrane at 2000 RPM until the chambers were completely drained (45 minutes). Finally, a post-wash step (500 μL chase buffer, 2000 RPM, 500 sec) was performed to remove any excess sample from the membrane.

3.2.5 Detection of Ebola Virus-Like Particles on the Centrifugal Microfluidic Orthogonal Flow Immunoassay Disc

Ebola reagents were prepared in the Diagnostics Discovery Laboratory (School of Medicine, University of Nevada, Reno, NV, U.S.A.) as per the protocol in DeMers et al.²⁴ The large volume cOFI disc was assembled as described in Section 2.1. The membranes were blotted post-lamination with 2.5 μL of 1HK7 IgG2b (Eb-mAb) (Ebola virus-like particle specific mAb, 10.2 mg/mL), then the discs were incubated at 37°C for 1 hour in a convection oven (Binder 056FD –

Convection Oven, P.O. Box 102, 78502 Tuttlingen, Germany). Next, each membrane was blocked with blocking buffer solution (2.5 μ L) through the 2 mm access port in layer 7 then placed in the oven at 37°C for 1 hour.

A pre-wash step (400 μ L) was performed using Ebola chase buffer, or Dulbecco's PBS buffer with 1% 10G surfactant at pH = 7.4, (Thermo Fisher Scientific, Waltham, MA USA 02451), pipetted into the sample chamber (2000 RPM, until the pre-wash solution was drained). Sample solutions (6 mL) of the Ebola virus-like particles (EBOV) were prepared at 10-0.1 ng/mL in chase buffer. Aliquots of each antigen dilution were mixed with 10 μ L of 1HK11 gold conjugate (Eb-AuNP, OD 10.5 at 520 nm), and incubated in-tube at room temperature for 20 min. Negative controls consisted of 6 mL of chase buffer and 10 μ L of Eb-AuNP; blank controls consisted of 6 mL chase buffer. Sample solutions were loaded into the sample chambers and centrifugally driven through the membrane at 2000 RPM until the chambers were completely drained (45 minutes). Finally, a post-wash step (500 μ L chase buffer, 2000 RPM, 500 sec) was performed to remove any excess sample from the membrane.

3.2.6 Detection in Artificial Urine and Human Urine

Artificial urine (AU) was prepared using the reagents described in **Table 1** dissolved in 50 mL of deionized water.²⁵ AU was spiked with m-AuNP (300x dilution), one set of samples (n=3) were diluted 1:4 with deionized water and another set was undiluted. Sample solution preparation followed the same procedure as stated in sections 2.3 and 2.4 with a change in the pre- and post-wash steps. A pre-wash step (400 μ L) of deionized water was pumped through the membrane (2000 RPM, until all fluid was drained). The urine samples (6 mL, n=3)

were pumped through the membrane (2000 RPM, 45 minutes). A post-wash step (500 μ L) of deionized water was pumped through the membrane (2000 RPM, 5 min) to remove any excess sample from the membrane. Human urine samples were collected, de-identified, and stored according to University of Virginia's Institutional Review Board (IRB) policies (HSR #210278) then spiked

	Chemical	MW (g/mol)	mM (mmol/L)	Quantity (g/50 mL)
Na_2SO_4	Sodium Sulfate	142.04	11.965	0.085
$\text{C}_5\text{H}_4\text{N}_4\text{O}_3$	Uric Acid	168.11	1.487	0.0125
$\text{Na}_3\text{C}_6\text{H}_5\text{O}_7 \cdot 2\text{H}_2\text{O}$	Sodium Citrate Dihydrate	294.1	2.45	0.036
$\text{C}_4\text{H}_7\text{N}_3\text{O}$	Creatinine	113.12	7.791	0.04405
$\text{CH}_4\text{N}_2\text{O}$	Urea	60.06	249.75	0.75
KCl	Potassium Chloride	74.55	30.953	0.1154
NaCl	Sodium Chloride	58.44	30.053	0.0878
CaCl_2	Calcium Chloride	110.98	1.663	0.00925
NH_4Cl	Ammonium Chloride	53.49	23.667	0.0633
$\text{K}_2\text{C}_2\text{O}_4 \cdot \text{H}_2\text{O}$	Dipotassium Oxalate monohydrate	166.22	0.19	0.00175
$\text{MgSO}_4 \cdot 7\text{H}_2\text{O}$	Magnesium Sulfate Heptahydrate	246.47	4.389	0.0541
$\text{NaH}_2\text{PO}_4 \cdot 2\text{H}_2\text{O}$	Sodium Dihydrogen Phosphate Dihydrate	156.01	18.667	0.1456
$\text{Na}_2\text{HPO}_4 \cdot 2\text{H}_2\text{O}$	Sodium Phosphate Dibasic Dihydrate	177.99	4.667	0.04155

Table 3-1: Composition of the artificial urine in 50 mL of deionized water.

with m-AuNP (300x dilution) and *Y. pestis* F1 antigen (0.05 ng/mL).

3.2.7 Detection in Artificial Blood Plasma

Artificial blood plasma (ABP, pH = 8.13) was spiked with m-AuNP (300x dilution), F1 antigen (0.05 ng/mL), and EBOV (10 ng/mL). ABP consisted of potassium chloride (0.0131 g, KCl), sodium chloride (0.4030 g, NaCl), disodium phosphate (0.0086 g, Na_2HPO_4), sodium bicarbonate (0.0173 g, NaHCO_3), magnesium chloride (0.1545 g, $\text{MgCl}_2 \cdot 6\text{H}_2\text{O}$), and calcium chloride (0.0193 g CaCl_2) dissolved in 50 mL of deionized water.²⁶ Sample solution preparation followed the same procedure as stated in sections 2.3, 2.4, and 2.5 with a change in the pre- and post-wash steps; a pre-wash step (400 μ L) of deionized water was

driven through the membrane (2000 RPM, until all water was drained), then the ABP samples (6 mL, n=3) were driven through the membrane (2000 RPM, 45 minutes), and A post-wash step (500 μ L) of deionized water was pumped through the membrane (2000 RPM, 5 min) to remove any excess sample from the membrane.

3.2.8 Image Processing and Data Analysis

Each large volume cOFI disc was digitally imaged (1200 dpi, TIF format) using a Perfection V100 desktop scanner (Epson, Suwa, Nagano, Japan), before and after each assay. Circular regions of interest (50-pixel diameter) from the NC membranes were selected using the Microsoft Windows 64-bit Fiji distribution of ImageJ v.1.52p (<https://imagej.net/Fiji/Downloads>), as described in Woolf *et al.*²⁷ The ROI for each membrane was converted in ImageJ to weighted 8-bit grayscale and the grayscale value (GV) was analyzed. Fiji ImageJ measures the GV from 0-255, where 0 is completely black and 255 is entirely white.

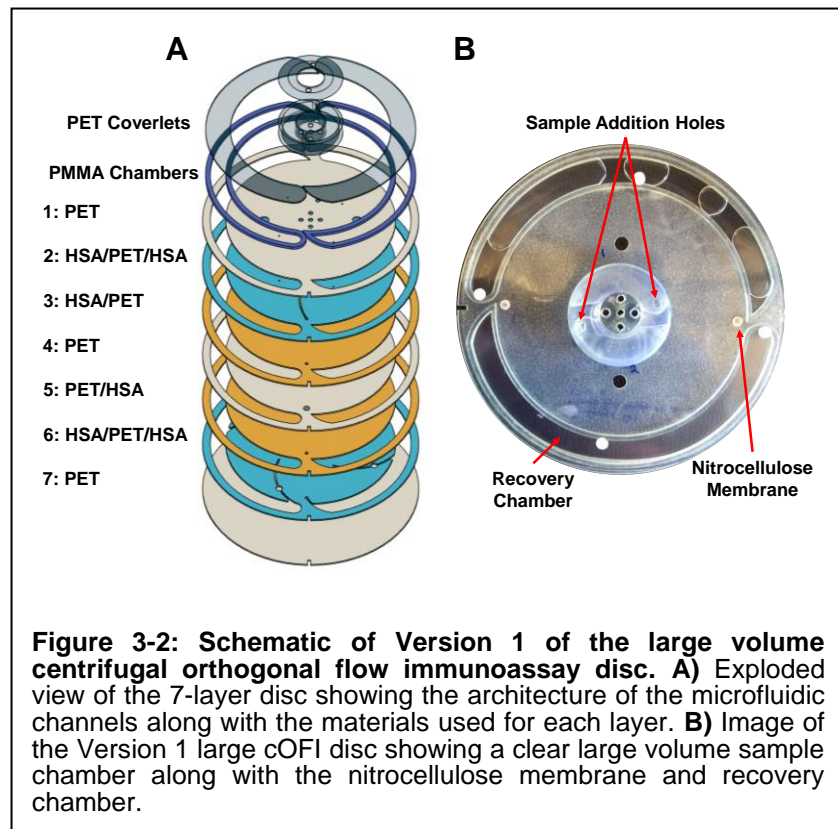
3.3 Results and Discussion

3.3.1 Fabrication of the Microfluidic cOFI Disc

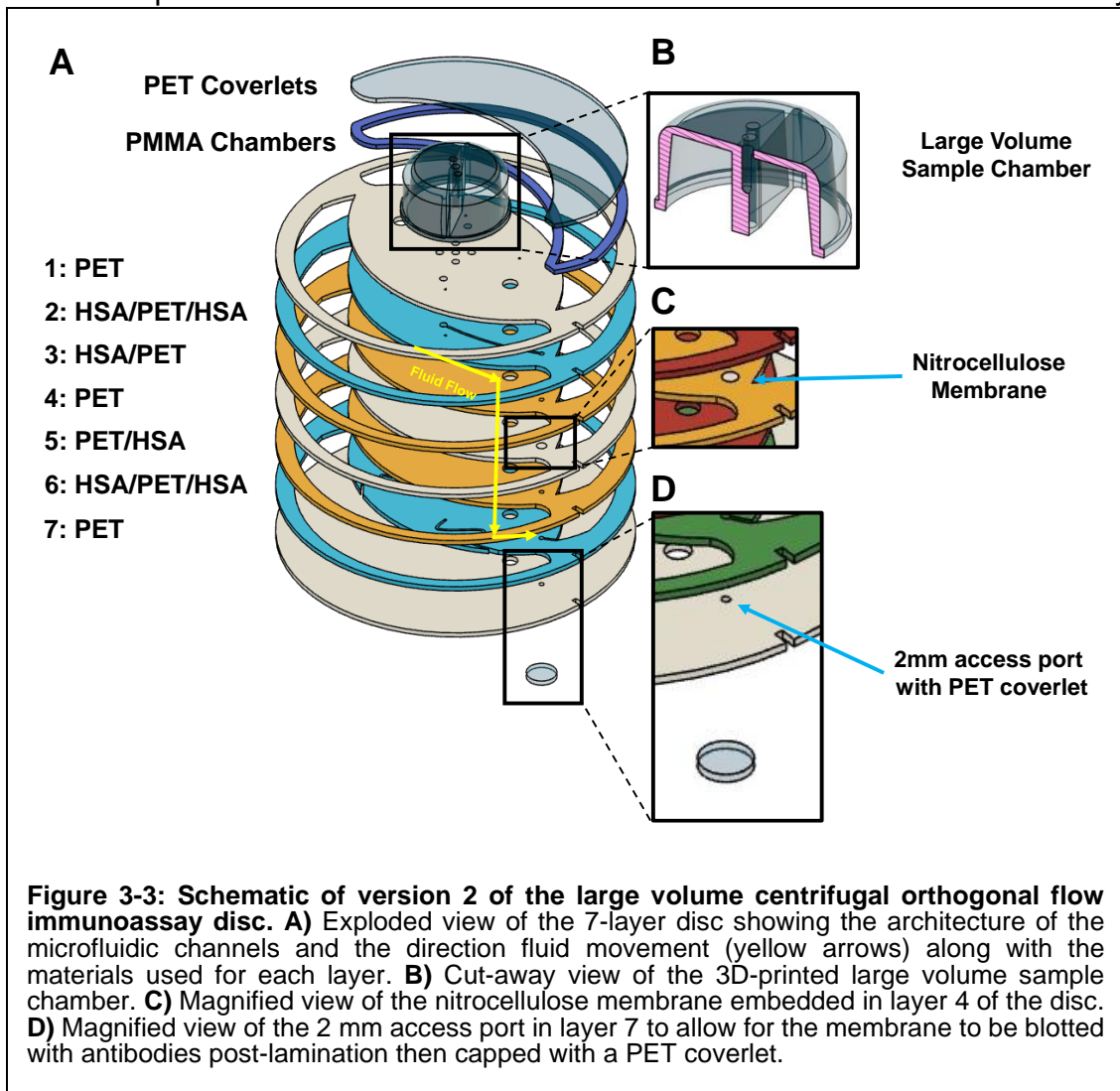
The large volume cOFI discs described here built upon the cOFI disc developed by Woolf *et al.* and the cOFI disc discussed in **Chapter 2**.¹⁹ The goal here was to develop a cOFI disc that could be used at the POC and analyze milliliter sized volumes of fluid. As previously reported by Chen *et al.*, analyzing a larger volume of sampled can increase the sensitivity of an immunoassay; therefore, in order to provide the flexibility to handle both small volumes (0.2 mL) and large volumes (6 mL), Version 1 of the large volume cOFI disc leveraged 3D printed technology to make a sample chamber that could hold 4 mL in total, or 2

mL per sub-chamber (**Figure 3-2**). Additionally, the recovery chambers were designed to handle the increased volume of fluid that would be pumped through the membranes (**Figure 3-2B**). The disc maintained the 7-layer design as the cOFI disc in **Chapter 2**. The large volume chamber provided the needed structural rigidity without leaking under centrifugal force while the disc rotated at 2000 RPM for extended periods of time; the sample chamber design and architecture will be further described in section 3.2. As for the disc design, the membranes in version 1 needed to be blotted and blocked before all the layers were laminated together because there was no access port in layers 1 or 7 allow for post-lamination blotting. Further, the laminator has the temperature set between 185-195°C in order to activate the HSA to bond the layers together, but after multiple passes through the

laminator, there was significant decreased signal on membrane which was hypothesized to be the result of the antibodies on the membrane becoming heat denatured by the laminator.²⁸



To prevent the antibodies from being heat denatured by the laminator, Version 2 of the large cOFI disc was designed (**Figure 3-3**). Version 2 incorporated a 2mm access port in layer 7 that allowed for the capture antibodies to be blotted on the membrane post-lamination; therefore, eliminating denaturing of the antibodies. Additionally, the volumetric capacity of the sample chamber was increased to 12 mL, 6 mL per chamber, (**Figure 3-3B**) by increasing the height of the chamber; the recovery chambers were also increased to allow for the increased fluid volume being driven through the membranes. It's interesting to note that the 3D printed chamber could handle the increased volume but the recovery



chambers could not handle the g-forces generated by the fluid rotating at 2000 RPM. The HSA would eventually fail during each experiment, causing the sample to leak inside the spin system. In order to prevent failure of the recovery chambers, the PMMA would need to be made wider in order for more PSA to cover more surface area. Another alternative would be to injection mold the recovery chambers; therefore, eliminating the need to bond PMMA-PET together to form the chambers. Both solutions to repair the HSA failure were not address because they were beyond the scope of this study, but the HSA issue will need to be fixed in the future if this disc design were to be manufactured. Ultimately, we were able to increase the sample volume on disc to 12 mL and developed a method that will allow for membranes to be blotted after the disc is completely assembled.

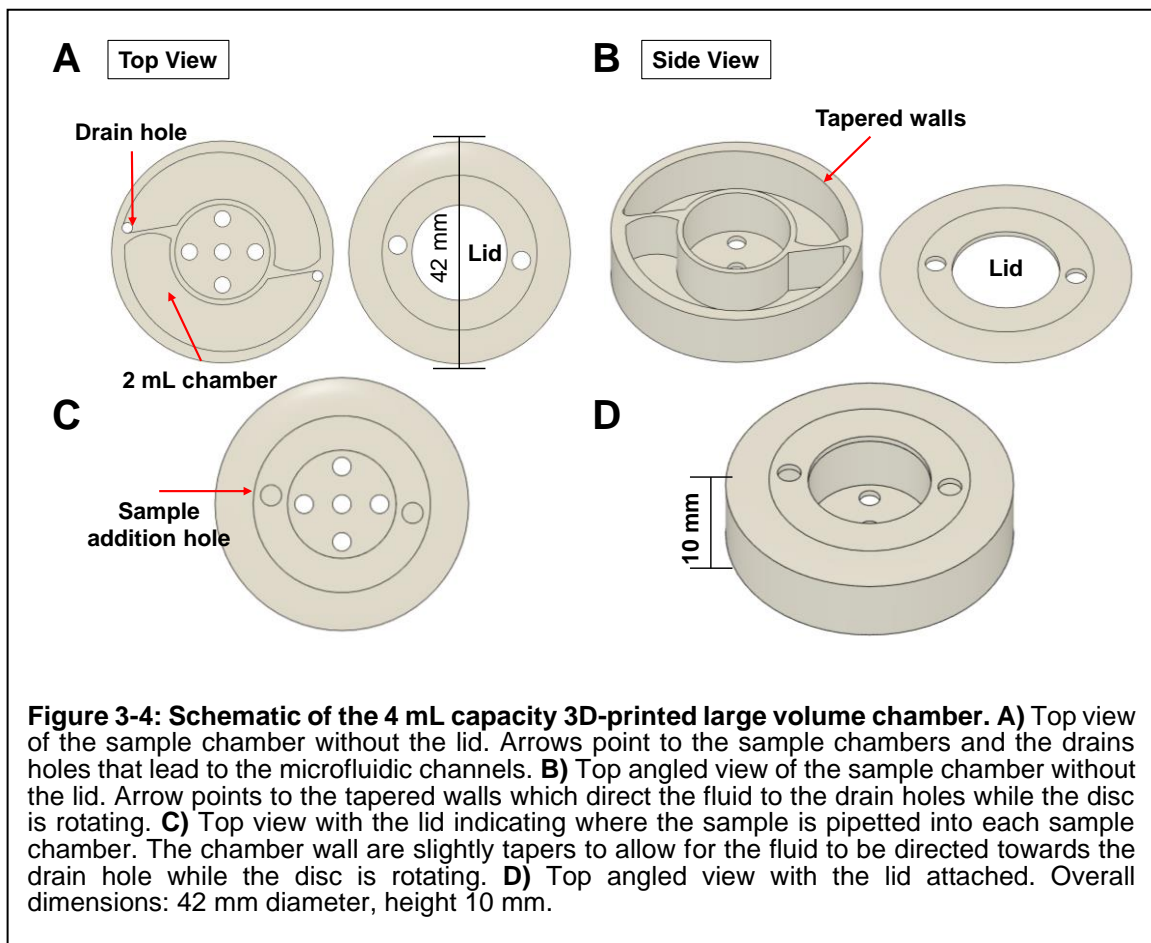
3.3.2 3D-Printed Large Volume Chamber

Early designs of a centrifugal microfluidic discs for OFI were focused on the architecture, type of membrane, pore size, consistent flow strategies and simplified image analysis.¹⁹ While sample volume was not a focus with those designs, once the parameters mentioned were optimized, sample volume becomes paramount as this directly impacts limit of detection (LOD). Microfluidic devices in the past have had the challenge of mitigating issues associated with the stochastic effects experienced with many POC systems, as they try to overcome the macro-to-micro interface hurdle; which is the ability to take a milliliter size sample and pump it through a device designed for nanoliter or picoliter sized volumes.²⁹ Collecting human samples (e.g., urine, blood plasma, and saliva) involves storing and handling milliliter sized volumes then injecting them into an instrument to be analyzed via an external pump or reservoir. As stated previously, the additional

equipment required to analyze these large volumes is not ideal for a POC device; therefore, the integration of a reservoir in or on a microfluidic chip must be explored in order to overcome the macro-to-micro interface.

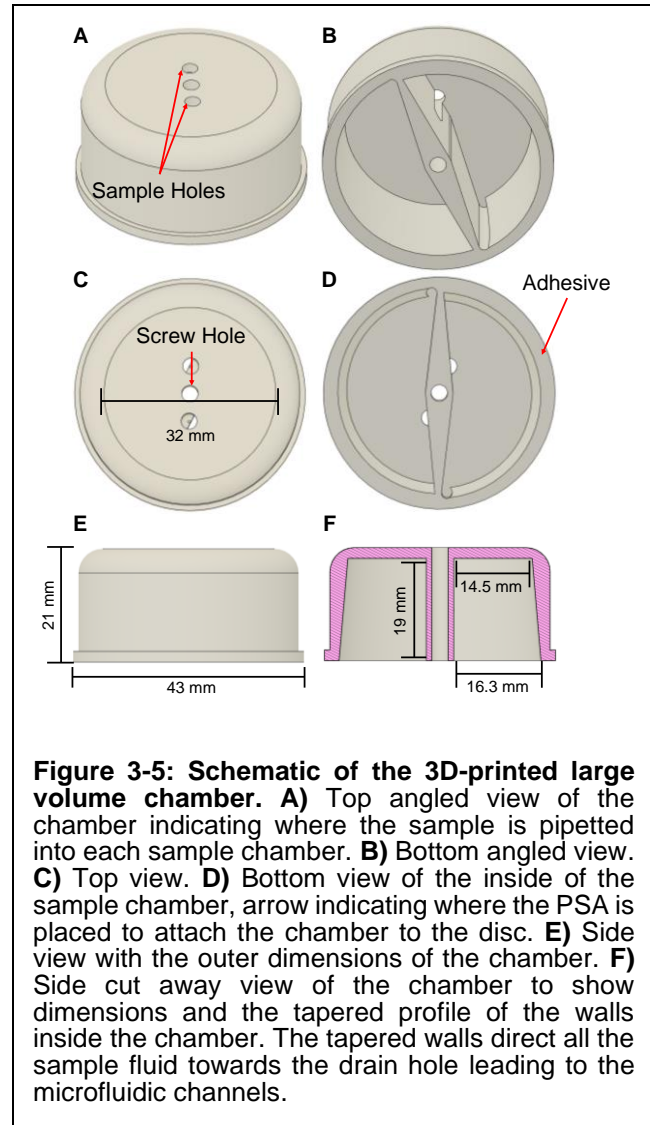
Here, we described the design and implementation of the large volume sample chamber onto the previously described cOFI discs. The sample chambers used in **Chapter 2** were made with 1.5 mm thick PMMA and bonded to the disc with PSA, but PSA does not have enough bond strength to handle large amounts of centrifugal force.¹⁹ Preliminary experiments tested 2 mL of fluid in PMMA sample chambers on a disc; ultimately, there was adhesive failure and the sample chambers leaked fluid. This is problematic for multiple reasons, e.g., the waste of valuable testing supplies, the invalidation of the test due to sample loss, and the potential aerosolization of contaminated fluid. Additionally, the amount of force applied to the PSA is 313 times the earth's gravitational field (g-force). To overcome this issue, 3D-printing technology was leveraged to manufacture a more structurally sound sample chamber that could handle larger volumes which would lead to greater sensitivity and a lower LOD.¹⁰ The initial design had an overall volumetric capacity of 4 mL, or 2 mL per sub-chamber (**Figure 3-4**). The chamber and lid were printed as one piece to limit assembly steps as well as to eliminate any potential of leaking from the chamber. The walls on the interior of the chamber were slightly tapered to direct the fluid towards the drains which lead to the microfluidic channels on the cOFI disc (**Figure 3-4A and B**). The chamber was attached to the disc with PSA and no leaking or failure of the adhesive occurred during the experiments due to the monolithic design of the chamber. 3D-printing

has provided the ability to handle milliliter sized volumes without compromising the integrity (e.g., chamber leaks) and architectural size (i.e., disc diameter) of the cOFI disc.



Next, we wanted to increase the ability of disc to handle up to 6 mL per sample sub-chamber (**Figure 3-5**). Increasing the volume on disc, allows for the ability to analyze biological samples that are extremely dilute (e.g., urine) without having to perform off-disc sample preparation (i.e., extraction, purification, or amplification) as well as enable the ability to detect infectious diseases in the early stages.^{30,31} This new design, similar to the design in **Figure 3-4** allows fluid to stay close to the center of rotation (CoR) which is important for two reasons. First, there is less g-forces applied the closer the object is to the CoR. Second, we keep the

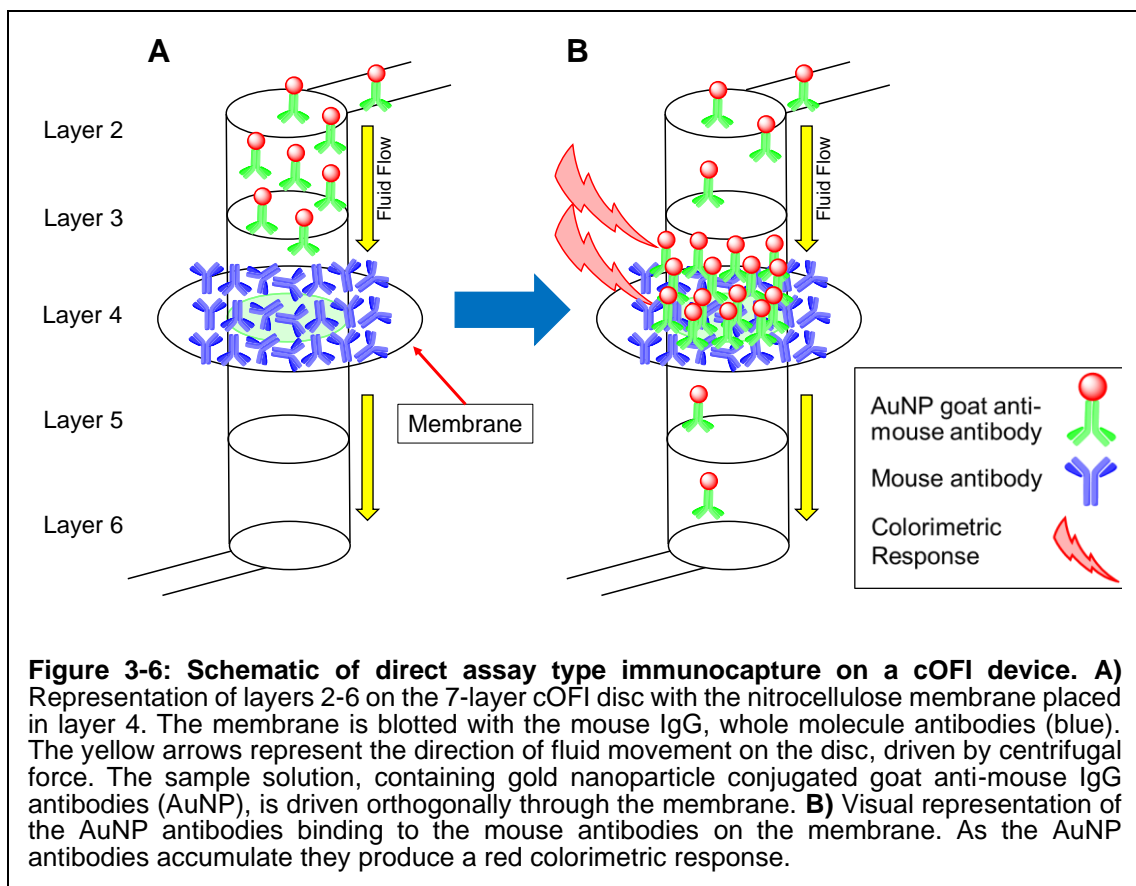
long inlet channel (43 mm) to the membrane which is important in maintaining hydraulic pressure as the sample chamber drains.³² The internal walls of the chamber were designed with a slight 5 degree taper down the vertical wall towards the drainage hole which leads to the microfluidic channel. The tapered wall was designed to ensure that the fluid would not be driven against the wall by centrifugal force and result in incomplete fluid drainage. (Figure 3-5D & F). The chamber was attached to the disc with PSA;



the additional volume on the disc resulted in no adhesive failures or leaks throughout the experiments. This is because the force generated from the spinning disc and the sample fluid is evenly distributed along the internal walls of the chamber and is made of an extremely durable proprietary acrylic resin.²² This chamber design has provided the end user the ability to analyze a range of sample fluid types (i.e., urine, saliva, blood plasma) and volumes on a centrifugal microfluidic device that is an ideal POC device.

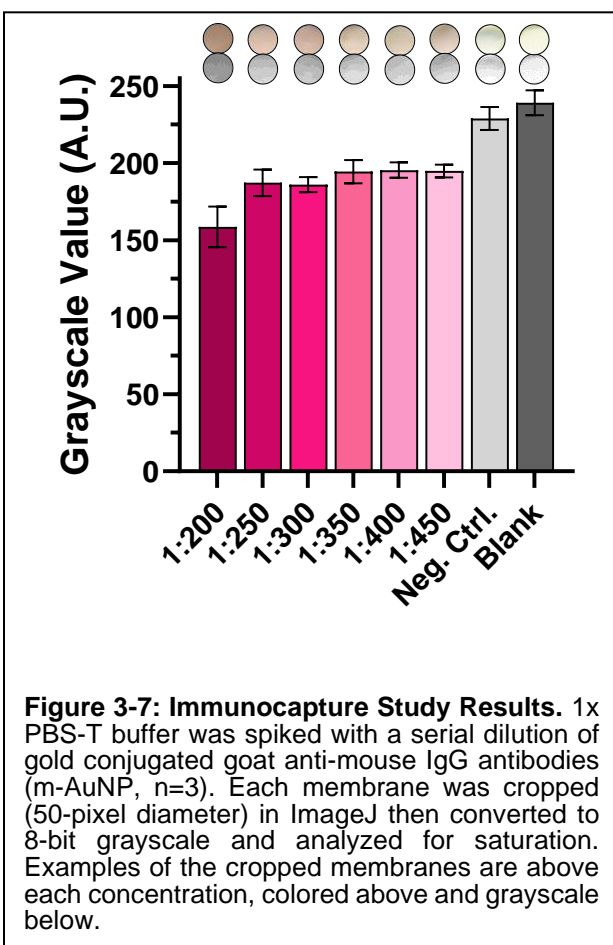
3.3.3 Proof-of-Concept: Large Volume Immunocapture Study

Similar to a traditional LFI, the core of the method with on-disc detection was ‘direct assay’ (**Figure 3-6**) through the formation of the m-AuNP-mIgG complex on the nitrocellulose membrane.³³ A positive result was when the m-AuNP containing sample solution produced a reddish color due to the accumulation of m-AuNPs that bind to the mIgG on the membrane, while a negative result was when a sample (no m-AuNP) produced no color on the membrane.^{34,35} The colorimetric response was quantified by cropping a 50-pixel diameter area in the center of the membrane using ImageJ and converting the image to 8-bit grayscale to measure the grayscale value (GV). GV was used, compared to other parameters (e.g., hue), because on a color wheel, the colors red, green, and blue (RGB) are given a numerical value of 0-255. AuNPs display a range of colors based off of



their surface plasmon resonance; the m-AuNPs used in this study (40 nm, OD = 2.0) emit a reddish hue.³⁶ On the hue color wheel, red falls at a numerical value of 0 and spans a range from 0-31 and 225 to 255, which produces a split spectrum. Depending on the color responses within the red region, peaks can be generated at both the high and low values of the hue scale.²⁷ By converting the NC membrane images to 8-bit grayscale, it eliminates the split spectrum generated by the hue scale and produces a black and white image that can easily be analyzed.

To show proof-of-concept of the large volume cOFI, we immobilized mIgG onto the membrane and centrifugally drove (0.1 mL/min) 6 mL of AuNP spiked in 1x PBS-T through the membrane. The study involved diluting the m-AuNP (OD 2.0) stock solution with PBS-T in 200x to 450x dilutions (increments of 50x). As predicted, the GVs increased as the sample was diluted (note: the GV is inverse of the membrane saturation).²⁷ At the lowest concentration (450x dilution, $GV = 195 \pm 4$), the membranes could visually be distinguished from the negative ($GV = 229 \pm 7$) and blank samples ($GV = 239 \pm 8$) (Figure 3-7). A one-way analysis of variance (ANOVA) was performed

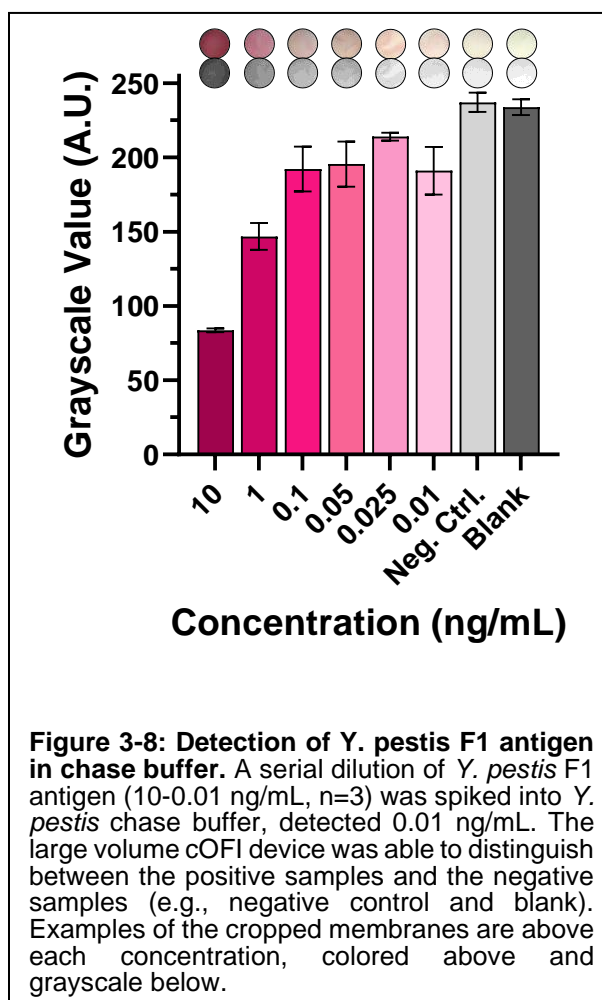


to determine if there was a statistical difference among the mean GVs of all the samples; the analysis indicated there was a significant difference among the GV means ($\alpha = 0.05$, $p < 0.0001$). A Tukey's multiple comparison test was performed to determine if there was a statistical difference between the 450x sample and the negative and blank samples; the analysis revealed there was a statistical difference among the mean GVs (respectively, $p = 0.0013$ and $p < 0.0001$), indicating that this assay can distinguish between a positive and negative sample. Examples of the cropped membranes are placed above the respective sample concentration.

Previous publications by Chen et al. and Devadhasan et al. describe a syringe pump driven VFI system with the capability to analyze up to 15 mL of sample. With that system, the membrane manifold needed to be disassembled in order to access the membrane for image analysis.^{10,14} As described in **Chapter 2**, the cOFI device was developed to allow the user to analyze the membrane directly on the disc, circumventing the need for any form of disassembly. We built on our previous work and integrated a long inlet channel (43 mm) from the sample chamber to the nitrocellulose membrane (**Figure 3-3**), and integrated a 3D-printed chamber onto the device. Our data shows that our microfluidic device can pump 6 mL sample volumes through the membranes while detecting a low concentration of m-AuNPs in solution and is able to delineate between a positive and negative sample.

3.3.4 Detection of *Y. Pestis F1* antigen on Large Volume Centrifugal Orthogonal Flow Microfluidic Disc

Previous sections have described the design of the sample chamber and proof of immunocapture with large sample volumes. Here, we demonstrate the sensitivity of the assay to detect *Y. pestis* F1 antigen spiked in chase buffer (10-0.01 ng/mL) with **Figure 3-8** showing the mean GV (n=3) for each sample. It is important to note that, unlike the results presented in section 3.2, this experimental setup comprised a full sandwich-type immunoassay (**Chapter 2, Figure 2-2**). As expected, the GVs increased as the F1 antigen concentration decreased. At 10 ng/mL, there was a very intense red color with a GV = 84 ± 1 (**Figure 3-8**). From the 0.1-0.01 ng/mL, the GVs plateau but there is still a visual and statistical difference from the positive samples compared to the negative (GV = 237 ± 6) and blank (GV = 234 ± 5) samples. The sample containing 0.025 ng/mL of F1 antigen (GV = 214 ± 3) had a greater average GV than the 0.01 ng/mL sample (192 ± 14). The greater GV at 0.025 ng/mL could be explained by the non-uniform binding of the Yp-AuNP-F1 antigen complex to the Yp-mAb on the membrane, as seen in examples of the cropped membranes above each bar in **Figure 3-8**. A one-way

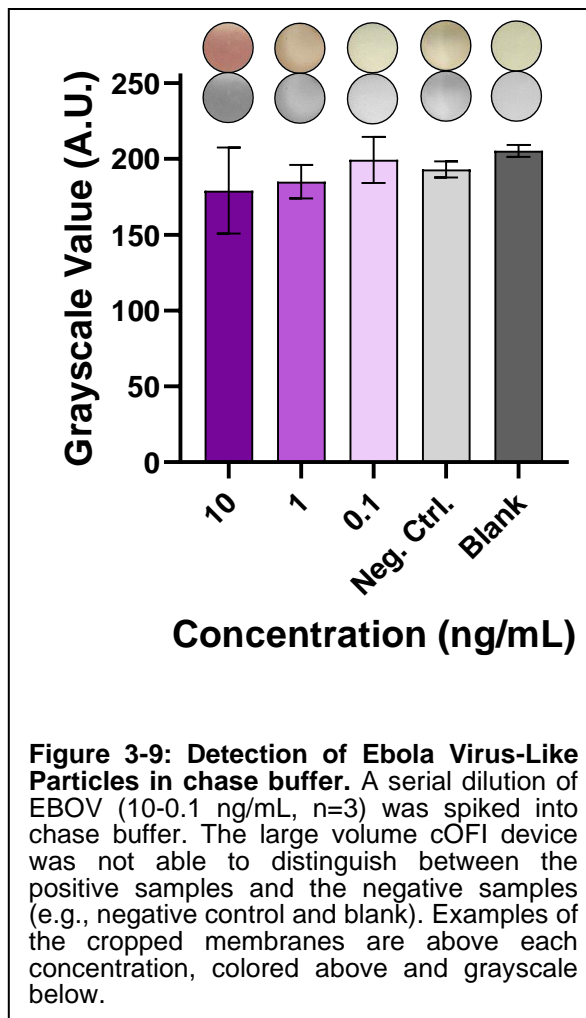


ANOVA ($\alpha = 0.05$) was performed to compare the difference among the four lowest F1 antigen concentrations (0.1, 0.05, 0.025, 0.01 ng/mL) on the mean GV; a Tukey's multiple comparison test revealed that there was no statistical difference among the mean GVs (respectively, $p > 0.99$, $p = 0.46$, $p = 0.23$); the analysis shows that the large volume cOFI device is qualitative and is unable to quantify the concentration of F1 antigen present in a sample. Ultimately, the large volume cOFI was able to detect a 0.01 ng/mL sample solution ($GV = 192 \pm 14$) which is more sensitive than the VFI device reported by Devadhasan et al. ($LOD = 0.025$ ng/mL).¹⁴

3.3.5 Detection of Ebola Virus-Like Particles on Large Volume Centrifugal Orthogonal Flow Microfluidic Disc

In this section, we describe the flexibility of the large volume cOFI disc by detecting another infectious disease, EBOV spiked in Ebola chase buffer (10-0.1 ng/mL) with **Figure 3-9** showing the mean GV ($n=3$) for each sample. The experimental setup was similar to what was described in section 3.4 and comprised of a full sandwich-type immunoassay. The results presented in **Figure 3-9** were unexpected and inconsistent. Visually and statically, there is no difference between the GV's of the 10-0.1 ng/mL samples (respectively, $GV = 179 \pm 28$, 185 ± 11 , and 199 ± 15), the negative control ($GV = 193 \pm 5$), and the blank ($GV = 205 \pm 4$). A one-way ANOVA was performed to compare the mean GVs among all the samples; the analysis determined there was no significant difference

among the results ($\alpha = 0.05$, $p = 0.20$). These results could be caused by either the cOFI method of detection or the binding affinity of the Ebola antibodies to the EBOV. The Ebola reagents were initially designed and optimized to be used on LFI strips; therefore, the flow rate and pressure generated on the cOFI may be too fast for the sandwich complex to form on the membrane.²⁴ One experiment that could be performed, is to compare the results between the cOFI and a traditional LFI strip.



On an LFI strip, the flow rate is measured in millimeter per second (mm/s), with the average flow rate on a NC membrane being 0.16-0.66 mm/s; therefore, the antigen interacts with the immobilized antibodies in the test zone for about 1-6 seconds.³⁷ The short interaction time requires the antibodies to have a high affinity to the target analyte. Additionally, if the flow rate is too fast, reducing the interaction time between the antibody and target antigen, there will be reduction in signal. By verifying the Ebola reagents with an LFI strip designed for the Ebola antibodies, we could confirm if the antibodies still maintain functionality or if they are passed

their expiration date (~ 6 months from production). If the LFI strip determines that the reagents are producing a visible signal with the same concentrations as tested on the cOFI disc, then we could hypothesize that the flow rate is too fast on the cOFI disc for the Ebola reagents used in these experiments. Ultimately, new antibody reagents would need to be designed with a higher binding affinity that would have the ability to bind the target antigen at the higher flow rate used on the cOFI disc.

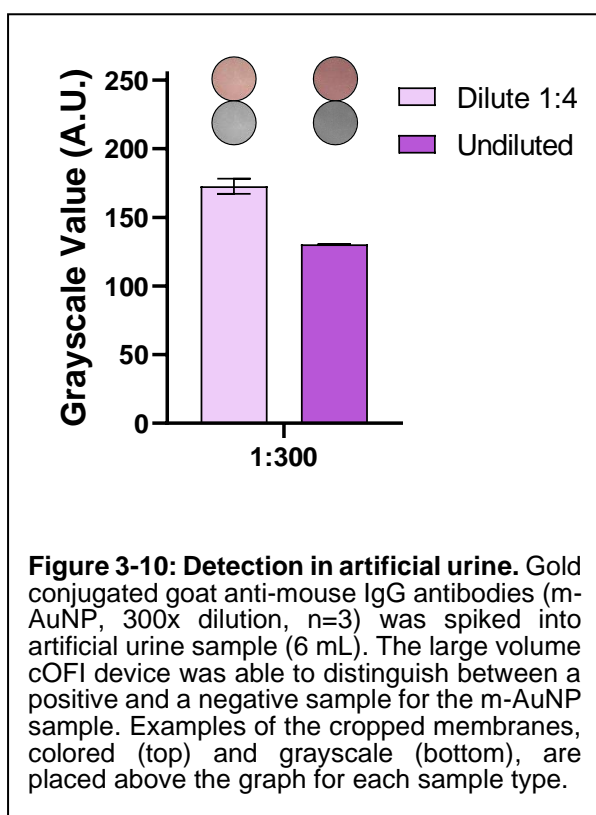
3.3.6 Analysis of Human Samples on Large Volume Centrifugal Orthogonal Flow Microfluidic Disc

Having shown proof-of-principle for immunocapture with large sample volumes and detected 0.01 ng/mL of F1 antigen with the large volume cOFI, we explored real world applications by testing human biological samples, both simulated and real, on the device. The purpose was to determine if the large volume assay could detect target analytes in complex samples in addition to the prepared buffer solutions. Both AU and real human urine was chosen for these studies for its ease of sample collection and storage compared to other biological fluids (e.g., blood).^{38,39} Human urine typically contains over 3000 metabolites and has been used to identify various biomarkers and diseases.⁴⁰ For example, the *Y. pestis* bacterium has been identified by culturing samples from human urine, saliva, and blood.^{25,41–43} Additionally, a human urine sample varies in composition, concentration, and volume from person to person (i.e., gender, race, sex, types of food consumed, water consumption, amount of exercise, and medication).^{25,44,45} Chateau et al. presented a study describing out of 194 patients diagnosed with *Y. pestis*, there was average of 13.5 ng/mL of F1 antigen present in urine.⁴² Based

off of this data, we tailored the following experiments to detect a lower concentration of F1 antigen (0.05 ng/mL) to show the capability of early detection in human urine.

First, we wanted to determine if the diluting the urine sample would have an effect on the flow rate and most importantly the signal produced. Using AU and m-AuNP (300x dilution, $n=3$) antibodies as a model, we compared the signals generated from 6 mL of concentration AU and AU diluted 1:4 (**Figure 3-10**). The results show the diluted AU sample produce a weaker signal ($GV = 173 \pm 6$) compared to the concentrated AU sample ($GV = 130 \pm 0.01$), which was expected due to the diluted sample containing less m-AuNP. What the data doesn't show is the difference in flow rate. During the study, the concentrated AU sample stopped flowing through the membrane after 4 mL, leaving 2 mL left in the sample chamber.

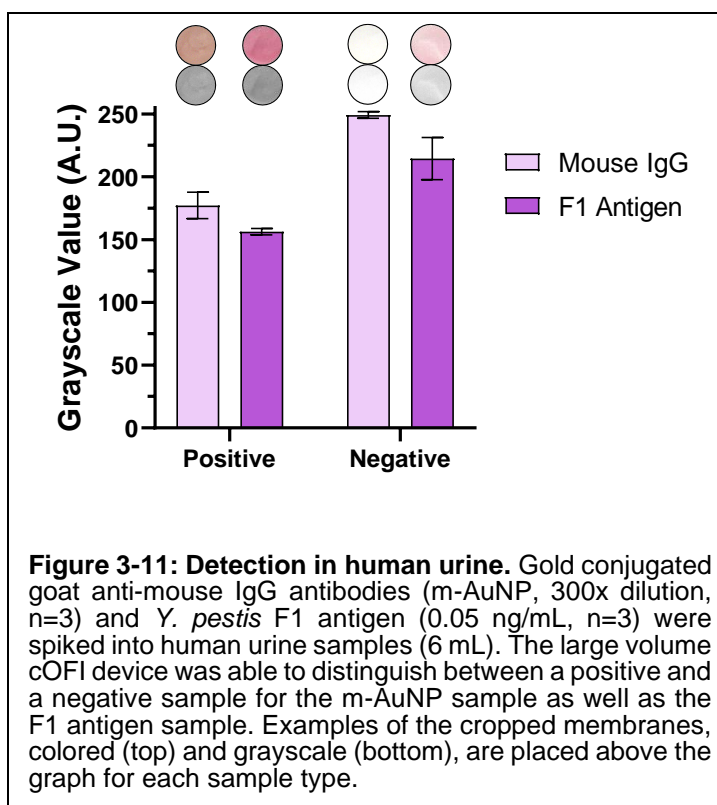
This confirms the findings described by Geise et al. that salt concentration effects pore size (i.e., swelling or deswelling) in polymer membranes (i.e., nitrocellulose).⁴⁶ As previously stated, urine contains a significantly large number of metabolites and these can vary from sample to sample. Based off of the results from **Figure 3-10**, the human urine sample will need to be diluted 1:4 with deionized water in



order for to prevent, or limit, the amount of membrane swelling caused by the presence of salt in urine.⁴⁶⁻⁴⁸ We hypothesized that the amount and type of salt in the artificial urine, and human urine, is causing swelling of the NC membrane due to the sheer volume and assay duration; the swelling of the NC pores is resulting in decreased fluidic discharge and increased membrane fouling. The membrane fouling is clogging the pores causing the m-AuNP to “get stuck’ or non-specifically bind to the NC membrane. Therefore, future studies will need to be performed to eliminate membrane swelling by either removing the salts present in the sample or by using a membrane which is immune to swelling.

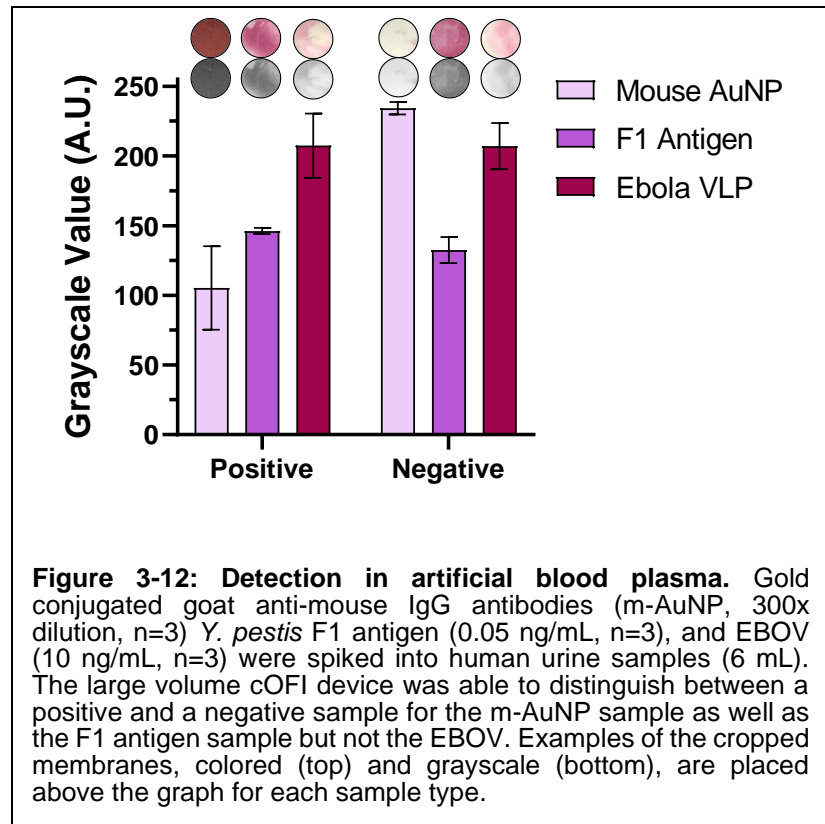
Next, human urine samples, were spiked with *Y. pestis* F1 antigen (0.05 ng/mL, n=3) and m-AuNP (300x dilution, n=3) (**Figure 3-11**). The positive and negative sample GVs were compared for each sample type: m-AuNP positive GV = 177 ± 11 , negative GV = 249 ± 3 ; F1 antigen positive GV = 156 ± 3 , negative GV = 215 ± 17 . When visually inspecting the negative F1 antigen samples, there was a red colorimetric change on the membrane which is an indication of the Yp-AuNP non-specifically binding to the membrane (**Figure 3-11**). It was hypothesized that the salt composition and concentration in the urine samples causes the Yp-AuNP to ‘salt-out’. Previous research has described that the salt concentration in a solution can cause either salting-in or salting-out, and is explained by the Hofmeister effect; this is the strength of specific ions to enable aggregation (precipitation) of proteins in water.⁴⁹⁻⁵⁰ It’s interesting to note that non-specific binding did not occur with the m-AuNP. Even so, the large volume cOFI device

was able to detect the target analytes (F1 antigen and m-AuNP) in a urine sample (**Figure 3-11**). In future work, methods to remove the salts present in biological fluids should be explored by using ion exchange resin either in-tube or by integrating onto the cOFI device.



Lastly, ABP samples (n=3) were prepared then spike with m-AuNP (300x dilution), F1 antigen (0.05 ng/mL), and EBOV (10 ng/mL) (**Figure 3-12**); both F1 antigen and Ebola can be identified in blood serum and plasma.^{24,42,51} A report by Chanteau et al. has described that out of 194 patients who were positive for *Y. pestis* and lived had an average of 42 ng/mL of F1 antigen present in serum. Ebola present in serum or plasma is measure by its viral load, which on average is between 5×10^1 to 7×10^7 pfu/mL (plaque forming unit/mL).²⁴ It is important to note that the conversion from pfu/mL to ng/mL or mg/mL is not possible due to the nature of how the plaque forming assay is performed, but for experimental purposes the EBOV samples were prepared from a stock solution measured in

ng/mL. The positive and negative samples' GV's, respectively, were compared to each sample type: m-AuNP = 105 ± 30 , 234 ± 4 ; F1 antigen = 146 ± 2 , 132 ± 9 ; EBOV = 207 ± 23 , 207 ± 17 . An unpaired, two-tail t-



test ($\alpha = 0.05$) was performed for each of the samples to determine if there was a significant difference between the positive and negative samples. The analysis determined there was a significant difference for m-AuNP samples ($p = 0.005$), there was no significant difference between the F1 antigen samples ($p = 0.179$), and there was no significant difference between the EBOV samples ($p = 0.979$). It can be concluded that the salt content and ionic strength of the ABP has caused non-specific binding to occur on the membrane for both the *Y. pestis* and Ebola reagents.

Similar to removing salts from urine as stated previously, ion exchange resin could be implemented on-disc or in-tube to remove the salts. The ABP used in this study isn't an exact replicate of human blood plasma because there are still other

proteins, immunoglobulins, vitamins, enzymes, and hormones present that may non-specifically bind to the capture and detection antibodies.⁵² Ultimately, when designing an immunoassay, the antibodies used will need to be both specific and sensitive to the target analyte present in complex matrices. With our method of detection, we have been able to show proof-of-concept to detect infectious diseases in human urine with the large volumes cOFI device.

3.4 Conclusions

We presented a novel, centrifugally driven OFI device that can analyze large volumes of fluid (6 mL per sub-chamber, 12 mL total) on a microfluidic disc that employs colorimetric detection and greater sensitivity compared to legacy POC immunoassays (e.g., LFI). First, we leveraged 3D printed technology to design a chamber that holds large volumes under tremendous centrifugal forces during sample analysis, then integrated the chamber onto a centrifugally driven microfluidic disc, increasing the sample volume that can be analyzed 60-fold. Further, by flowing a larger sample volume through the assay, we increased the cOFI sensitivity 2.5-fold, from the Devadhasan *et al.* of 0.025 ng/ml of *Y. pestis* F1 antigen down to 0.01 ng/mL.¹⁴ Finally, we showed real world application with our device by testing 6mL of AU, human urine, and ABP samples spiked with F1 antigen and EBOV; however, we observed non-specific binding on the membrane due to the large amounts of salt present in both human urine and ABP. Future work will entail a method to remove the salts from samples using ion exchange resins to decrease non-specific binding and membrane swelling; next, a multiplexed and automated large volume cOFI disc will be designed to create an easy, portable point-of-need device (**Chapter 4**).

3.5 References

- (1) Mark, D.; Haeberle, S.; Roth, G.; Stetten, F. Von; Zengerle, R. Microfluidic Lab-on-a-Chip Platforms: Requirements, Characteristics and Applications. *Chem. Soc. Rev.* **2010**, *39* (3), 1153–1182. <https://doi.org/10.1039/b820557b>.
- (2) Gorkin, R.; Park, J.; Siegrist, J.; Amasia, M.; Lee, B. S.; Park, J.-M.; Kim, J.; Kim, H.; Madou, M.; Cho, Y.-K. Centrifugal Microfluidics for Biomedical Applications. *Lab Chip* **2010**, *10*, 1758–1773. <https://doi.org/10.1039/b924109d>.
- (3) Reyes, D. R.; Iossifidis, D.; Auroux, P.-A.; Manz, A. Micro Total Analysis Systems. 1. Introduction, Theory, and Technology. *Anal. Biochem.* **2002**, *74*, 2623–2636. <https://doi.org/10.1021/ac0202435>.
- (4) Gong, M. M.; Sinton, D. Turning the Page: Advancing Paper-Based Microfluidics for Broad Diagnostic Application. *Chem. Rev.* **2017**, *117*, 8447–8480. <https://doi.org/10.1021/acs.chemrev.7b00024>.
- (5) Madou, M.; Zoval, J.; Jia, G.; Kido, H.; Kim, J.; Kim, N. Lab on a CD. *Annu. Rev. Biomed. Eng.* **2006**, *8*, 601–628. <https://doi.org/10.1146/annurev.bioeng.8.061505.095758>.
- (6) Xie, Y.; Dai, L.; Yang, Y. Microfluidic Technology and Its Application in the Point-of-Care Testing Field. *Biosens. Bioelectron.* **2022**, *10*. <https://doi.org/10.1016/j.biosx.2022.100109>.
- (7) Gubala, V.; Harris, L. F.; Ricco, A. J.; Tan, M. X.; Williams, D. E. Point of Care Diagnostics: Status and Future. *Anal. Chem.* **2012**, *84*, 487–515. <https://doi.org/10.1021/ac2030199>.
- (8) Posthuma-Trumpie, G. A.; Korf, J.; Van Amerongen, A. Lateral Flow (Immuno)Assay: Its Strengths, Weaknesses, Opportunities and Threats. A Literature Survey. *Anal. Bioanal. Chem.* **2009**, *393*, 569–582. <https://doi.org/10.1007/s00216-008-2287-2>.
- (9) Jiang, N.; Ahmed, R.; Damayantharan, M.; Ünal, B.; Butt, H.; Yetisen, A. K. Lateral and Vertical Flow Assays for Point-of-Care Diagnostics. *Adv. Healthc. Mater.* **2019**, *8* (14). <https://doi.org/10.1002/ADHM.201900244>.
- (10) Chen, P.; Gates-Hollingsworth, M.; Pandit, S.; Park, A.; Montgomery, D.; AuCoin, D.; Gu, J.; Zenhausern, F. Paper-Based Vertical Flow Immunoassay (VFI) for Detection of Bio-Threat Pathogens. *Talanta* **2019**, *191* (August 2018), 81–88. <https://doi.org/10.1016/j.talanta.2018.08.043>.
- (11) Li, F.; You, M.; Li, S.; Hu, J.; Liu, C.; Gong, Y.; Yang, H.; Xu, F. Paper-Based Point-of-Care Immunoassays: Recent Advances and Emerging Trends. *Biotechnol. Adv.* **2019**, *39*. <https://doi.org/10.1016/j.biotechadv.2019.107442>.
- (12) Kim, S.; Hao, Y.; Miller, E. A.; Tay, D. M. Y.; Yee, E.; Kongsuphol, P.; Jia, H.; Mcbee, M.; Preiser, P. R.; Sikes, H. D. Vertical Flow Cellulose-Based Assays for SARS-CoV-2 Antibody Detection in Human Serum. *ACS Sensors* **2021**, *6*, 1891–1898. <https://doi.org/10.1021/acssensors.1c00235>.
- (13) Joung, H.-A.; Ballard, Z. S.; Ma, A.; Tseng, D. K.; Teshome, H.; Burakowski, S.; Garner, O. B.; Di, D.; Eg, C.; Ozcan, A. Paper-Based Multiplexed Vertical Flow Assay for Point-of-Care Testing. *Lab Chip* **2019**, *19*, 1027.

- <https://doi.org/10.1039/c9lc00011a>.
- (14) Devadhasan, J. P.; Gu, J.; Chen, P.; Smith, S.; Thomas, B.; Gates-Hollingsworth, M.; Hau, D.; Pandit, S.; AuCoin, D.; Zenhausern, F. Critical Comparison between Large and Mini Vertical Flow Immunoassay Platforms for *Yersinia Pestis* Detection. *Anal. Chem.* **2021**, *acs.analchem.0c05278*. <https://doi.org/10.1021/acs.analchem.0c05278>.
 - (15) Hsu, H.-L.; Chuang, C.-C.; Liang, C.-C.; Chiao, D.-J.; Wu, H.-L.; Wu, Y.-P.; Lin, F.-P.; Shyu, R.-H. Rapid and Sensitive Detection of *Yersinia Pestis* by Lateral-Flow Assay in Simulated Clinical Samples. *BMC Infect. Dis.* **2018**, *18* (402). <https://doi.org/10.1186/s12879-018-3315-2>.
 - (16) Loïez, C.; Herwegh, S.; Wallet, F.; Armand, S.; Guinet, F.; Courcol, R. J. Detection of *Yersinia Pestis* in Sputum by Real-Time PCR. *J. Clin. Microbiol.* **2003**, *41* (10), 4873–4875. <https://doi.org/10.1128/JCM.41.10.4873-4875.2003/FORMAT/EPUB>.
 - (17) Jauset-Rubio, M.; Tomaso, H.; El-Shahawi, M. S.; Bashammakh, A. S.; Al-Youbi, A. O.; O’Sullivan, C. K. Duplex Lateral Flow Assay for the Simultaneous Detection of *Yersinia Pestis* and *Francisella Tularensis*. *Anal. Chem.* **2018**, *90* (21), 12745–12751. https://doi.org/10.1021/ACS.ANALCHEM.8B03105/SUPPL_FILE/AC8B03105_SI_001.PDF.
 - (18) Choi, S. Y.; Rhie, G. eun; Jeon, J. H. Development of a Double-Antibody Sandwich ELISA for Sensitive Detection of *Yersinia Pestis*. *Microbiol. Immunol.* **2020**, *64* (1), 72–75. <https://doi.org/10.1111/1348-0421.12751>.
 - (19) Woolf, M.; Dignan, L.; Karas, S.; Lewis, H.; Hadley, K.; Nauman, A.; Gates-Hollingsworth, M.; AuCoin, D.; Green, H.; Geise, G.; et al. Characterization of a Centrifugal Microfluidic Orthogonal Flow Platform. *Micromachines* **2022**, *13* (3), 487. <https://doi.org/10.3390/MI13030487>.
 - (20) Jansen, H. J.; Breeveld, F. J.; Stijnis, C.; Grobusch, M. P. Biological Warfare, Bioterrorism, and Biocrime. *Clin. Microbiol. Infect.* **2014**, *20* (6), 488–496. <https://doi.org/10.1111/1469-0691.12699>.
 - (21) Thompson, B. L.; Ouyang, Y.; Duarte, G. R. M.; Carrilho, E.; Krauss, S.; Landers, J. P. Inexpensive, Rapid Prototyping of Microfluidic Devices Using Overhead Transparencies and a Laser Print, Cut, and Laminate Fabrication Method. *Nat. Protoc.* **2015**, *10* (6), 875–886. <https://doi.org/10.1038/nprot.2015.051>.
 - (22) *Standard Materials for High-Resolution Rapid Prototyping*; 2017.
 - (23) Hau, D.; Wade, B.; Lovejoy, C.; Pandit, S. G.; Reed, D. E.; DeMers, H. L.; Green, H. R.; Hannah, E. E.; McLarty, M. E.; Creek, C. J.; et al. Development of a Dual Antigen Lateral Flow Immunoassay for Detecting *Yersinia Pestis*. *PLoS Negl. Trop. Dis.* **2022**, *16* (3), e0010287. <https://doi.org/10.1371/JOURNAL.PNTD.0010287>.
 - (24) Demers, H. L.; He, S.; Pandit Id, S. G.; Hannah Id, E. E.; Zhang, Z.; Yan, F.; Greenid, H. R.; Reyes, D. F.; Huid, D.; Mclartyid, M. E.; et al. Development of an Antigen Detection Assay for Early Point-of-Care Diagnosis of Zaire Ebolavirus. *PLoS Negl. Trop. Dis.* **2020**, *14* (11). <https://doi.org/10.1371/journal.pntd.0008817>.

- (25) Sarigul, N.; Korkmaz, F.; Kurultak, İ. A New Artificial Urine Protocol to Better Imitate Human Urine. *Sci. Rep.* **2019**, *9*. <https://doi.org/10.1038/s41598-019-56693-4>.
- (26) Liu, L.; Shou, L.; Yu, H.; Yao, J. Mechanical Properties and Corrosion Resistance of Vulcanized Silicone Rubber after Exposure to Artificial Urine. *J. Macromol. Sci. Part B Phys.* **2015**, *54* (8), 962–974. <https://doi.org/10.1080/00222348.2015.1042624>.
- (27) Woolf, M. S.; Dignan, L. M.; Scott, A. T.; Landers, J. P. Digital Postprocessing and Image Segmentation for Objective Analysis of Colorimetric Reactions. *Nat. Protoc.* **2020**, *16*, 218–238. <https://doi.org/10.1038/s41596-020-00413-0>.
- (28) Akazawa-Ogawa, Y.; Nagai, H.; Hagihara, Y. Heat Denaturation of the Antibody, a Multi-Domain Protein. *Biophys. Rev.* **2018**, *10* (2), 255–258. <https://doi.org/10.1007/S12551-017-0361-8>.
- (29) Fredrickson, C. K.; Fan, Z. H. Macro-to-Micro Interfaces for Microfluidic Devices. *Lab Chip* **2004**, *4*, 526–533. <https://doi.org/10.1039/b410720a>.
- (30) Everitt, M. L.; Tillery, A.; David, M. G.; Singh, N.; Borison, A.; White, I. M. A Critical Review of Point-of-Care Diagnostic Technologies to Combat Viral Pandemics. *Anal. Chim. Acta* **2021**, *1146*, 184–199. <https://doi.org/10.1016/J.ACA.2020.10.009>.
- (31) Wang, C.; Liu, M.; Wang, Z.; Li, S.; Deng, S.; He, N. Point-of-Care Diagnostics for Infectious Diseases: From Method to Devices. *Nano Today* **2021**, *37*. <https://doi.org/10.1016/j.nantod.2021.101092>.
- (32) Al-Faqheri, W.; Hwai Gilbert Thio, T.; Ameen Qasaimeh, M.; Dietzel, A.; Madou, M.; Al-Halhouli, A. Particle/Cell Separation on Microfluidic Platforms Based on Centrifugation Effect: A Review. *Microfluid. Nanofluidics* **2017**, *21*, 102. <https://doi.org/10.1007/s10404-017-1933-4>.
- (33) Bailes, J.; Mayoss, S.; Teale, P.; Soloviev, M. Gold Nanoparticle Antibody Conjugates for Use in Competitive Lateral Flow Assays. *Methods Mol. Biol.* **2012**, *906*, 45–55. https://doi.org/10.1007/978-1-61779-953-2_4.
- (34) Dykman, L.; Khlebtsov, N. Gold Nanoparticles in Biomedical Applications. *Gold Nanoparticles in Biomedical Applications*. 2017, pp 1–332. <https://doi.org/10.1201/b22465>.
- (35) Products, M. S.; Science, C.; Products, N.; Nanofibers, C.; Nanostructures, G.; Mesoporous, G.; Nanoparticles, G.; Nanoparticles, S.; Dots, Q.; Advantage, Q.; et al. Gold Nanoparticles: Properties and Applications Optical & Electronics Properties of Gold Nanoparticles. *Sigma Aldrich* **2016**, 8–12.
- (36) Yeh, Y.-C.; Creran, B.; Rotello, V. M. Gold Nanoparticles: Preparation, Properties, and Applications in Bionanotechnology. *Nanoscale* **2012**, *4* (6), 1871–1880. <https://doi.org/10.1039/c1nr11188d>.
- (37) Wong, R. C.; Tse, H. Y. *Lateral Flow Immunoassay*; Humana Press, 1981; Vol. 53.
- (38) Rabinovitch, A.; Sarewitz, S. J.; Woodcock, S. M.; Allinger, D. B.; Azar, M.; Dynek, D. A.; Robinowitz, M.; Slade, B. A. *Urinalysis and Collection, Transportation, and Preservation of Urine Specimens; Approved Guideline*

— *Second Edition Serving the World ' s Medical Science Community Through Voluntary Consensus*; 2001; Vol. 21.

- (39) Lifshitz, E.; Kramer, L. Outpatient Urine Culture. *Arch. Intern. Med.* **2000**, *160* (16), 2537. <https://doi.org/10.1001/archinte.160.16.2537>.
- (40) Bouatra, S.; Aziat, F.; Mandal, R.; Guo, A. C.; Wilson, M. R. The Human Urine Metabolome. *PLoS One* **2013**, *8* (9). <https://doi.org/10.1371/journal.pone.0073076>.
- (41) Choi, S.-Y.; Rhie, G.; Jeon, J. H. Development of a Double-Antibody Sandwich ELISA for Sensitive Detection of Yersinia Pestis. *Microbiol. Immunol.* **2020**, *64* (1), 72–75. <https://doi.org/10.1111/1348-0421.12751>.
- (42) Chanteau, S.; Rahalison, L.; Ratsitorahina, M.; Mahafaly; Rasolomaharo, M.; Boisier, P.; O'Brien, T.; Aldrich, J.; Keleher, A.; Morgan, C.; et al. Early Diagnosis of Bubonic Plague Using F1 Antigen Capture ELISA Assay and Rapid Immunogold Dipstick. *Int. J. Med. Microbiol.* **2000**, *290* (3), 279–283. [https://doi.org/10.1016/S1438-4221\(00\)80126-5](https://doi.org/10.1016/S1438-4221(00)80126-5).
- (43) Ren Schubert, S.; Cuenca, S.; Fischer, D.; Rgen Heesemann, J. High-Pathogenicity Island of Yersinia Pestis in Enterobacteriaceae Isolated from Blood Cultures and Urine Samples: Prevalence and Functional Expression. *J. Infect. Dis.* **2000**, *182*, 1268–1271.
- (44) Barr, D. B.; Wilder, L. C.; Caudill, S. P.; Gonzalez, A. J.; Needham, L. L.; Pirkle, J. L. Urinary Creatinine Concentrations in the U.S. Population: Implications for Urinary Biologic Monitoring Measurement. *Environ. Health Perspect.* **2005**, *113* (2).
- (45) Taylor, E. N.; Curhan, G. C. Differences in 24-Hour Urine Composition between Black and White Women Materials and Methods Study Population and Ascertainment of Race. *J. Am. Soc. Nephrol.* **2007**, *18*, 654–659. <https://doi.org/10.1681/ASN.2006080854>.
- (46) Geise, G. M.; Paul, D. R.; Freeman, B. D. Fundamental Water and Salt Transport Properties of Polymeric Materials. *Prog. Polym. Sci.* **2014**, *39*, 1–42. <https://doi.org/10.1016/j.progpolymsci.2013.07.001>.
- (47) Sun, S.; Feng, S.; Ji, C.; Shi, M.; He, X.; Xu, F.; Lu, J. Microstructural Effects on Permeability of Nitrocellulose Membranes for Biomedical Applications. *J. Memb. Sci.* **2020**, *595*, 117502. <https://doi.org/10.1016/j.memsci.2019.117502>.
- (48) Geise, G. M.; Hickner, M. A.; Logan, B. E. Ammonium Bicarbonate Transport in Anion Exchange Membranes for Salinity Gradient Energy. *ACS Macro Lett.* **2013**, *2* (9), 814–817. <https://doi.org/10.1021/mz4003408>.
- (49) Arosio, P.; Jaquet, B.; Wu, H.; Morbidelli, M. On the Role of Salt Type and Concentration on the Stability Behavior of a Monoclonal Antibody Solution. *Biophys. Chem.* **2012**, *168–169*, 19–27. <https://doi.org/10.1016/j.bpc.2012.05.004>.
- (50) Zhang, L.; Zhang, J. Specific Ion-Protein Interactions Dictate Solubility Behavior of a Monoclonal Antibody at Low Salt Concentrations. *Mol. Pharm.* **2012**, *9* (9), 2582–2590. <https://doi.org/10.1021/mp300183a>.
- (51) Breechin, N. J.; Fenech, M.; Houlihan, C. F. Ebola Virus Disease. *Br. Med. J.* **2014**, *349*. <https://doi.org/10.1136/bmj.g7348>.

- (52) Issaq, H. J.; Xiao, Z.; Veenstra, T. D. Serum and Plasma Proteomics. *Chem. Rev.* **2007**, *107*, 3601–3620. <https://doi.org/10.1021/cr068287r>.

CHAPTER 4 – The Development of a Smartphone Point-of-Care Diagnostic Device a Centrifugal Microfluidic Orthogonal Flow Immunoassay

4.1 Introduction

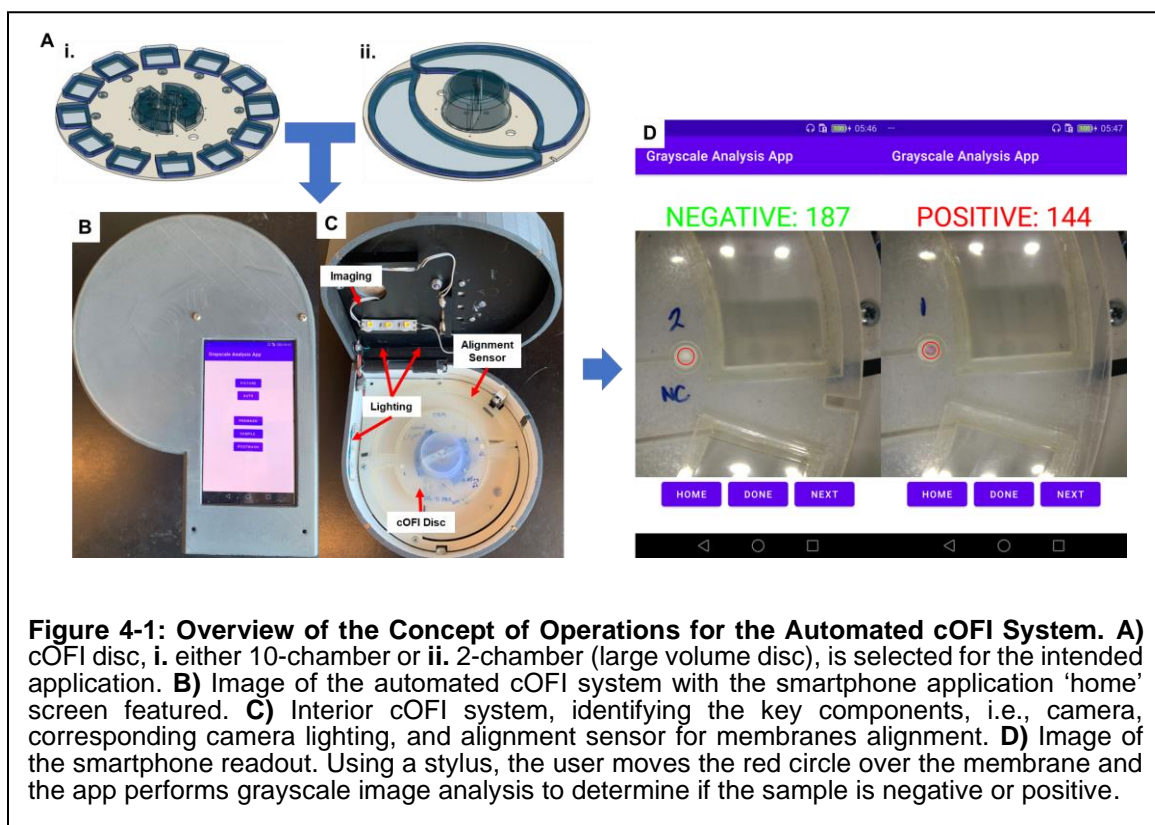
Point-of-Care (POC) testing has become a household phrase since the outbreak of the SARS-CoV-2 (COVID-19) pandemic in 2020 due to the rapid need to test and diagnose large populations of people.¹ POC testing, or POC diagnostics, is defined as the ability to provide fast, real-time, and accurate diagnosis of an individual at or near the point-of-need (PoN).²⁻⁴ The World Health Organization (WHO) has defined a set of criteria for the consideration of POC devices; they must be affordable, sensitive, specific, user-friendly, rapid and robust.⁴ These “ASSURED” criteria set the guidelines for manufactures and researchers to follow in order to meet the requirements of the healthcare system.⁴ POC devices enable decentralized testing, whereby a conventional laboratory is not required and the need for highly trained personnel and expensive laboratory equipment is eliminated.^{2,5} There has been significant research and growth in the microfluidic community to develop small, rapid, and sensitive POC devices to be used at the PoN. Despite these efforts, the majority of viral pathogen testing takes place in a laboratory environment, far from the location the sample was collected.¹

Microfluidic devices, including micro total analysis systems (μ TAS) and lab-on-a-chip (LOC) based systems, have been on the leading edge of POC devices since the concept of miniaturizing laboratory analysis was developed in the 1990s.⁶ Some common POC microfluidic devices used every day include the pregnancy test (i.e., lateral flow immunoassay (LFI)) and blood glucose assay for diabetes monitoring.^{5,7} These applications are popular because they are inexpensive, easy-

to-use, fast, and sensitive; which follows the WHO ASSURED criteria. Another advantage of POC devices is their ability to provide the user with a result, direct from the sample without requiring any sample preparation (i.e., extraction, purification, or amplification) and in approximately 10 minutes.^{1,4} Ideally, a 'sample-to-answer' POC device is inexpensive, requires no sample preparation by the user, and utilizes a small, portable interfacing technology, often an instrument; previously reported research has shown centrifugal microfluidics helping propel sample-to-answer devices to meet these requirements, especially during the COVID-19 pandemic.^{1,8,9} Centrifugal microfluidics employs rotational forces to samples and reagents on a compact-disc to move fluid through the microfluidic channels, radially outward from the center of rotation (CoR).¹⁰ This method of fluid movement eliminates the need for large equipment or clean-room manufacturing during development, bringing costs per device down. Lab-on-a-disc (LoaD) systems have been developed to perform sample lysis and extraction, purification, and targeted amplification steps, among other things. In total, the capacity of LoaD devices to enable sample-to-answer POC diagnosis makes them popular and attractive.⁸⁻¹⁰

Here, we describe the development of a portable, smartphone controlled POC diagnostic system that uses the centrifugal orthogonal flow immunoassay (cOFI) discs, described in **Chapters 2** and **3**. The system described permits either a 10-chamber multiplex or large volume sample analysis, depending on the end-user's need (**Figure 4-1A**). For operation, the cOFI disc is placed into the POC system and each step is controlled using the custom smartphone application (e.g.,

app) (**Figure 4-1B**). The cOFI analysis system includes an onboard motor to control the disc's rotational frequency, a camera to image the nitrocellulose (NC) membrane, and a sensor for disc alignment to perform automated image analysis via a corresponding smartphone. The smartphone app was programmed to capture an image of the NC membrane and complete image analysis to determine if the sample was positive or negative for the target analyte (**Figure 4-1D**). Using *Y. pestis* as a model organism, we demonstrated the system's ability to perform all three assay steps on the cOFI disc (i.e., pre-wash, sample, and post-wash) and detect *Y. pestis* F1 antigen as low as 0.01 ng/mL. Ultimately, we showed a proof-of-concept, portable, POC device that detects infectious diseases with an android smartphone application.



4.2 Experimental Section

4.2.1 Fabrication of the Multiplexed cOFI Disc

Microfluidic cOFI devices were fabricated using the print-cut-laminate (PCL) method.¹¹ Each device was comprised of seven polyethylene terephthalate (PET, 101.6 μm thickness, Film Source Inc., Maryland Heights, MO U.S.A.) sheets alternated with heat sensitive adhesive (HSA, 50.8 μm thickness, EL-7970-39, Adhesive Research Inc., Glen Rock, PA U.S.A) (**Figure 4-2**). The disc architecture for each layer was designed using AutoCAD® 2020 (Autodesk Inc., San Rafael, CA, U.S.A.) and laser ablated using a 50W CO₂ laser engraving system (VLS3.50, Universal Laser Systems®, Scottsdale, AZ, U.S.A.). Layers 1 and 7 were considered capping layers, while layers 2 and 6 contained the microfluidic channels. Layers 3 and 5 were via layers containing circular orthogonal flow ports (2 mm diameter). The flow ports directed flow to and through layer 4, which contained 4 mm circular cutouts of the nitrocellulose (NC) membranes (0.2 μm pore size, Whatman ProTran BA 83, Marlborough, MA U.S.A.). To activate the HSA, the disc layers were aligned and lamination bonded (185-195°C) (UltraLam 250B, Akiles Products Inc., Mira Loma, CA, U.S.A.) in three separate steps. First, disc layers 3-5 were aligned, NC membrane cutouts were inserted in layer 4 and bonded together when passed through an office laminator (2 passes). Second, layers 6 and 7 were aligned and laminated to layers 3-5 (2 passes). Finally, layers 1 and 2 were aligned and laminated to the previously bonded layers (2 passes). The three separate lamination steps were completed to allow the HSA to properly bond the PET layers together.

Polymethyl methacrylate (PMMA, 1.5 mm McMaster-Carr, Elmhurst, IL U.S.A.) was used to increase sample recovery chamber volumes. PMMA pieces and PET coverlets were affixed to the cOFI disc using pressure sensitive adhesive (PSA, 55.8 μm thickness, ARcare 7876, Adhesive Research Inc., Glen Rock, PA U.S.A.). Layer 1 contains a 2 mm access port to allow for the NC membranes to be blotted with assay reagents post-lamination and capped with PET using PSA. Completely assembled discs were placed in foil moisture barrier bags (Dri-shield™, Uline, Pleasant Prairie, WI, U.S.A.) with two 3-gram silica moisture absorbent packets (S-3904, Uline) overnight and pressed (15 lbs) to ensure PSA adhesions.

4.2.2 Fabrication of the Multiplexed 3D-Printed Sample Chamber

The sample chamber was designed using Autodesk Fusion 360 (Autodesk Inc., San Rafael, CA, U.S.A.); designs were printed with a FormLabs 3B stereolithography 3D-printer (FormLabs Inc., Somerville, MA, U.S.A.) with clear v4 resin (Formlabs Inc., Somerville, MA, U.S.A.).¹² The inside of each sample sub-chamber was blocked with 100 μL of blocking buffer solution (0.25% phosphate buffered saline-tween, PBS-T; 0.1% Bovine Serum Albumin) and placed in a convection oven (Binder 056FD – Convection Oven, P.O. Box 102, 78502 Tuttlingen, Germany) at 37°C for 1 hour. The multiplexed chamber was manually aligned and attached to the cOFI disc using PSA (**Figure 4-2**).

4.2.3 Automated cOFI System, Image Processing and Data Analysis

The automated cOFI system included three assay steps with a combined image processing and data analysis step. Each step is controlled using a Huawei p9 smartphone (Huawei Technologies Co., Shenzhen, China) and an android

application featuring custom programming. The three assay steps, controlled using the app, included a pre-wash step (2000 RPM, 200 sec), a sample step (2000 RPM, 2000 sec), and a post-wash step (2000 RPM, 200 sec) (**Figure 4-3**). For each assay step, the user manually pipettes assay reagents (e.g., wash buffer or sample fluid) into the sample chamber(s) and executes the next step using the app.

Following these steps, each membrane on the cOFI disc is digitally imaged using the camera on the Huawei p9 smartphone with each image being manually captured by the user. Next, the user drags and centers a red circle (diameter = 100 pixels) over the NC membrane using either their finger or a stylus. The app automatically analyzes a 50-pixel diameter region of interest (ROI) in the center of the red circle. Simultaneously, the app converts the 50-pixel area from RGB to weighted 8-bit grayscale, whereby the average grayscale value (GV) is determined for the selected ROI. For clarity, the GV can fall within 0-255, where 0 is black and 255 is pure white.

For the proof-of-concept studies utilizing the *Y. pestis* F1 antigen, the app is programmed to complete analysis with a corresponding GV threshold of 165; here, any GV that was equal to or greater than 165 is considered a negative result and any GV less than 165 is considered a positive result. Further, a positive result will produce a 'red' color change to the NC membrane and indicates the sample fluid contains the target analyte. The threshold GV was determined by calculating the limit-of-detection (LOD) of the automated cOFI system (LOD = Negative Control Mean – (3 x Standard Deviation of the Negative Control Mean)).

4.2.4 Proof-of-Concept: Multiplexed Immunocapture Study

In this study, 2.5 μL of mouse whole molecule, IgG antibodies (mIgG) (Jackson ImmunoResearch Laboratories Inc., West Grove, PA, U.S.A.) were manually blotted and immobilized onto 4 mm NC membranes through the 2 mm access port in layer 1 (2.5 μL , 5.5 mg/mL). The NC membranes were dried at 37°C for 1 hour in a convection oven (Binder 056FD – Convection Oven, P.O. Box 102, 78502 Tuttlingen, Germany). mIgG was not immobilized on the membranes for the negative control. Each membrane was subsequently blocked with a blocking buffer solution (2.5 μL /membrane) and dried in the convection oven at 37°C for 1 hour. The discs were placed in foil moisture barrier bags (Dri-shield™, Uline, Pleasant Prairie, WI, U.S.A.) with two 3-gram silica moisture absorbent packets (S-3904, Uline) for a minimum of 24 hours.

A pre-wash step (40 μL) was performed using 1x PBS-T, pH = 7.5 (Thermo Fisher Scientific, Waltham, MA USA 02451) pipetted into the sample chamber (2000 RPM, 200 sec). Sample solutions were prepared using 40 nm colloidal gold nanoparticle conjugated goat anti-mouse IgG antibodies (m-AuNP; OD 10.0 at 529 nm, Jackson ImmunoResearch Laboratories, Inc., West Grove, PA, U.S.A.), diluted (200-800x) with PBS-T, and incubated in-tube at room temperature for 20 min. Negative controls consisted of PBS-T buffer and m-AuNP (200x dilution). Each sample solution (200 μL) was pipetted into the sample chamber and centrifugally-driven through the membrane at 2000 RPM for 2000 sec. A final post-wash step (40 μL PBS-T buffer, 2000 RPM, 200 sec) was performed to remove any excess sample from the membrane.

4.2.5 Detection of *Y. pestis* F1 Antigen on the Multiplexed cOFI Disc

Y. pestis reagents were prepared in the Diagnostics Discovery Laboratory (School of Medicine, University of Nevada, Reno, NV, U.S.A.) as per the protocol described in Hau et al.¹³ The multiplexed cOFI disc was assembled as described in Section 4.2.1. The membranes were blotted post-lamination with 2.5 μ L of Yp11C7 0416 IgG1 (Yp-mAb) (*Y. pestis* F1 antigen specific mAb, 5.85 mg/mL), then the discs were incubated at 37°C for 1 hour in a convection oven (Binder 056FD – Convection Oven, P.O. Box 102, 78502 Tuttlingen, Germany). Next, each membrane was blocked with blocking buffer solution (2.5 μ L) through the 2 mm access port in layer 1 and placed in the oven at 37°C for 1 hour.

A pre-wash step (40 μ L) was performed using *Y. pestis* chase buffer, or 50 mM carb-bicarbonate buffer at pH = 9.6, prepared from sodium bicarbonate (Thermo Fisher Scientific, Waltham, MA USA 02451) and sodium carbonate (Thermo Fisher Scientific, Waltham, MA USA 02451), pipetted into the sample chamber (2000 RPM, 200 sec). Sample solutions (200 μ L) of the *Y. pestis* F1 antigen were prepared at concentrations ranging from 10-0.025 ng/mL and diluted in chase buffer. Aliquots of each antigen dilution were mixed with 10 μ L of Yp3F2 gold conjugate (Yp-AuNP, OD 10.1 at 520 nm), and incubated in-tube at room temperature for 20 min. Negative controls consisted of 200 μ L of chase buffer and 10 μ L of Yp-AuNP. Sample solutions were loaded into the sample chambers and centrifugally-driven through the membrane at 2000 RPM for 2000 sec. To complete the on-disc assay, a post-wash step (40 μ L chase buffer, 2000 RPM, 200 sec) was performed to remove any excess sample from the membrane.

4.2.6 Detection of *Y. pestis* F1 Antigen on the Large Volume cOFI Disc

The large volume cOFI disc was assembled as described in Section 4.2.1.

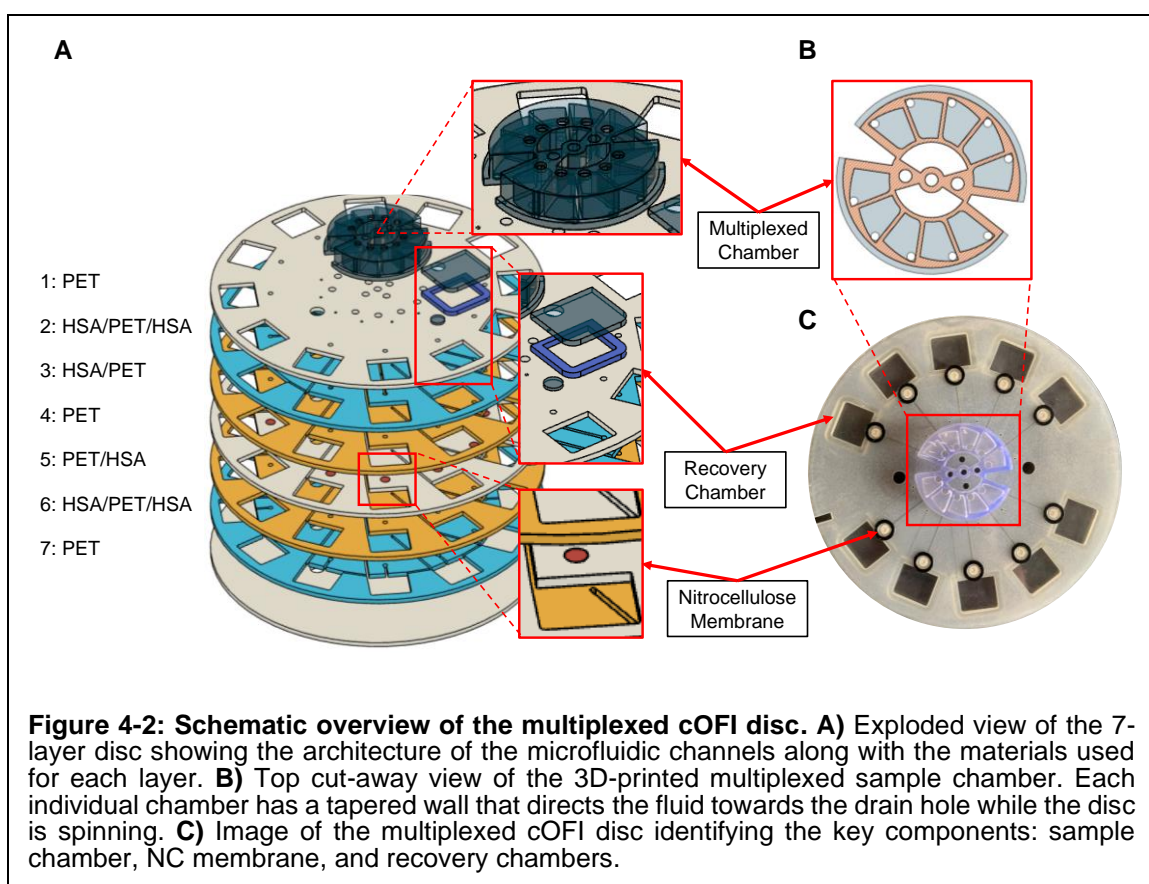
The membranes were blotted post-lamination with 2.5 μ L of Yp11C7 0416 IgG1 (Yp-mAb) (*Y. pestis* F1 antigen specific mAb, 5.85 mg/mL), then the discs were incubated at 37°C for 1 hour in a convection oven (Binder 056FD – Convection Oven, P.O. Box 102, 78502 Tuttlingen, Germany). Next, each membrane was blocked with blocking buffer solution (2.5 μ L) through the 2 mm access port in layer 1 and placed in the oven at 37°C for 1 hour.

A pre-wash step (400 μ L) was performed using *Y. pestis* chase buffer, or 50 mM carb-bicarbonate buffer at pH = 9.6, prepared from sodium bicarbonate (Thermo Fisher Scientific, Waltham, MA USA 02451) and sodium carbonate (Thermo Fisher Scientific, Waltham, MA USA 02451), and pipetted into the sample chamber (2000 RPM, 200 sec). A total of 6 mL of sample solutions of the *Y. pestis* F1 antigen were prepared at 10-0.01 ng/mL in chase buffer. Aliquots of each antigen dilution were mixed with 10 μ L of Yp3F2 gold conjugate (Yp-AuNP, OD 10.1 at 520 nm), and incubated in-tube at room temperature for 20 min. Negative controls consisted of 6 mL of chase buffer and 10 μ L of Yp-AuNP. Sample solutions were loaded into the sample chambers and centrifugally pumped through the membrane at 2000 RPM for 2000 sec. Finally, a post-wash step (500 μ L chase buffer, 2000 RPM, 200 sec) was performed to remove any excess sample from the membrane.

4.3 Results and Discussion

4.3.1 Fabrication and Design of the Multiplexed cOFI Disc

Previous designs and characterization studies of the cOFI discs were described in **Chapters 2** and **3**. Here, focus will shift to the modification of an 8-plex cOFI disc to a 10-plex disc; this is achieved with 3D-printed architectural features, incorporated into the 7-layer design (**Figure 4-2**). The 10-plex design increased the capability of the system, enabling the detection of more target analytes from a single sample, while maintaining the long inlet channel (43 mm), described in **Chapter 2**. As discussed previously, the long channel is important for maintaining hydraulic pressure throughout the assay's duration as fluid drains from the sample chamber. Here, 3D-printing the sample chamber eliminates the potential for sample loss, as experienced with the previously designed 1.5 mm

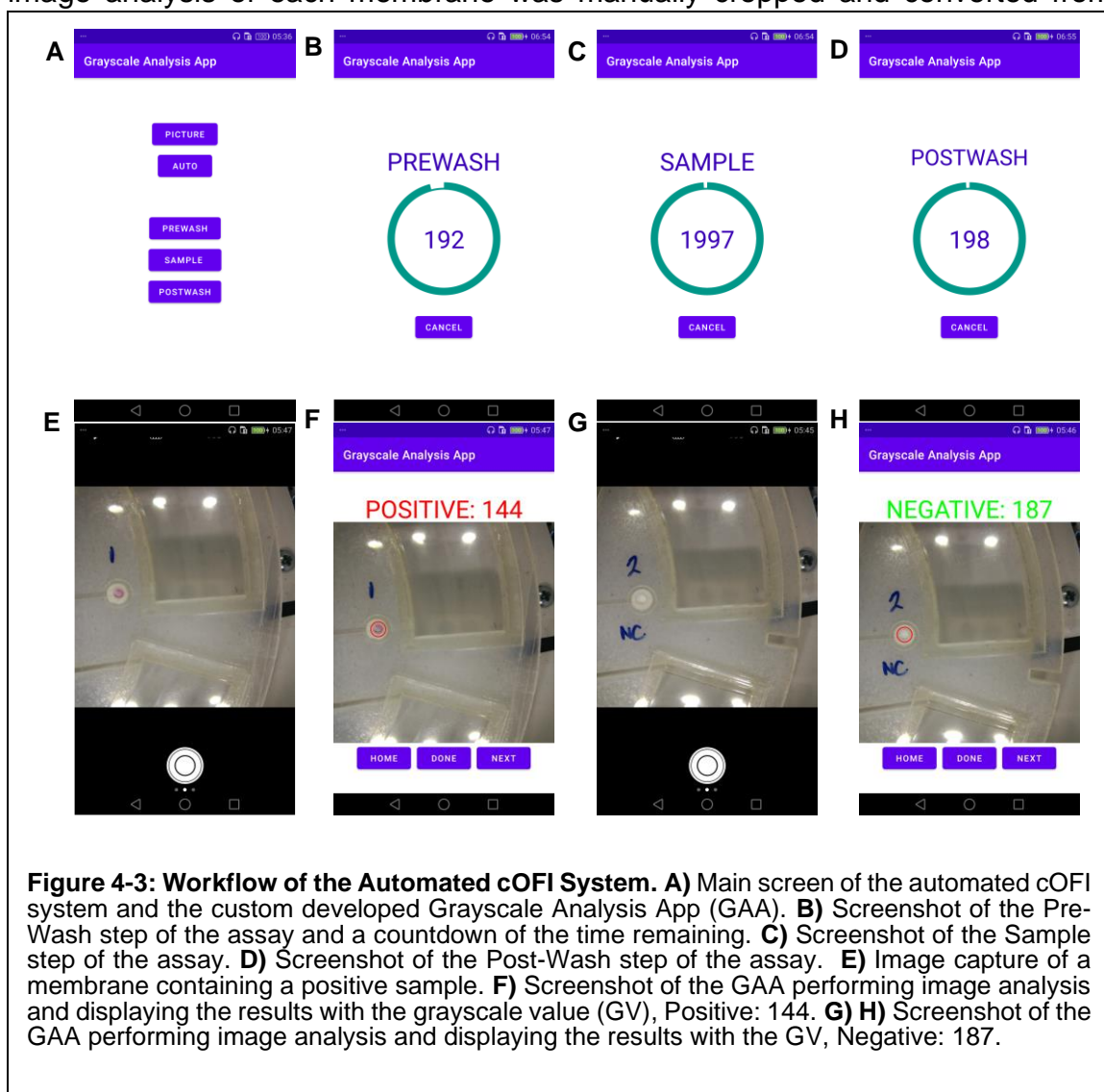


thick PMMA sample chamber(s). Further, the 3D printed chamber decreases the number of steps required for assembly and permits increased fluid volume retention, as each sub-chamber holds up to 440 μL . In the future, the multiplex cOFI disc could be injection molded, further simplifying the assembly and decreasing the overall cost of manufacturing the disc.

The multiplexed chamber was designed in a similar fashion as the large volume sample chamber described in **Chapter 3**. Each sub-chamber contains tapered walls to direct the sample fluid toward the drain hole during disc rotation (**Figure 4-2B**). The tapered wall was designed to ensure that fluid would not be driven against the wall by centrifugal force and result in improper fluid drainage. The multiplexed chamber was also designed to be modular; depending on the concept of operations, defined by the end user, the sample chamber can be modified to handle larger volumes, up to 1 mL per sub-chamber by simply making the overall height of the chamber taller. For this design, the chamber height is 9 mm, with 4.4 mL total capacity, and can be increased to accommodate the desired sample volume (e.g., 18 mm tall, for an 8.4 mL capacity), without effecting the integrity (i.e., leaking) of the chamber or cOFI disc. Increasing the volumetric capacity of the sample chamber will require increasing the size of the recovery chambers as well. The incorporated design changes permit multiplexed analysis of up to 10 different targets with a range of sample fluid types (i.e., urine, saliva, blood plasma). Further, the large chamber capacities mitigate issues associated with the stochastic effects experienced with many POC devices, as they struggle to overcome to macro-to-micro interface issue.

4.3.2 Automated cOFI System, Image Processing and Data Analysis

The previous section described a newly modified multiplexed cOFI disc. Here, we describe the development of an automated cOFI system which integrates the three assay steps with image processing and data analysis completed with a smartphone application featuring a custom program (**Figure 4-3**). Initially, the cOFI discs were spun using a custom-built mechatronic system which required the user to manually control the rotational frequency and spin duration. Once the assay steps were complete, the discs were manually imaged on a desktop scanner. The image analysis of each membrane was manually cropped and converted from



RGB to 8-bit grayscale using Fiji ImageJ.^{14,15} The mechatronic spin system and multistep analysis procedure, while effective and robust, is not ideal for a POC device in either developed countries or forward operating locations.

To enhance the portability of the system, we integrated a Huawei P9 smartphone into a small 3D-printed prototype (**Figure 4-1**). The system contains all of the same instrumentation as the benchtop mechatronic spin system, e.g., the desktop scanner, and image analysis software. The smartphone contains a custom designed android app that controls the three assay steps (i.e., pre-wash, sample, and post-wash), image processing and analysis steps (**Figure 4-3A**). Each assay step contains its own programmed setting and procedure (**Figure 4-3B-D**), e.g., the pre- and post-wash steps spin the disc at 2000 RPM for 200 sec and the sample step spins the disc at 2000 RPM for 2000 sec. These parameters were selected based off of the results described in **Chapters 2** and **3**. Once each step is complete, the app redirects to the main screen for the user to initiate the next step. It's important to note that the system is not completely automated, as user input is required for the manual addition of buffer solution and sample to the disc after each workflow step.

Once the assay steps are complete, each NC membrane is imaged with the Huawei P9 smartphone 12 MP camera and subsequently analyzed to determine if the sample contains the target analyte (**Figure 4-3 E and G**). The user then drags a red circle (100-pixel diameter) on the screen and centers it over the membrane (**Figure 4-3F and H**); the app analyzes only a 50-pixel diameter ROI in the center of the red circle; the ROI is converted from RGB to weighted 8-bit grayscale. Note,

that GV is inversely proportional to the amount of AuNP accumulated on the NC membrane. Simply, the more AuNP on the membrane, the lower the GV and the fewer AuNP the higher the GV. Section 4.2.3 describes how the GV threshold was determined and programmed into the app; **Figure 4-3F** and **H** shows a screen capture of the difference between a positive and negative readout from the automated cOFI system. As mentioned previously, while the system is not fully automated currently, it is amenable to the addition of further programming to automate the assay workflow and downstream image analysis, providing the user with a readout within 60 min. Ultimately, we have designed a portable, prototype POC system which requires minimal training and is not tethered to a laboratory environment.

4.3.3 Proof-of-Concept: Multiplexed cOFI Immunocapture Study

The on-disc detection method was 'direct assay' (**Chapter 3**) through the formation of the m-AuNP-mIgG complex on the NC membrane.¹⁶ A positive result occurred when the m-AuNP containing sample solution produced a reddish color due to the accumulation of m-AuNPs binding to the mIgG on the membrane, while a negative result produced no color change on the membrane.^{17,18} The colorimetric response was quantified using the automated cOFI system. A 0.2 μm pore sized membrane was used due to having a larger surface area, allowing for greater m-AuNP-mIgG binding and therefore a greater signal intensity compared to a larger pore sized membrane (i.e., 0.45 μm pore size).¹⁹⁻²¹

For proof-of-concept of the automated cOFI system, we utilized the multiplexed cOFI disc containing NC membrane-immobilized mIgG. Here, a total volume of 200 μL of AuNP-containing solutions were centrifugally-driven through

the membrane (n=3) for analysis. The study involved diluting the m-AuNP (OD 10.0) stock solution with PBS-T in 200x to 800x dilutions (increments of 50x). Interestingly, the GV produced inconsistent results as concentrations decreased, producing no identifiable trend in colorimetric values (**Figure 4-4**). Further, results at each dilution produced large standard deviations (SD); we hypothesize these large SDs could be attributed to multiple factors including insufficient washing, user error, or system design error. In the next section, these error modes will be discussed in more detail.

Insufficient washing is when the volume of buffer solution used during the wash step of the assay is not enough to remove all the unbound m-AuNP from the NC membrane; the limited amount of washing could result in a larger GV or false-positive due to unbound m-AuNP remaining on the NC membrane. At this point, the wash step involves the addition of only 40 μ L of PBS-T, flown over the

membrane, to remove any unbound antibodies. By increasing the amount of wash buffer to a larger volume, such as 100 μ L, we may increase the likelihood that all of the unbound m-AuNP will be

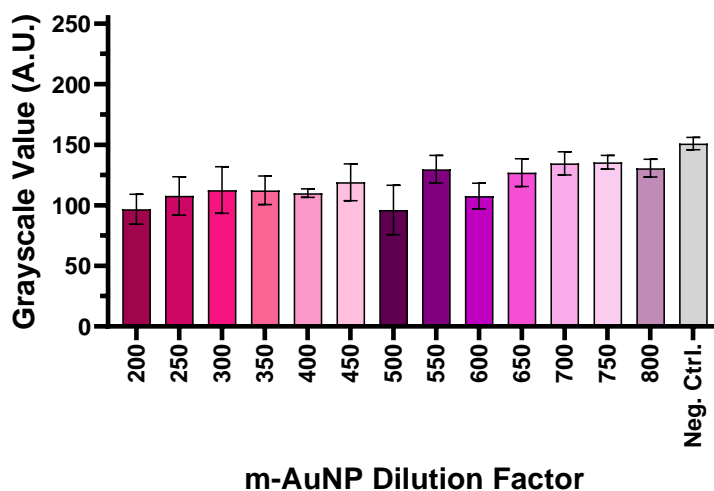


Figure 4-4: Multiplexed cOFI - Immunocapture Study Results. 1x PBS-T buffer was spiked with 200-800x dilutions of gold conjugated goat anti-mouse IgG antibodies (m-AuNP, n=3).

removed, ultimately eliminating false-positive results. With regard to 'user error,' we are referring specifically to selection of the ROI; more specifically, higher SDs may result from irregular manual alignment of the red circle over the NC membrane, ultimately decreasing the reproducibility of the system. This issue can be mitigated by programming the system to auto-align with the NC membrane and complete the image analysis without the user-intervention. Finally, system error can result in a lower GV due to insufficient lighting inside the system; insufficient lighting can produce shadows on the NC membrane, resulting in a lower GV. This error mode may be avoided with the addition of more lights, or brighter LEDs to the inside of the system to completely saturate the ROI with white light.

With the large variability in the results, a one-way analysis of variance (ANOVA) was performed to determine if there was a statistical difference among the mean GVs of all the samples; the analysis indicated there was a significant difference among the GV means ($\alpha = 0.05$, $p < 0.0001$). A Dunnett's multiple comparison test ($\alpha = 0.05$) was performed to determine if there was a statistical difference between the positive samples and negative control; the analysis demonstrated a significant difference between nine of the positive samples and the negative control, while there was not a significant difference among the mean GVs for four of the positive samples and the negative control (**Table 4-1**). Table 4-1 shows the mean sample GVs compared to the negative control GV, with each comparison receiving a p-value. The p-value determines if the comparison accepts or rejects the null hypothesis. The null hypothesis was defined as there not being a statistical difference among the mean sample GVs. If the p-value is less than the

alpha value ($\alpha = 0.05$), than the null hypothesis is rejected. Samples that have a p-value larger than the α are accepting the null hypothesis and do not have a statistical difference among the mean sample GVs compared to the negative control. These results describe that the system can statistically differentiate between a positive and negative sample as long as the sample is not diluted more than 500x. Overall, we have demonstrated the proof-of-concept of an automated cOFI system to perform all the assay steps as well as image processing and analysis to produce an easy-to-use POC system.

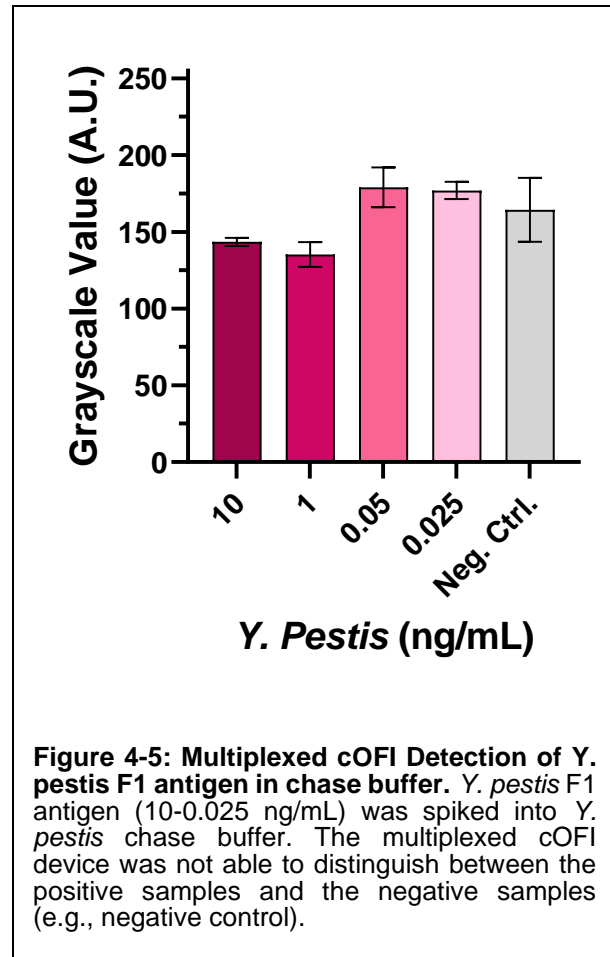
Dunnett's multiple comparisons test	Mean Diff.	95.00% CI of diff.	Significant Difference (Y/N)	P Value
200 vs. Neg. Ctrl.	-54.2	-77.68 to -30.72	Y	<0.0001
250 vs. Neg. Ctrl.	-43.25	-64.41 to -22.09	Y	<0.0001
300 vs. Neg. Ctrl.	-38.4	-61.88 to -14.92	Y	0.0002
350 vs. Neg. Ctrl.	-38.63	-59.79 to -17.46	Y	<0.0001
400 vs. Neg. Ctrl.	-41	-64.48 to -17.52	Y	<0.0001
450 vs. Neg. Ctrl.	-32	-53.16 to -10.84	Y	0.0006
500 vs. Neg. Ctrl.	-54.88	-76.04 to -33.71	Y	<0.0001
550 vs. Neg. Ctrl.	-21.2	-44.68 to 2.279	N	0.097
600 vs. Neg. Ctrl.	-43.4	-66.88 to -19.92	Y	<0.0001
650 vs. Neg. Ctrl.	-24	-47.48 to -0.5205	Y	0.0426
700 vs. Neg. Ctrl.	-16.4	-39.88 to 7.079	N	0.3136
750 vs. Neg. Ctrl.	-15.5	-37.98 to 6.980	N	0.3279
800 vs. Neg. Ctrl.	-20.4	-43.88 to 3.079	N	0.1204

Table 4-1: Multiplexed cOFI Immunocapture Study– One-Way ANOVA, Dunnett's Multiple Comparison Test Results. The multiple comparisons test determined there was not a statistical difference among the mean GVs for the 550x, 700x, 750x, and 800x samples compared to the negative control. There was a statistical difference among the mean GVs for the remaining samples compared to the negative control.

4.3.4 Detection of *Y. Pestis F1 Antigen on Multiplexed cOFI Disc*

Previous sections have described the multiplexed cOFI disc and the automated cOFI system with proof of immunocapture. Here, we demonstrate the sensitivity of the assay to detect *Y. pestis* F1 antigen spiked in chase buffer (10-

0.025 ng/mL) with **Figure 4-5** showing the mean GV for each sample (n=3). It is important to note that, unlike the detection method in section 4.3.3, this experimental setup comprised a full sandwich-type immunoassay, the details of which were described previously in **Chapter 2**. Similar to the results presented in section 4.3.3, the mean GVs did not produce a reliable trend as the F1 antigen concentration decreased. At 10 ng/mL, there was a mean GV of 144 ± 3 (**Figure 4-5**); the



1 ng/mL sample produced a lower mean GV of 135 ± 8 . The 0.05 ng/mL and 0.025 ng/mL samples produced expected results with higher mean GVs (179 ± 13 and 177 ± 6 , respectively). A one-way ANOVA ($\alpha = 0.05$) was performed to determine if there was a statistical difference among the mean GVs and the analysis determined the p-value ($p < 0.0006$) was less than the α (0.05); therefore, it rejected the null hypothesis defined as no difference in the mean GVs. A Dunnett's multiple comparisons test ($\alpha = 0.05$) was performed to determine if there was a statistical difference among the F1 antigen containing samples and the negative control; the analysis determine there was not a significant difference between the

F1 antigen samples (10, 0.05, and 0.025 ng/mL) and the negative control (**Table 4-2**). There was a significant difference between the mean GVs of the 1 ng/mL F1 antigen sample and the negative control; the p-value ($p < 0.0162$) was less than the α (0.05); therefore, the null hypothesis was rejected. The results presented here are consistent with those described section 4.3.3, in that there are inconsistencies in the mean GVs as the sample becomes less concentrated. We conclude this is the result of a limited volume of washing buffer being driven through membrane to remove any unbound Yp-AuNP, resulting in a false positives (i.e., lower GVs). Despite the inconsistent GVs, we have demonstrated that the multiplexed cOFI is capable of detecting two different target analytes via two separate methods of detection (i.e., direct and sandwich-type assay) with the automated cOFI system.

Dunnett's multiple comparisons test	Mean Diff.	95.00% CI of diff.	Significant Difference (Y/N)	P Value
10 vs. Neg. Ctrl.	-20.83	-44.55 to 2.881	N	0.0902
1 vs. Neg. Ctrl.	-29.08	-52.80 to -5.369	Y	0.0162
0.05 vs. Neg. Ctrl.	14.67	-10.69 to 40.02	N	0.3399
0.025 vs. Neg. Ctrl.	12.67	-12.69 to 38.02	N	0.4568

Table 4-2: Multiplexed cOFI Detection of *Y. pestis* F1 antigen in chase buffer – One-Way ANOVA, Dunnett's Multiple Comparison Test. The multiple comparisons test determined there was not a significant difference among the means of the 10, 0.05, and 0.025 ng/mL F1 antigen samples compared to the negative control samples.

4.3.5 cOFI Detection of *Y. Pestis* F1 Antigen on Large Volume cOFI

Next, we sought to demonstrate sensitivity of the automated cOFI in comparison with the large volume cOFI (0.01 ng/mL) described in **Chapter 3**. We spiked 1-0.01 ng/mL of F1 antigen into 6 mL of chase buffer; **Figure 4-6** shows the resultant mean GVs ($n=3$) for each sample. The mean GVs remained relatively unchanged as the F1 antigen concentrations decreased from 1-0.01 ng/mL (GV = 127 ± 6 , 125 ± 8 , and 136 ± 16 , respectively); additionally, a visual difference

between the mean GVs of the positive samples and the negative control was observed. A one-way ANOVA ($\alpha = 0.05$) was performed to determine if there was a statistical difference among all the mean GVs and the results reported that there was a significant difference among the means ($p = 0.0002$). A Dunnett's multiple comparisons test was performed to determine if there was a significant difference between the mean GVs of the positive samples and the

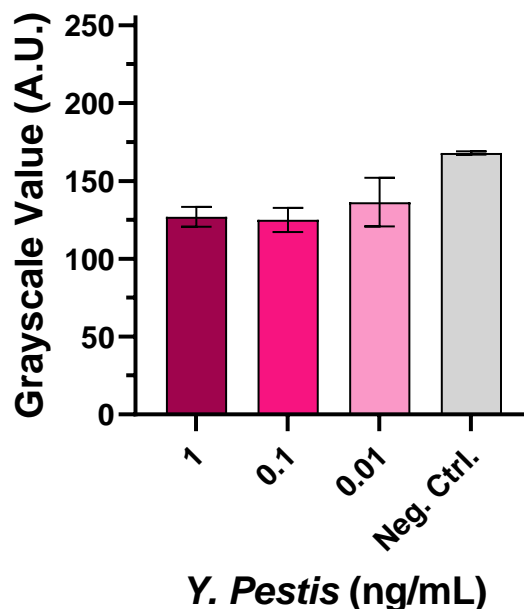


Figure 4-6: Large Volume cOFI Detection of *Y. pestis* F1 antigen in chase buffer. *Y. pestis* F1 antigen (10-0.01 ng/mL) was spiked into *Y. pestis* chase buffer. The automated cOFI system was able to detect 0.01 ng/mL F1 antigen while distinguishing between the positive samples and the negative samples (e.g., negative control).

mean GV of the negative control; the analysis determined that there was a statistical difference between the positive mean GVs and the negative control mean GV (**Table 4-3**). Table 4-3 shows the three-mean sample GVs compare to the negative control GV; each comparison resulted in a p-value less than the α (0.05), meaning that the null hypothesis is rejected. The null hypothesis was defined as there is no difference between the mean sample GVs. Therefore, these results indicate the automated cOFI system demonstrates comparable sensitivity to the large volume cOFI disc described in **Chapter 3**; recall that the large volume cOFI disc was able to detect as low as 0.01 ng/mL and distinguish between a

negative control sample. Thus, using this proof-of-concept study with the *Y. pestis* F1 antigen, we have demonstrated an automated, portable cOFI system with sensitivity down to 0.01 ng/mL in buffer solution; making this an ideal candidate for a POC diagnostic device.

Dunnett's multiple comparisons test	Mean Diff.	95.00% CI of diff.	Significant Difference (Y/N)	P Value
1 vs. Neg. Ctrl.	-41	-57.43 to -24.57	Y	<0.0001
0.1 vs. Neg. Ctrl.	-43	-61.97 to -24.03	Y	0.0002
0.01 vs. Neg. Ctrl.	-31.67	-50.64 to -12.69	Y	0.0023

Table 4-3: Large Volume cOFI Detection of *Y. pestis* F1 antigen in chase buffer – One-Way ANOVA, Dunnett's Multiple Comparison Test. The multiple comparisons test determined that there was a significant difference among the means of the F1 antigen containing samples compared to the negative control samples.

4.4 Conclusions

We described an automated cOFI system powered by a custom smartphone app. The system is capable of completing all immunoassay steps, including downstream image processing and analysis, all within a compact portable device. The automated system was designed to replace multiple pieces of benchtop laboratory equipment, while simplifying the cOFI procedure by limiting the amount of user intervention and eliminating the time-consuming steps associated with image analysis. Further, multiplexed and large volume cOFI discs were tested using the automated system to show proof-of-concept immunocapture and detection. We demonstrated the system could rapidly analyze the NC membrane to determine if the sample fluid was positive or negative for the target analyte. Further, we demonstrated comparable sensitivity with the large volume cOFI disc described in **Chapter 3**, detecting 0.01 ng/mL of the *Y. pestis* F1 antigen using a smartphone camera over the desktop scanner. Future work includes nano-

spotting reagents onto a NC membrane to create a micro-array which will allow for the detection of multiple target analytes from a single sample fluid.

4.5 References

- (1) Everitt, M. L.; Tillery, A.; David, M. G.; Singh, N.; Borison, A.; White, I. M. A Critical Review of Point-of-Care Diagnostic Technologies to Combat Viral Pandemics. *Anal. Chim. Acta* **2021**, *1146*, 184–199. <https://doi.org/10.1016/J.ACA.2020.10.009>.
- (2) Nichols, J. H. Point-of-Care Testing. *Immunoass. Handb.* **2013**, 455–463. <https://doi.org/10.1016/B978-0-08-097037-0.00031-2>.
- (3) He, W.; You, M.; Wan, W.; Xu, F.; Li, F.; Li, A. Point-of-Care Periodontitis Testing: Biomarkers, Current Technologies, and Perspectives. *Trends Biotechnol.* **2018**, *36* (11), 1127–1144. <https://doi.org/10.1016/J.TIBTECH.2018.05.013>.
- (4) Wang, C.; Liu, M.; Wang, Z.; Li, S.; Deng, S.; He, N. Point-of-Care Diagnostics for Infectious Diseases: From Method to Devices. *Nano Today* **2021**, *37*. <https://doi.org/10.1016/j.nantod.2021.101092>.
- (5) Gubala, V.; Harris, L. F.; Ricco, A. J.; Tan, M. X.; Williams, D. E. Point of Care Diagnostics: Status and Future. *Anal. Chem* **2012**, *84*, 487–515. <https://doi.org/10.1021/ac2030199>.
- (6) Reyes, D. R.; Iossifidis, D.; Auroux, P.-A.; Manz, A. Micro Total Analysis Systems. 1. Introduction, Theory, and Technology. *Anal. Biochem.* **2002**, *74*, 2623–2636. <https://doi.org/10.1021/ac0202435>.
- (7) Li, F.; You, M.; Li, S.; Hu, J.; Liu, C.; Gong, Y.; Yang, H.; Xu, F. Paper-Based Point-of-Care Immunoassays: Recent Advances and Emerging Trends. *Biotechnol. Adv.* **2019**, *39*. <https://doi.org/10.1016/j.biotechadv.2019.107442>.
- (8) Turiello, R.; Dignan, L. M.; Thompson, B.; Poulter, M.; Hickey, J.; Chapman, J.; Landers, J. P. Centrifugal Microfluidic Method for Enrichment and Enzymatic Extraction of Severe Acute Respiratory Syndrome Coronavirus 2 RNA. *Cite This Anal. Chem* **2022**, *2022*, 3295. <https://doi.org/10.1021/acs.analchem.1c05215>.
- (9) Dignan, L. M.; Turiello, R.; Layne, T. R.; O'Connell, K. C.; Hickey, J.; Chapman, J.; Poulter, M. D.; Landers, J. P. An Ultrafast SARS-CoV-2 Virus Enrichment and Extraction Method Compatible with Multiple Modalities for RNA Detection. *Anal. Chim. Acta* **2021**, *1180*. <https://doi.org/10.1016/J.ACA.2021.338846>.
- (10) Gorkin, R.; Park, J.; Siegrist, J.; Amasia, M.; Lee, B. S.; Park, J. M.; Kim, J.; Kim, H.; Madou, M.; Cho, Y. K. Centrifugal Microfluidics for Biomedical Applications. *Lab Chip* **2010**, *10* (14), 1758–1773. <https://doi.org/10.1039/b924109d>.
- (11) Thompson, B. L.; Ouyang, Y.; Duarte, G. R. M.; Carrilho, E.; Krauss, S.; Landers, J. P. Inexpensive, Rapid Prototyping of Microfluidic Devices Using Overhead Transparencies and a Laser Print, Cut, and Laminate Fabrication Method. *Nat. Protoc.* **2015**, *10* (6), 875–886. <https://doi.org/10.1038/nprot.2015.051>.
- (12) *Standard Materials for High-Resolution Rapid Prototyping*; 2017.
- (13) Hau, D.; Wade, B.; Lovejoy, C.; Pandit, S. G.; Reed, D. E.; DeMers, H. L.; Green, H. R.; Hannah, E. E.; McLarty, M. E.; Creek, C. J.; et al. Development

- of a Dual Antigen Lateral Flow Immunoassay for Detecting *Yersinia Pestis*. *PLoS Negl. Trop. Dis.* **2022**, *16* (3), e0010287. <https://doi.org/10.1371/JOURNAL.PNTD.0010287>.
- (14) Woolf, M.; Dignan, L.; Karas, S.; Lewis, H.; Hadley, K.; Nauman, A.; Gates-Hollingsworth, M.; AuCoin, D.; Green, H.; Geise, G.; et al. Characterization of a Centrifugal Microfluidic Orthogonal Flow Platform. *Micromachines* **2022**, *13* (3), 487. <https://doi.org/10.3390/MI13030487>.
- (15) Woolf, M. S.; Dignan, L. M.; Scott, A. T.; Landers, J. P. Digital Postprocessing and Image Segmentation for Objective Analysis of Colorimetric Reactions. *Nat. Protoc.* **2020**, *16*, 218–238. <https://doi.org/10.1038/s41596-020-00413-0>.
- (16) Bailes, J.; Mayoss, S.; Teale, P.; Soloviev, M. Gold Nanoparticle Antibody Conjugates for Use in Competitive Lateral Flow Assays. *Methods Mol. Biol.* **2012**, *906*, 45–55. https://doi.org/10.1007/978-1-61779-953-2_4.
- (17) Dykman, L.; Khlebtsov, N. Gold Nanoparticles in Biomedical Applications. *Gold Nanoparticles in Biomedical Applications*. 2017, pp 1–332. <https://doi.org/10.1201/b22465>.
- (18) Products, M. S.; Science, C.; Products, N.; Nanofibers, C.; Nanostructures, G.; Mesoporous, G.; Nanoparticles, G.; Nanoparticles, S.; Dots, Q.; Advantage, Q.; et al. Gold Nanoparticles: Properties and Applications Optical & Electronics Properties of Gold Nanoparticles. *Sigma Aldrich* **2016**, 8–12.
- (19) Manz; Pamme; Lossifidis. Molecular Recognition. In *Bioanalytical Chemistry*, London Imperial Press, 2004.
- (20) Devadhasan, J. P.; Gu, J.; Chen, P.; Smith, S.; Thomas, B.; Gates-Hollingsworth, M.; Hau, D.; Pandit, S.; AuCoin, D.; Zenhausern, F. Critical Comparison between Large and Mini Vertical Flow Immunoassay Platforms for *Yersinia Pestis* Detection. *Anal. Chem.* **2021**, acs.analchem.0c05278. <https://doi.org/10.1021/acs.analchem.0c05278>.
- (21) Chen, P.; Gates-Hollingsworth, M.; Pandit, S.; Park, A.; Montgomery, D.; AuCoin, D.; Gu, J.; Zenhausern, F. Paper-Based Vertical Flow Immunoassay (VFI) for Detection of Bio-Threat Pathogens. *Talanta* **2019**, *191* (August 2018), 81–88. <https://doi.org/10.1016/j.talanta.2018.08.043>.

CHAPTER 5 – The Design and Characterization of a Multiplexed Flow Through Assay for Rapid, Point-of-Need Diagnostics

5.1 Introduction

The early detection and identification of infectious diseases is paramount when triaging infected personnel for them to receive the necessary treatment. Pathogenic bacteria (e.g., *Yersinia pestis*) are a major threat to our health with potential to cause serious illness or death.^{1,2} Additionally, infectious diseases can turn into an epidemic or possibly a pandemic if the infected individuals are not properly identified and/or treated.² Traditional methods (e.g., enzyme-linked immunosorbent assay (ELISA) or polymerase chain reaction (PCR)), as explained in previous chapters, have been developed to detect an array of diseases and other target biomolecules.³ Unfortunately, these techniques are expensive, time consuming, and must be performed in a laboratory environment.⁴⁻⁶ Conversely, ELISA and PCR were not designed to be deployed as point-of-need (PoN) diagnostic devices.⁷ In order to prevent the spread of infection, rapid detection and identification of diseases must be performed in the field at the point of incident. Not only can PoN devices be used to test humans for illnesses, but they can also be used to test food, animals, and water for potential pathogens which could have a significant effect on the food chain as well as the global economy.⁸

To meet the demands for portable, rapid PoN diagnostics, there has been an increased interest in paper-based immunoassays because they are specific to a target molecule and can detect very small quantities, down to the nanogram or picogram amount.⁷ **Chapter 1** explained two major types of paper-based immunoassays, along with their pros and cons: lateral flow immunoassays (LFI)

and vertical flow immunoassays (VFI). These two assays have a mutual component: porous membranes (e.g., nitrocellulose (NC) or glass fiber). These types of assays have been coined flow through assays (FTA) because the sample is being driven through the porous membrane for the target analyte to bind to either a capture antibody (i.e., specific to the target analyte) or to the surface of the membrane.⁷⁻⁹ A porous membrane is used because of the large surface area available for the target analyte to binding or interact with and theoretically increasing the assay's sensitivity. This theory can be explained by the Damköhler (Da) and Péclet ($Pé$) numbers. The Da (**equation 1**) describes the interaction between the adsorption rate and the transport rate of the molecule to the surface of the membrane; the $Pé$ (**equation 2**), explained in **Chapter 2**, describes the interaction between the convection rate and the diffusion rate of the molecule to the membrane's surface.^{10,11}

Equation 1:
$$Da = \frac{\text{adsorption rate}}{\text{transport rate}} = \frac{k_{on}\gamma}{k_c}$$

k_{on} is the association constant of the target analyte, γ is the surface concentration of the capture agent (i.e., capture antibody), and k_c is the mass transfer coefficient. When $Da > 1$, the target analyte has a higher rate of binding to the capture antibody than the rate of transport through the membrane's pore.

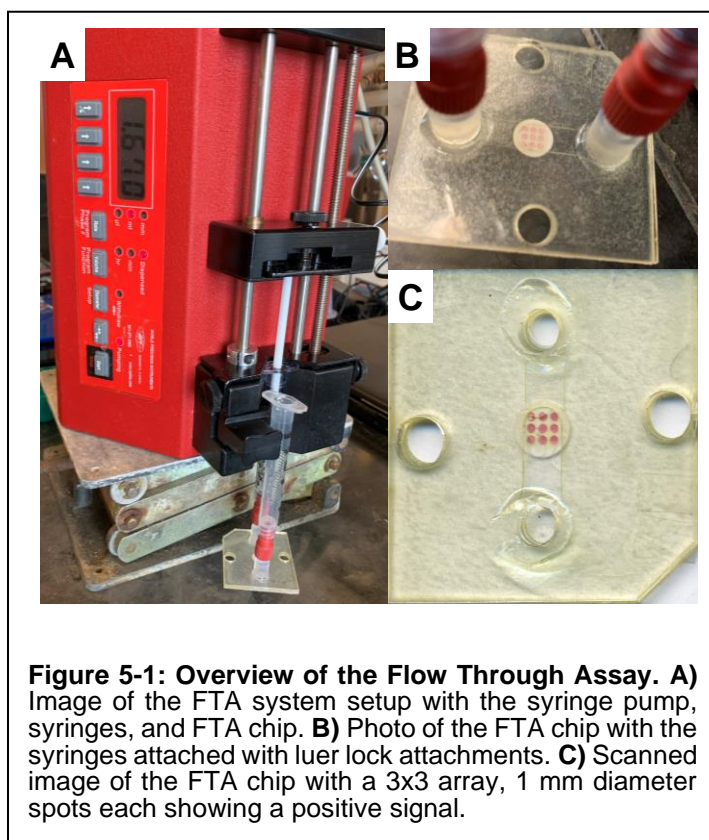
Equation 2:
$$Pé = \frac{\text{convection rate}}{\text{diffusion rate}} = \frac{U/\delta_m}{D/R_p^2}$$

U is the velocity (m/s) of the sample through the pore, δ_m is the membrane thickness, D is the diffusivity of the target analyte, and R_p is the radius of the pore. When $Pé < 1$, the target analyte diffuses to the pore wall faster than the target

analyte flows through the pore. Simply put, a slower sample flow rate and a smaller membrane pore size will lead to greater binding of the target analyte to the capture antibody, resulting increased signal and device sensitivity.

Based off of the *Da* and *Pé* knowledge, this chapter describes the development of the multiplexed PoN FTA chip using the same method of fluid flow (i.e., orthogonal flow) and detection (i.e., colorimetric) described in **Chapter 2-4**. Previously developed FTA-type devices for point-of-care (POC) testing have shown a proof-of-concept to detect nucleic acids, *Escherichia coli* (*e. coli*), and trypanosomosis.^{1,10,12} Unfortunately, many of these FTA devices were not ideal for use at the PoN because they required off device sample preparation; plus once the sample was pumped through the device, the end-user needed to disassemble

then perform image analysis or visual inspection to determine the assay's results. The FTA chip described here is a syringe-driven, fully enclosed, and multiplexed design that requires no off-chip sample preparation or disassembly (**Figure 5-1**); the chip uses a 7-layer, print-cut-laminate (PCL) method with 3D-



printed luer locks to attach the syringes.¹³ Two syringes are used: one for the sample and one to act as a waste chamber (**Figure 5-1B**). This FTA was demonstrated using a syringe pump to drive the sample through the chip but the syringe pump is optional. If needed, the end-user could manually pump the sample through the chip. Additionally, the 7-layer design produced 1 mm detection regions on the NC membrane allowing for easy deposition of small volumes of reagents (0.25 $\mu\text{L}/\text{spot}$) without the need for expensive nano-spotter instruments; furthermore, this micro-array design allows for the detection of up to nine different target analytes as well as simple, repeatable image analysis without chip disassembly (**Figure 5-1C**). Ultimately, the FTA chip design here is capable of rapidly detecting and identifying a variety of infectious diseases at the PoN with little to no instrumentation.

5.2 Experimental Section

5.2.1 Fabrication of the Flow Through Assay

The flow through assay (FTA) chips were fabricated using the print-cut-laminate (PCL) method.¹³ Each device was comprised of six polyethylene terephthalate (PET, 101.6 μm thickness, Film Source Inc., Maryland Heights, MO U.S.A.) sheets alternated with heat sensitive adhesive (HSA, 50.8 μm thickness, EL-7970-39, Adhesive Research Inc., Glen Rock, PA U.S.A) and a polymethyl methacrylate (PMMA, 1.5 mm McMaster-Carr, Elmhurst, IL U.S.A.) layer (**Figure 5-2**). The chip architecture for each layer was designed using AutoCAD® 2020 (Autodesk Inc., San Rafael, CA, U.S.A.) and cut using a 50W CO₂ laser engraving system (VLS3.50, Universal Laser Systems®, Scottsdale, AZ, U.S.A.). Layers 1 and 7 were the capping layers, while layers 2 and 6 contained the microfluidic

channels. Layers 3 and 5 were via layers containing six circular orthogonal flow ports (1 mm diameter). The flow ports directed flow to and through layer 4, which contained 7 mm circular cutouts of the nitrocellulose (NC) membranes. Two types of NC membranes were used: Whatman ProTran BA 83 (0.2 μm , Marlborough, MA U.S.A.) and UniSart® CN140 (0.45 μm , Sartorius, Göttingen, DE). To activate the HSA, the disc layers were aligned and lamination bonded (185-195°C) (UltraLam 250B, Akiles Products Inc., Mira Loma, CA, U.S.A.) in three separate steps. First, disc layers 3-5 were aligned, NC membrane cutouts were inserted in layer 4 and bonded together when passed through an office laminator (2 passes). Second, layers 1 and 2 were aligned with and laminated to layers 3-5 (2 passes). Finally, layer 6 was aligned and laminated to the previously bonded layers (2 passes). The three separate lamination steps were performed to allow the HSA to properly bond each of the PET layers together.

PMMA, layer 7, was affixed to layers 1-6 with pressure sensitive adhesive (PSA, 55.8 μm thickness, ARcare 7876, Adhesive Research Inc., Glen Rock, PA U.S.A), after the NC membranes were blotted with assay reagents. Completely assembled discs were placed in foil moisture barrier bags (Dri-shield™, Uline, Pleasant Prairie, WI, U.S.A.) with two 3-gram silica moisture absorbent packets (S-3904, Uline) overnight and pressed (15 lbs) to ensure PSA adhesions.

The luer lock attachments were designed using Autodesk Fusion 360 (Autodesk Inc., San Rafael, CA, U.S.A.) then printed on a FormLabs 3B stereolithography 3D-printer (FormLabs Inc., Somerville, MA, U.S.A.) with clear v4 resin (Formlabs Inc., Somerville, MA, U.S.A.).¹⁴ The attachments were manually

aligned and bonded to layer 7 using ultra-violet light curing adhesive (SuperWeld – Light Activated Instant Glue, J-B Weld, Sulphur Springs, TX, U.S.A.).

5.2.3 Proof-of-Concept: Immunocapture Study

5.2.3.1 Antibody Blotting Volume Study

In this study, different volumes of mouse whole molecule, IgG antibodies (m-IgG) (Jackson ImmunoResearch Laboratories Inc., West Grove, PA, U.S.A.) were manually blotted and immobilized onto the 7 mm NC membranes (0.1, 0.25, 0.5, 0.75, and 1 μ L). The NC membrane was blotted with m-IgG through the 1 mm via ports in layer 5 (5.5 mg/mL). The NC membranes were dried at 37°C for 1 hour in a convection oven (Binder 056FD – Convection Oven, P.O. Box 102, 78502 Tuttlingen, Germany). M-IgG was not immobilized on the membranes of the negative control. Each membrane was subsequently blocked with a blocking buffer solution (0.25 μ L/membrane; 0.25% phosphate buffered saline-tween, PBS-T; 0.1% Bovine Serum Albumin) then dried in the convection oven at 37°C for 1 hour. The discs were placed in foil moisture barrier bags (Dri-shield™, Uline, Pleasant Prairie, WI, U.S.A.) with two 3-gram silica moisture absorbent packets (S-3904, Uline) for a minimum of 24 hours.

Sample solutions (5mL) were prepared using 40 nm colloidal gold nanoparticle conjugated goat anti-mouse IgG antibodies (m-AuNP; OD 10.0 at 529 nm, Jackson ImmunoResearch Laboratories, Inc., West Grove, PA, U.S.A.), diluted (500x) with 1x phosphate buffered saline-tween, pH = 7.5 (PBS-T; Thermo Fisher Scientific, Waltham, MA USA 02451), and incubated in-tube at room temperature for 20 minutes. Negative controls consisted of PBS-T buffer and m-AuNP (500x dilution). Each sample solution (5 mL) was pumped through the

FTA chip with a syringe pump set at 0.1 mL/min flow rate. A post-wash step (1 mL PBS-T buffer, 0.1 mL/min) was performed to remove any excess sample from the membrane.

5.2.3.2 Flow Rate Study

To optimize immunocapture on the FTA chip, each 1 mm spot on the 7 mm NC membranes (both Whatman and Sartorius membranes) were blotted with 0.25 μ L of mIgG. Samples solutions (5 mL) were prepared using m-AuNP, diluted (500x) with PBS-T, and incubated in-tube at room temperature for 20 min. Using a syringe pump, each sample solution (5 mL) was pumped through the FTA chips at five different flow rates (0.1, 0.25, 0.5, 0.75, 1 mL/min). A post-wash step (1 mL PBS-T buffer) was performed at the same flow rate as the sample solution to remove any excess sample from the membrane.

5.2.4 Detection of *Y. pestis* F1 Antigen on the Flow Through Assay Chip

Y. pestis reagents were prepared in the Diagnostics Discovery Laboratory (School of Medicine, University of Nevada, Reno, NV, U.S.A.) as per the protocol described in Hau et al.¹⁵ The FTA chip was assembled as described in Section 5.2.1. The membranes were blotted post-lamination with 0.25 μ L of Yp11C7 0416 IgG1 (Yp-mAb) (*Y. pestis* F1 antigen specific mAb, 5.85 mg/mL); note, only 3 out of the 6 spots were blotted with Yp-mAb, the other 3 spots served as negative controls (no Yp-mAb). After blotting, the discs were incubated at 37°C for 1 hour in a convection oven (Binder 056FD – Convection Oven, P.O. Box 102, 78502 Tuttlingen, Germany). Next, each membrane was blocked with blocking buffer solution (0.25 μ L) through the 1 mm access port in layer 5 then placed in the oven at 37°C for 1 hour.

Sample solutions (5 mL) of the *Y. pestis* F1 antigen were prepared at 0.075-0.01 ng/mL in *Y. pestis* chase buffer, or 50 mM carb-bicarbonate buffer at pH 9.6, prepared from sodium bicarbonate (Thermo Fisher Scientific, Waltham, MA USA 02451) and sodium carbonate (Thermo Fisher Scientific, Waltham, MA USA 02451). Aliquots of each antigen dilution were mixed with 10 μ L of Yp3F2 gold conjugate (Yp-AuNP, OD 10.1 at 520 nm), and incubated in-tube at room temperature for 20 min. Using a syringe pump, sample solutions were pumped through the FTA chip at 0.25 mL/min flow rate. Finally, a post-wash step (1 mL chase buffer, 0.25 mL/min flow rate) was performed to remove any excess sample from the membrane.

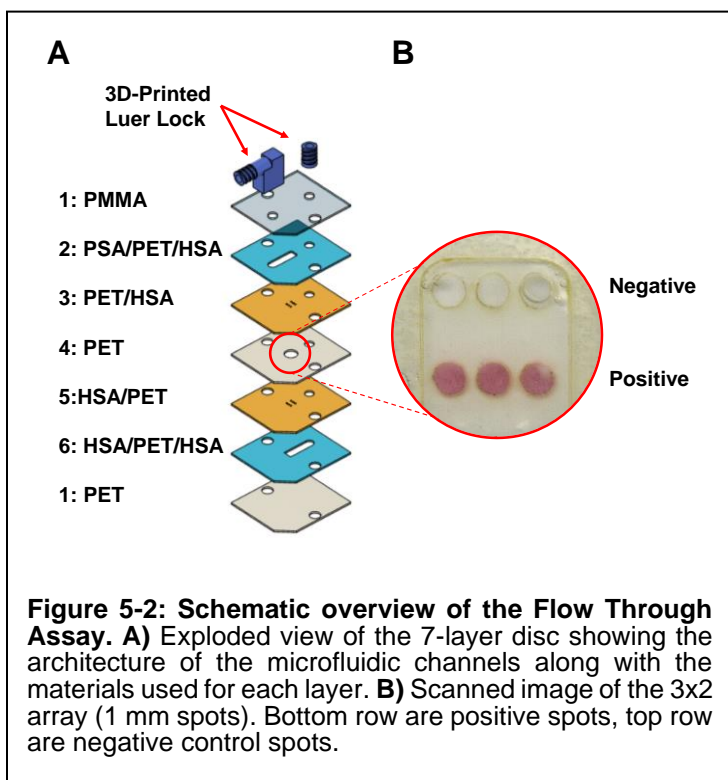
5.2.5 Image Processing and Data Analysis

Each FTA chip was digitally imaged (1200 dpi, TIF format) using a Perfection V100 desktop scanner (Epson, Suwa, Nagano, Japan) after each assay. Circular regions of interest (ROI) (45-pixel diameter) from the NC membranes were selected using the Microsoft Windows 64-bit Fiji distribution of ImageJ v.1.52p (<https://imagej.net/Fiji/Downloads>), as described in Woolf *et al.*¹⁶ The ROI for each membrane was converted in ImageJ to weighted 8-bit grayscale and the grayscale value (GV) was analyzed. Fiji ImageJ measures the GV from 0-255, where 0 is completely black and 255 is entirely white.

5.3 Results and Discussion

5.3.1 Fabrication and Design of the Flow Through Assay Chip

The FTA chip was developed as a rapid and easy to use PON device that could be used with or without an external pump (i.e., syringe pump). The chip is small and compact measuring 45 mm x 40 mm with a 3x2 microarray for the detection of up to six target analytes (**Figure 5-2**). The sample solution is driven through the chip with a syringe, attached to the chip with a luer lock, providing quick, leak free connections (**Figure 5-2A**). Using a syringe to drive the solution through the chip, allows the user to analyze, in theory, an unlimited amount of sample because the only limiting factor in the volume being driven through the chip is the size of the syringe. By eliminating the centrifugally-driven method of fluid flow, we can eliminate the variation in flow rate (e.g., slowed or halted fluid flow) through the NC membrane as described in **Chapters 2 and 3**, because a constant flow rate is maintained with the syringe pump. Additionally, the large volume disc experienced leaking from the PMMA sample recovery chambers due to the large amount of centrifugal force applied by the 6 mL sample volume against the PMMA PSA. The design of the FTA chip



eliminates the need for a large volume reservoir on the chip by leveraging the pumping method to house the liquid sample while also providing improvements to the stability of the flow rate. The 7-layer FTA chip followed a similar design and assembly as the cOFI disc described in **Chapters 2-4**. Briefly, the 7-layer design produces true orthogonal flow, eliminating lateral flow across the NC membrane, and creating uniform, circular detection regions on the NC membrane allowing for easy, repeatable image analysis (**Figure 5-2B**).

The 3x2 microarray on the FTA chip was designed to eliminate the need for an expensive nano-spotter, e.g., a base model nano-spotter from BioDot costs \$45,000 (cost estimate provided by vender). The 3x2 array was fabricated by laser cutting 1 mm diameter holes in PET layers 3 and 5. These two layers contained HSA on one side, sandwiching the NC membrane and forming a water tight seal. The 1 mm diameter holes allowed for pipetting of reagents onto the NC membrane, creating a uniform detection region, as shown in **Figure 5-2B**. Subsequent chapters describe the optimization of the volume of antibodies immobilized on each 1mm spot and the characterization of sample flow rate through the FTA chip.

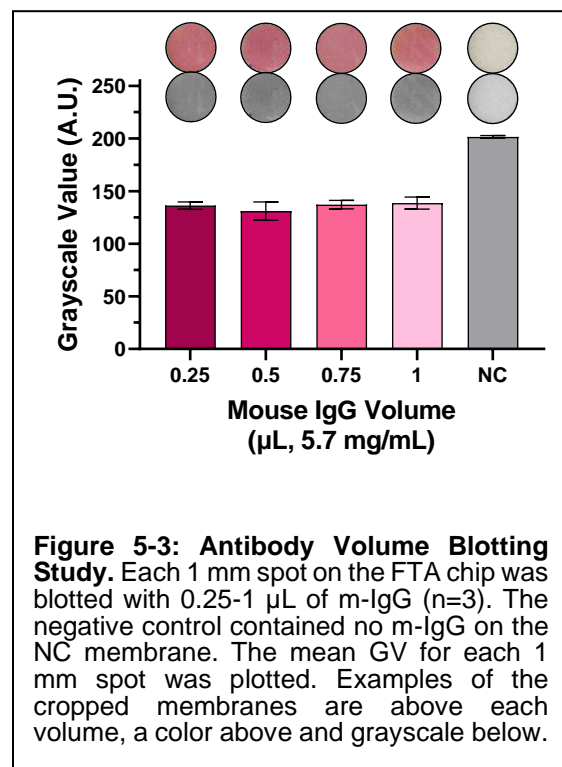
5.3.2 Proof-of-Concept: Immunocapture Study

5.3.2.1 Antibody Blotting Volume Study

An antibody blotting study was performed to determine if the volume of antibodies blotted on the 1 mm spot would affect the amount of colorimetric change on the NC membrane, i.e., GV. We hypothesized blotting a larger volume of antibodies on the membrane would produce a greater colorimetric change because the more m-IgG present on the membrane provides more binding sites for the m-AuNP to bind as well as more of the NC membrane surface will be coated

with m-IgG allowing for greater sensitivity.¹¹ The 1 mm spots on the FTA chip were blotted with 0.25-1 μL ($n=3$) of m-IgG (5.7 mg/mL) and blocked with an equal volume of blocking buffer. Sample solutions containing m-AuNP (500x dilution) were pumped through the FTA chip at 0.1 mL/min flow rate. A slow flow rate was chosen to ensure the m-AuNP had the greatest amount of time to diffuse to the pores' walls which allows the m-AuNP an opportunity to bind to the m-IgG on pores' surface; a future sub-section will explore the optimization of the flow rate through the FTA chip.^{7,9,17,18} The mean grayscale values (GV) for each spot was measured and recorded (**Figure 5-3**).

A one-way analysis of variance (ANOVA) with a Tukey's multiple comparisons test ($\alpha = 0.05$) was performed to determine if there was a statistical difference among the mean GVs for each volume of m-IgG (**Table 5-1**). The analysis determined there was not a significant difference between the mean GVs, except for the GVs between 0.5 μL and 1 μL of m-IgG; the p-value ($p = 0.0423$) was less than the alpha (0.05); therefore, it rejected the null hypothesis defined as there is no difference between the mean GVs. The comparisons between the other m-IgG volumes resulted in p-values larger than alpha and accepted the null hypothesis



where there is no difference between the mean GVs. Based off of these results, 0.25 μ L of m-IgG was blotted on each 1 mm spot for all future experiments.

Tukey's multiple comparisons test	Mean Diff.	Significant Difference (Y/N)	P Value
0.25 vs. 0.5	5.337	N	0.2338
0.25 vs. 0.75	-0.8222	N	0.9906
0.25 vs. 1	-2.338	N	0.8311
0.5 vs. 0.75	-6.159	N	0.1358
0.5 vs. 1	-7.674	Y	0.0423
0.75 vs. 1	-1.516	N	0.9459

Table 5-1: Tukey's Multiple Comparison's Test. The multiple comparisons test determined there was not a statistical difference among the mean GVs, except for the GVs comparing 0.5 μ L to 1 μ L m-IgG volumes blotted on the 1 mm spots. The mean GVs for 0.5 μ L vs. 1 μ L resulted in a p-value (0.0423) that was less than the alpha (0.05) which rejected the null hypothesis of there being no difference in the mean GVs.

5.3.2.2 Flow Rate Study

Once the volume of m-IgG blotted on membrane was characterized, a flow rate study was performed in order to achieve the greatest amount of m-AuNP binding to m-IgG on the membrane while limiting the potential for non-specific binding. We hypothesized that a slower flow rate would result in the greatest amount of binding between the m-IgG and the m-AuNP, therefore producing a greater red colorimetric change on the membrane. A slower flow rate would allow for greater binding interaction time between the two antibodies compared to a faster flow rate, which could lead to enhanced assay sensitivity.¹⁹ Samples were prepared (500x dilution m-AuNP, n=3) and pumped through the FTA chips with flow rates from 0.1 mL/mm to 1 mL/mm. Each 1 mm spot was blotted with 0.25 μ L of m-IgG and the mean GVs for each spot were analyzed and compared; the negative controls 1 mm spots contained no m-IgG (**Figure 5-4**).

The slowest flow rate (0.1 mL/min) resulted in the greatest colorimetric change, or lowest mean GV (44 ± 2), on the membrane but the negative control contained a large amount of non-specific binding with a mean GV of 133 ± 3 . Visually comparing the negative controls between 0.1 mL/min and 0.25 mL/min, the 0.25 mL/min flow rate negative control had a mean GV of

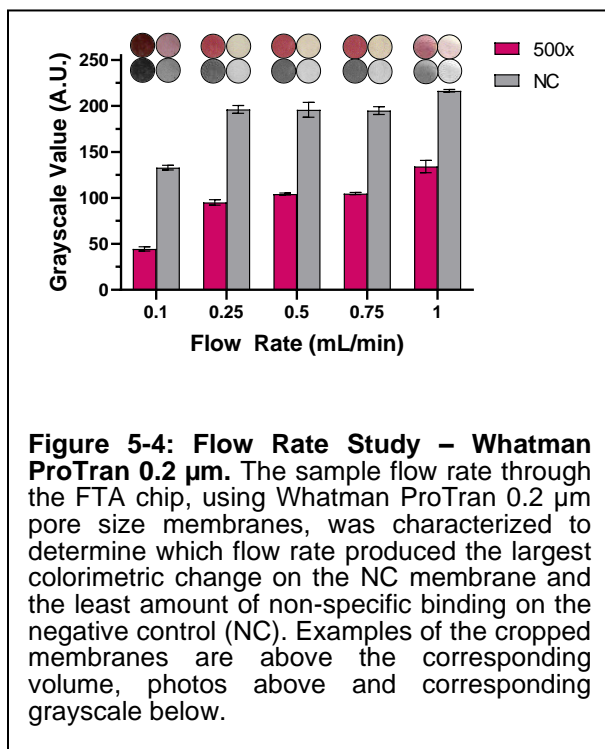
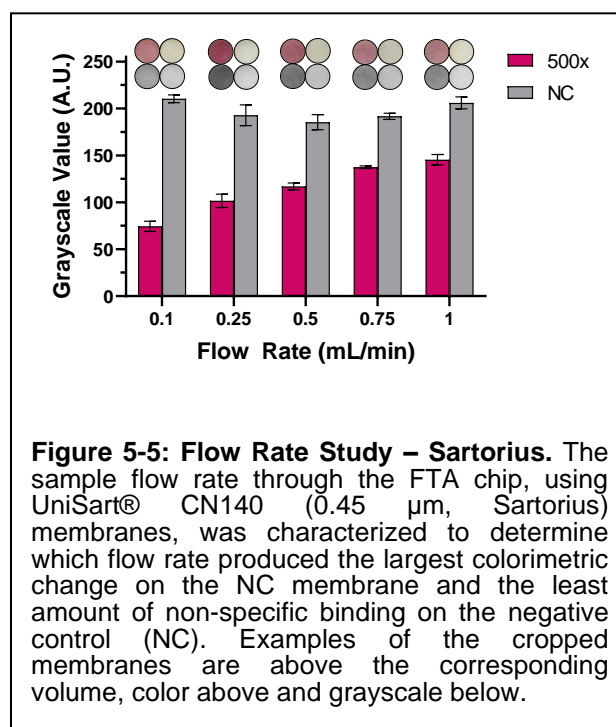


Figure 5-4: Flow Rate Study – Whatman ProTran 0.2 μm . The sample flow rate through the FTA chip, using Whatman ProTran 0.2 μm pore size membranes, was characterized to determine which flow rate produced the largest colorimetric change on the NC membrane and the least amount of non-specific binding on the negative control (NC). Examples of the cropped membranes are above the corresponding volume, photos above and corresponding grayscale below.

196 \pm 4. With there being little to no non-specific binding occurring at flow rates higher than 0.25 mL/min, a two-way ANOVA ($\alpha = 0.05$) and a Tukey's multiple comparisons test was performed to determine if there was a statistical difference between the mean GVs of the negative controls for each flow rate. The analysis determined there was a statistical difference between 0.1 mL/min and 0.25-1 mL/min, the p-values were < 0.0001 . As the 0.25 mL/min flow rate showed little to no non-specific binding in the negative control spots, as can be seen by the higher GV in **Figure 5-4**, a comparison between this flow rate and all other flow rates tested was done to examine if there is any benefit to flowing at faster rates. The analysis revealed that there was no significant difference between the negative control spots of the 0.25 mL/min sample versus the 0.5 mL/min ($p > 0.9999$) and 0.75 mL/min ($p > 0.9958$) samples. However, there was a significant difference

when compared to the 1 mL/min sample ($p < 0.0001$). The fastest flowing sample resulted in the least non-specific binding as evidenced by the highest GV of 217 ± 1 . Next, these two sample flow rates were compared with regards to the positive spots. It was determined that the positive spots in the 1 mL/min sample ($p < 0.0001$) were significantly different compared to the 0.25 mL/min sample flow rate. Thus, while less non-specific binding can be gained from flowing at a faster rate, there is a significant loss of sensitivity due to the m-AuNP not having sufficient time to diffuse and bind to the m-IgG immobilized on the NC membrane.¹⁹

Next, the use of another membrane with a larger pore size, Sartorius 0.45 μm , was explored in an effort to eliminate the non-specific binding occurring at the 0.1 mL/min flow rate while obtaining the strongest colorimetric change in the positive spot or higher signal on the membrane (i.e., lower GV). Using the same flow rates and positive sample dilutions (500x m-AuNP) as in **Figure 5-4**, the mean GVs for both the positive samples and negative controls were compared (**Figure 5-5**). It was interesting to see the 0.1 mL/min negative control had a mean GV of 210 ± 4 and the 0.25 mL/min negative control had a lower mean GV of 193 ± 11 ; stated another way, the faster flow rate (0.25 mL/min) had more non-specific binding than



the 0.1 mL/min flow rate. Comparing the mean GV for the 0.1 mL/min positive sample to the 0.25 mL/min positive sample, the 0.1 mL/min had a lower GV (74 ± 5) than 0.25 mL/min (102 ± 7). A two-way ANOVA and Tukey's multiple comparisons test ($\alpha = 0.05$) was performed to determine if there was a statistical difference between the mean GVs for the 0.1 mL/min and 0.25 mL/min flow rates. The analysis determined there was a statistical difference between 0.1 mL/min and 0.25 mL/min mean GVs for both the positive samples ($p = 0.0014$) and the negative controls ($p = 0.0474$). These results show there is less non-specific binding at 0.1 mL/min with the Sartorius membrane compared to the Whatman membrane. Therefore, in subsequent studies, the Sartorius membranes will be used along with a 0.1 mL/min flow rate to achieve the greatest amount of antibody binding and colorimetric change on the membrane (i.e., lower GV).

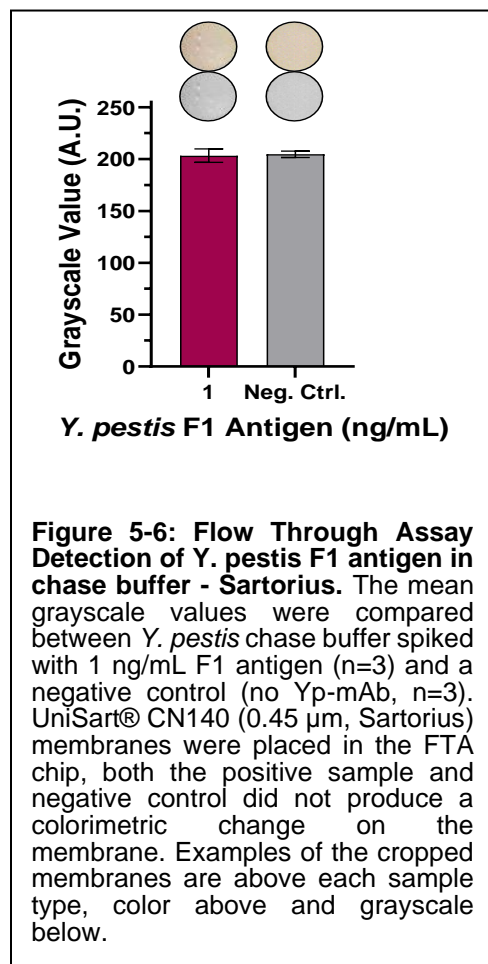
It is important to note that the flow rate studies have revealed that the FTA chip's sensitivity can be tailored to the end users' needs. As shown in both **Figures 5-4** and **5-5**, the slower flow rate (0.01 mL/min) results in a greater colorimetric change, lower GV, but takes 10x as long to complete the assay (50 min) compared to the 1 mL/min flow rate (5 min) (note: assay times based off of a 5 mL total sample volume). Interestingly, the 0.1 mL/min flow rate (GV = 74 ± 5) does not result in a 10x lower GV than the 1 mL/min sample (GV = 145 ± 6) but only a 2x lower GV (**Figure 5-5**). Consequently, one could weigh the issue if the 50-minute assay time at 0.1 mL/min is worth the increased sensitivity. Ultimately, the flow rate studies have shown the flexibility in the FTA chip's sensitivity as well as how the

non-specific binding can be eliminated by changing the flow rate and the type of membrane used (e.g., pore size).

5.3.3 Detection of *Y. pestis* F1 Antigen on the Flow Through Assay Chip

Previous sections describe the characterization of the volume of m-IgG blotted per 1 mm spot and the sample flow rate through the FTA chip. Here, we show proof-of-concept to detect *Y. pestis* F1 antigen on the FTA chip. Based off of the results from section 5.3.2, the experiments were performed using the Sartorius membranes blotted with 0.25 μ L Yp-mab per 1 mm spot and the sample flow rate was 0.1 mL/min. Sample solutions include *Y. pestis* chase buffer (5 mL) spiked with F1 antigen (1 ng/mL) with **Figure 5-6** showing the mean GV (n=3) for each 1

mm spot. It is important to note that this assay was comprised of a full sandwich-type immunoassay (**Chapter 2, Figure 2-2**). Unexpectedly, the positive spots and the negative control spots produced similar GVs, 203 ± 6 and 205 ± 3 , respectively. An unpaired two-tail t-test was performed to determine if there was a statistical difference between the two mean GVs; the analysis determined there was not a significant difference between the positive spots and negative control spots ($\alpha = 0.05$, $p = 0.76$). We conclude that these results are due to the larger pore size (0.45 μ m) and increased



diffusion distance for the analytes to interact with the Yp-mAb, reducing the interaction time to form the sandwich-complex.^{11,19} The membrane pore size and diffusion distance can be explained by the Péclet number (Pe) described earlier. Pe describes the relationship between the flow rate through the NC membrane and the diffusion rate of the analyte to the walls of the pores.^{10,19,20} With the large pore size and increased diffusion distance to the Yp-mAb, the Yp-AuNP-F1 antigen complex could not bind to the Yp-mAb; the inability to bind resulted in a decreased colorimetric change on the membrane because the Yp-AuNP could not accumulate on the membrane. To overcome the lack of binding interaction time, we changed back to the Whatman 0.2 μm pore size membrane to decrease the diffusion distance for the analytes.

As described in section 5.3.2.2, the 0.2 μm pore size experienced large amounts of non-specific binding at the 0.1 mL/min flow (**Figure 5-4**). To eliminate the non-specific binding or false-positive results, the flow rate was increased to 0.25 mL/min. The *Y. pestis* sample solutions were prepared in *Y. pestis* chase buffer spiked with F1 antigen (0.75-0.01 ng/mL) with **Figure 5-7** showing the mean GV (n=3) for each 1 mm spot; the negative control spots contained no Yp-mAb. Unfortunately, the

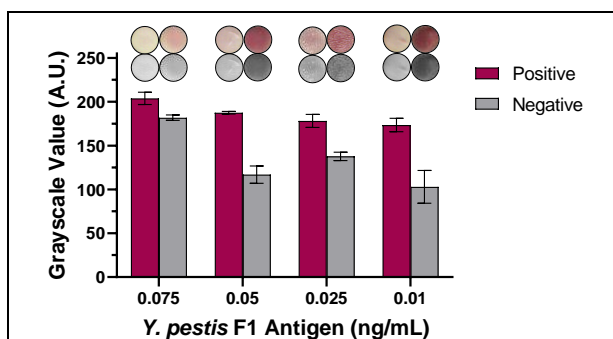


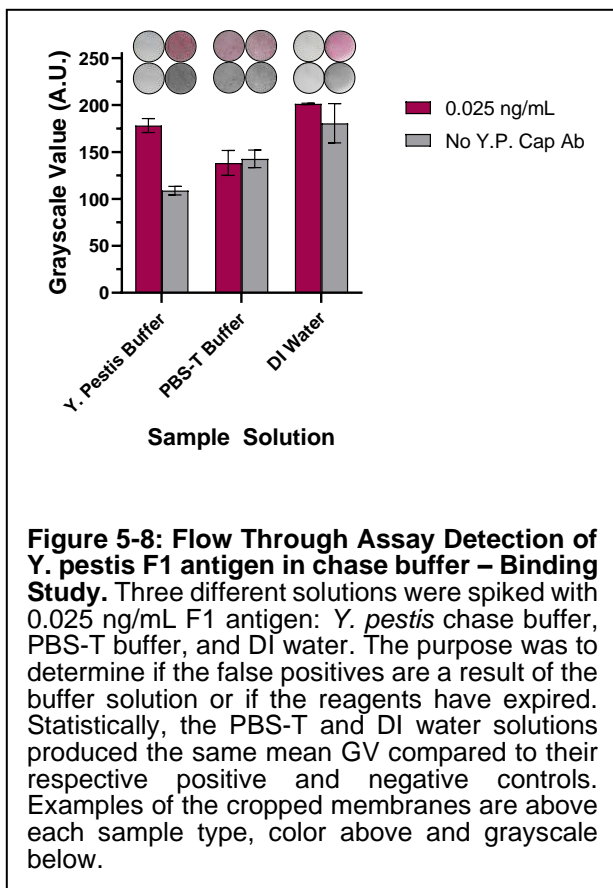
Figure 5-7: Flow Through Assay Detection of *Y. pestis* F1 antigen in chase buffer – Whatman ProTran 0.2 μm . *Y. pestis* samples were prepared with 0.075-0.01 ng/mL F1 antigen in chase buffer (n=3) and a negative control (no Yp-mAb, n=3). Whatman ProTran 0.2 μm membranes were placed in the FTA chip, both the positive samples produced little to no colorimetric change, while the negative control samples produced false-positives. Examples of the cropped membranes are above each sample type, color above and grayscale below.

results were the opposite of what was expected; the positive spots had little to no signal and the negative control spots experienced a high signal indicative of non-specific binding; this is a unique situation because these results were not experienced in the cOFI discs described in **Chapters 2-4**. We hypothesize the major contributor to the contradicting results are the new set of reagents, (i.e., different lot), we received from the AuCoin lab, our collaborator at the Discovery Lab.

In order to test our hypothesis, we designed a binding study which entailed spiking different buffer solutions with F1 antigen (0.025 ng/mL, n=3) along with not blotting the Yp-mAb (negative control, n=3) on the NC membrane (**Figure 5-8**).

The mean GV for both positive and negative samples were compared using the

three sample solutions: *Y. pestis* chase buffer (pH = 9.6), PBS-T buffer (pH = 7.5), and DI water (pH = 7). Each buffer has a different pH, ionic strength, and salt composition; these characteristics can affect the binding affinity of the Yp-mAb and/or Yp-AuNP to the F1 antigen by disrupting the hydrogen bonding, e.g., a buffer solution with too high or too low of a pH.²¹ Ideally to achieve good binding of antibodies,



the buffer solution should be at or near the neutral pH, at or near the isoelectric point, of the antibody and the antigen.^{22,23}

The results presented in **Figure 5-8** show an interesting phenomenon, specifically with the *Y. pestis* chase buffer. When there was no Yp-mAb on the NC membrane, there was a red colorimetric change with a mean GV of 109 ± 5 , while the positive sample containing the Yp-mAb on the NC membrane had no red colorimetric change (GV = 178 ± 7). It appears that the F1 Antigen-Yp-AuNP is binding and accumulating on the NC membrane only when there is no Yp-mAb present. This must mean that the Yp-mAb is not binding to the F1 antigen because of two potential reasons. First, the Yp-mAb has been denatured either via its journey being shipped across the country or it was not maintained at the necessary storage temperature. Second, the Yp-mAb antibody has lost its binding affinity due to it being past its expiration date, typically ~6 months, but the expiration date theory is least likely because these were brand new reagents.

Another hypothesis is that the buffer solution could have gone bad, but a new solution of buffer was prepared just before the experiments. Therefore, it is likely that the Yp-mAb have been denatured and lost their binding ability to the F1 antigen. Alternatively, based off of these results it is difficult to determine if the F1 antigen is binding to the Yp-AuNP. The Yp-AuNP may not be binding to the F1 antigen but could be non-specifically binding to the membrane when the Yp-mAb is not present on the NC membrane. Finally, the AuNP on the Yp-AuNP could possibly be dissociating off the antibody because the AuNP is non-covalently bound to the Yp-mAb through electrostatic interactions and hydrogen bonding,

which are sensitive to salt concentration, pH, and presence of proteins.²⁴⁻²⁶ If this is the case, then the AuNP may be aggregating together and getting stuck in the 0.2 μm pores; this could also be occurring with the PBS-T and DI sample solutions.

Both PBS-T and DI water sample solutions have different ionic strengths but similar pH values; the ionic strength of either solution was not measured but DI water contains no ions while PBS-T does contain some in the form of sodium chloride, potassium chloride, sodium phosphate, and potassium phosphate. As previously stated, the ionic strength of a solution does affect the binding affinity of antibodies.^{21,22} The DI water positive sample had a mean GV of 201 ± 1 and the negative control sample had a mean GV of 181 ± 21 . An unpaired t-test ($\alpha = 0.05$) was performed to determine if there was a statistical difference between the DI water sample's mean GV; the analysis determined there was not a significant difference among the mean GVs ($p = 0.144$). The PBS-T solution positive sample had a mean GV of 138 ± 13 and the negative control had a mean GV of 143 ± 9 . An unpaired t-test ($\alpha = 0.05$) was performed to determine if there was a statistical difference between the PBS-T sample's mean GV; the analysis determined there was not a significant difference among the mean GVs ($p = 0.666$). Both the positive sample and negative control sample for the DI water and PBS-T, resulted in similar mean GVs respectively. What we can conclude is that the PBS-T solution and DI water solution did not solve the false-positive and false-negative results that were received in the *Y. pestis* chase buffer solution. Ultimately, we can conclude there is something wrong with *Y. pestis* reagents because we did not experience these

results when performing the immunocapture studies in section 5.3.2; therefore, we can eliminate the FTA chip and fluid flow as a potential variable.

5.4 Conclusions

We described a syringe-driven FTA chip with the capability to detect up to six different target analytes. The FTA chip was designed to be multiplexed with a 3x2 array with 1 mm diameter detection spots; the 1 mm spots allow for easy deposition of the capture antibodies on the NC membrane without requiring an expensive nano-spotter instrument. Additionally, the FTA chip was designed to limit the amount of external instrumentation required to analyze a sample, e.g., the chip can be human powered and does not require a syringe pump to drive the sample through the chip. Further, there is no disassembly required to perform the image analysis which reduces overall assay time while reducing exposure of a potentially contaminated sample to the user. We demonstrated proof-of-immunocapture on the 3x2 array, characterized the volume of the capture antibodies to be immobilized on each 1 mm spot without negatively affecting the sensitivity of the assay, and we characterized the sample flow rate in order to eliminate false-positives on the NC membrane. When detecting *Y. pestis* F1 antigen in buffer solution, we experienced both false-positive and false-negative results and we believe that the *Y. pestis* reagents have lost their binding ability as well as specificity. Therefore, new reagents will need to be acquired to continue characterization and to show proof-of-concept to detect infectious diseases on the FTA chip. Future work includes detecting *Y. pestis* spiked into human samples (e.g., human urine) to demonstrate in-field application. Finally, integrating the 3x2 array onto the cOFI disc, described in **Chapters 2-4**, will allow for multiplexing on

a single NC membrane to further increase the capability of detecting multiple target analytes on a centrifugally-driven device.

5.5 References

- (1) Chorti, P.; Kazi, A. P.; Wiederoder, M.; Christodouleas, D. C. High-Throughput Flow-Through Direct Immunoassays for Targeted Bacteria Detection. *Anal. Chem.* **2021**, *93*, 14586–14592. <https://doi.org/10.1021/acs.analchem.1c02867>.
- (2) Jansen, H. J.; Breeveld, F. J.; Stijnis, C.; Grobusch, M. P. Biological Warfare, Bioterrorism, and Biocrime. *Clin. Microbiol. Infect.* **2014**, *20* (6), 488–496. <https://doi.org/10.1111/1469-0691.12699>.
- (3) Crowther, J. R. *The ELISA Guidebook*, Second.; Springer US, 2009.
- (4) Choi, S.-Y.; Rhie, G.; Jeon, J. H. Development of a Double-Antibody Sandwich ELISA for Sensitive Detection of Yersinia Pestis. *Microbiol. Immunol.* **2020**, *64* (1), 72–75. <https://doi.org/10.1111/1348-0421.12751>.
- (5) Jauset-Rubio, M.; Tomaso, H.; El-Shahawi, M. S.; Bashammakh, A. S.; Al-Youbi, A. O.; O'Sullivan, C. K. Duplex Lateral Flow Assay for the Simultaneous Detection of Yersinia Pestis and Francisella Tularensis. *Anal. Chem.* **2018**, *90* (21), 12745–12751. https://doi.org/10.1021/ACS.ANALCHEM.8B03105/SUPPL_FILE/AC8B03105_SI_001.PDF.
- (6) Loñez, C.; Herwegh, S.; Wallet, F.; Armand, S.; Guinet, F.; Courcol, R. J. Detection of Yersinia Pestis in Sputum by Real-Time PCR. *J. Clin. Microbiol.* **2003**, *41* (10), 4873–4875. <https://doi.org/10.1128/JCM.41.10.4873-4875.2003/FORMAT/EPUB>.
- (7) Li, F.; You, M.; Li, S.; Hu, J.; Liu, C.; Gong, Y.; Yang, H.; Xu, F. Paper-Based Point-of-Care Immunoassays: Recent Advances and Emerging Trends. *Biotechnol. Adv.* **2019**, *39*. <https://doi.org/10.1016/j.biotechadv.2019.107442>.
- (8) Jiang, N.; Ahmed, R.; Damayantharan, M.; Ünal, B.; Butt, H.; Yetisen, A. K. Lateral and Vertical Flow Assays for Point-of-Care Diagnostics. *Adv. Healthc. Mater.* **2019**, *8* (14). <https://doi.org/10.1002/ADHM.201900244>.
- (9) Wong, R. C.; Tse, H. Y. *Lateral Flow Immunoassay*; Humana Press, 1981; Vol. 53.
- (10) Schlappi, T. S.; Mccalla, S. E.; Schoepp, N. G.; Ismagilov, R. F. Flow-through Capture and in Situ Amplification Can Enable Rapid Detection of a Few Single Molecules of Nucleic Acids from Several Milliliters of Solution. *Anal. Chem.* **2016**, *88*, 7647–7653. <https://doi.org/10.1021/acs.analchem.6b01485>.
- (11) Chen, P.; Gates-Hollingsworth, M.; Pandit, S.; Park, A.; Montgomery, D.; AuCoin, D.; Gu, J.; Zenhausern, F. Paper-Based Vertical Flow Immunoassay (VFI) for Detection of Bio-Threat Pathogens. *Talanta* **2019**, *191* (August 2018), 81–88. <https://doi.org/10.1016/j.talanta.2018.08.043>.
- (12) Kumar, R.; Yadav, S. C.; Kumar, S.; Dilbaghi, N. Development of Membrane-Based Flow-through Assay for Detection of Trypanosomosis in Equines. *J. Parasit. Dis.* **2020**, *44* (1), 99–104. <https://doi.org/10.1007/S12639-019-01166-8>.
- (13) Thompson, B. L.; Ouyang, Y.; Duarte, G. R. M.; Carrilho, E.; Krauss, S.; Landers, J. P. Inexpensive, Rapid Prototyping of Microfluidic Devices Using

- Overhead Transparencies and a Laser Print, Cut, and Laminate Fabrication Method. *Nat. Protoc.* **2015**, *10* (6), 875–886. <https://doi.org/10.1038/nprot.2015.051>.
- (14) *Standard Materials for High-Resolution Rapid Prototyping*; 2017.
- (15) Hau, D.; Wade, B.; Lovejoy, C.; Pandit, S. G.; Reed, D. E.; DeMers, H. L.; Green, H. R.; Hannah, E. E.; McLarty, M. E.; Creek, C. J.; et al. Development of a Dual Antigen Lateral Flow Immunoassay for Detecting *Yersinia Pestis*. *PLoS Negl. Trop. Dis.* **2022**, *16* (3), e0010287. <https://doi.org/10.1371/JOURNAL.PNTD.0010287>.
- (16) Woolf, M. S.; Dignan, L. M.; Scott, A. T.; Landers, J. P. Digital Postprocessing and Image Segmentation for Objective Analysis of Colorimetric Reactions. *Nat. Protoc.* **2020**, *16*, 218–238. <https://doi.org/10.1038/s41596-020-00413-0>.
- (17) Joung, H.-A.; Ballard, Z. S.; Ma, A.; Tseng, D. K.; Teshome, H.; Burakowski, S.; Garner, O. B.; Di, D.; Eg, C.; Ozcan, A. Paper-Based Multiplexed Vertical Flow Assay for Point-of-Care Testing. *Lab Chip* **2019**, *19*, 1027. <https://doi.org/10.1039/c9lc00011a>.
- (18) Devadhasan, J. P.; Gu, J.; Chen, P.; Smith, S.; Thomas, B.; Gates-Hollingsworth, M.; Hau, D.; Pandit, S.; AuCoin, D.; Zenhausem, F. Critical Comparison between Large and Mini Vertical Flow Immunoassay Platforms for *Yersinia Pestis* Detection. *Anal. Chem.* **2021**, acs.analchem.0c05278. <https://doi.org/10.1021/acs.analchem.0c05278>.
- (19) Squires, T. M.; Messinger, R. J.; Manalis, S. R. Making It Stick: Convection, Reaction and Diffusion in Surface-Based Biosensors. *Nat. Biotechnol.* **2008**, *26* (4). <https://doi.org/10.1038/nbt1388>.
- (20) Zimmermann, M.; Delamarche, E.; Wolf, M.; Hunziker, P. Modeling and Optimization of High-Sensitivity, Low-Volume Microfluidic-Based Surface Immunoassays. *Biomed. Microdevices* **2005**, *7* (2), 99–110.
- (21) Susan, R.; Wiley, J. Antibodies. In *Bioanalytical Chemistry*; 2016.
- (22) Urh, M.; Simpson, D.; Zhao, K. Affinity Chromatography: General Methods. In *Methods in Enzymology*; Elsevier Inc., 2009; Vol. 463, pp 417–438. [https://doi.org/10.1016/S0076-6879\(09\)63026-3](https://doi.org/10.1016/S0076-6879(09)63026-3).
- (23) Wild, D.; Kusnezow, W. Separation Systems. In *The Immunoassay Handbook*; Elsevier, 2013; pp 287–299. <https://doi.org/10.1016/B978-0-08-097037-0.00019-1>.
- (24) Dominguez-Medina, S.; Kisley, L.; Tausin, L. J.; Hoggard, A.; Shuang, B.; D. S. Indrasekara, A. S.; Chen, S.; Wang, L. Y.; Derry, P. J.; Liopo, A.; et al. Adsorption and Unfolding of a Single Protein Triggers Nanoparticle Aggregation. *ACS Nano* **2016**, *10* (2), 2103–2112. <https://doi.org/10.1021/acs.nano.5b06439>.
- (25) Yeh, Y.-C.; Creran, B.; Rotello, V. M. Gold Nanoparticles: Preparation, Properties, and Applications in Bionanotechnology. *Nanoscale* **2012**, *4* (6), 1871–1880. <https://doi.org/10.1039/c1nr11188d>.
- (26) Bailes, J.; Mayoss, S.; Teale, P.; Soloviev, M. Gold Nanoparticle Antibody Conjugates for Use in Competitive Lateral Flow Assays. *Methods Mol. Biol.* **2012**, *906*, 45–55. https://doi.org/10.1007/978-1-61779-953-2_4.

CHAPTER 6 – Final Remarks

6.1 Conclusions

All of the projects described in this dissertation focused on improving previously time-intensive workflows and bioassays used in clinical diagnostics to make them more sensitive, efficient, and cost-effective. Specifically, the research presented here described the development and characterization of centrifugal microfluidic lab-on-a-disc (LoaD) systems for immunoassay detection of infectious diseases at the point-of-need (PoN). This work facilitated the development of traditional assays down to the microscale while integrating novel fabrication techniques which will provide the necessary PoN diagnostics over traditional benchtop methods.

Chapter 2 focused on the development of a PoN centrifugally-driven orthogonal flow immunoassay (cOFI) that used a colorimetric method of detection to identify infectious diseases. We described a 7-layer print-cut-laminate (PCL) disc design that overcame the shortfalls of a previously designed 5-layer cOFI design.¹ Comparatively, the precursor cOFI device incorporated a short microfluidic inlet channel (3mm) that resulted in a decreased flow rate from the sample chamber, with flow rate experiencing exponential decay over time. Further, this design produced a region of non-orthogonal flow, resulting in membrane irregularities and, ultimately, difficulty with reproducible image analysis.² We designed a 7-layer cOFI disc with a significantly lengthened microfluidic inlet channel (26 mm) that forms a long fluid column on the device. The elongated column maintained the hydraulic pressure in the system as the fluid volume decreased in the sample chamber, resulting in a constant flow rate for the duration

of the assay. Using this design, both the flow rate and total assay time can be adjusted simply by changing the rotational frequency of the disc. The added polymeric layers work to eliminate the region of non-orthogonal flow and provide a uniform, circular 2 mm detection region, permitting reproducible image analysis. This demonstrated that the new cOFI device was capable of detecting the *Yersinia pestis* (*Y. pestis*) F1 antigen down to 1 ng/mL, and with a total analysis time of 25 min. This new cOFI device paved the path for a fast, inexpensive, automated, and tunable (e.g., adjustable assay runtime and flow rates) PoN device.

Chapter 3 built upon the cOFI disc described in **Chapter 2** and focused on overcoming the limitations of the lateral flow immunoassay (LFI), e.g., inability to control flow rate and the sample pad is easily oversaturated, while maintaining simple, rapid analysis of biological fluids. 3D-printed technology was leveraged to develop a large volume cOFI disc that could analyze up to 12 mL of fluid and used a colorimetric-based detection method. The 3D-printed sample chamber was integrated onto the 7-layer cOFI microfluidic disc and overcame the macro-to-micro interface typically encountered in microfluidic devices. The cOFI disc described in **Chapter 2** could only analyze 200 μ L of sample per chamber; the large volume cOFI disc had 400 times greater sensitivity compared to an LFI strip and was 2.5 times more sensitive than previously developed vertical flow immunoassays (VFI).³ Real world proof-of-concept was demonstrated by detecting *Y. pestis* F1 antigen in both spiked buffer solution and human urine. With 3D-printed technology and a custom mechatronic system to centrifugally pump fluid,

a rapid, cost effective PoN microfluidic device was presented that could detect down to 0.025 ng/mL of *Y. pestis* F1 antigen.

The work in **Chapter 4** described the development of a portable, smartphone controlled PoN diagnostic system that used the cOFI discs, described in **Chapters 2** and **3**. Depending on the end-user's need, the cOFI system could run a 10-chamber multiplexed disc or large volume disc. Each assay step was performed and controlled using an in-house designed smartphone application (e.g., app). The cOFI system included an onboard motor to control the disc's rotational frequency, a camera phone to image the nitrocellulose (NC) membrane, and an optical sensor to align the disc under the camera phone for image analysis. The app was programmed to capture an image of the NC membrane and complete image analysis to determine if the sample was positive or negative for the target analyte. The system demonstrated the ability to perform all three assay steps (i.e., pre-wash, sample, and post-wash) and detect *Y. pestis* F1 antigen as low as 0.01 ng/mL. Continued development of the app and cOFI system, will produce a portable diagnostic device that will automatically analyze and detect infectious diseases at the PoN.

Finally, **Chapter 5** described the development of a flow through assay (FTA) chip which contained a 3x2 array of 1 mm diameter detection spots. The FTA chip was a syringe-driven method of fluid flow that used the OFI detection technique, described in **Chapters 2-4**. The syringe driven flow eliminated the need for cumbersome, external equipment and could be hand powered to pump the sample. The 3x2 array provided multiplexed capability to detect up to 6 target

analytes from a single sample. The amount of capture antibodies blotted on the membrane was characterized, and the sample flow rate was optimized to eliminate non-specific binding. The FTA chip was specifically designed to be portable, easy to operate, and cost-effective to produce. With further research, the 3x2 array could be integrated onto the cOFI disc to further increase the detection and multiplexing capability of the PoN devices previously described.

6.2 Ongoing Studies, Persistent Challenges, and Future Work

The work outlined in this dissertation focused on PCL devices which have the ability to perform a series of different bioanalytical assays used in clinical workflows. The projects mainly focused on the development of novel microfluidic OFI devices to improve assay analysis time and sample-to-answer processing. After successfully characterizing and optimizing fluid flow through the OFI devices, additional development is needed to increase reliability and sensitivity of the assays. Finally, the manufacturing method and architectural design of the cOFI discs will need to be improved for total assay automation and functional integrity of the PoN device.

6.2.1 Disc Design and Fabrication

The major hurdle that still remains is the materials used for the cOFI discs and the method of assembly. The PCL method is great for research and development of centrifugal microfluidic chips but the inconsistencies involved in the cutting and assembly of individual components has resulted in sample loss and incomplete experiments. Each cOFI disc will need to be injection molded in order for the discs to advance to manufacturing and become an approved PoN device.

6.2.1.1 Large Volume Sample Handling

Chapter 3 described overcoming the macro-to-micro interface on a microfluidic device by increasing the sample volume on disc. This was achieved through 3D-printing a large volume chamber. The addition of more sample to the disc increases the weight and force applied to the materials (i.e., the pressure sensitive adhesive) while the disc is rotating. The increased force stresses the adhesive leading to the recovery chamber failing and spraying sample inside the mechatronic spin system. Obviously, this is an issue if the cOFI disc was to be manufactured and deployed to the PoN. Injection molding the large volume disc will form a monolithic disc and eliminate any potential leaking. Additionally, injection molded parts are easy to manufacture, decreasing overall device cost, and producing an overall more reliable device. The end user expects the system to be reliable and not fail at the worst possible moment. It is especially important that the device doesn't fail when testing a human sample that could be contaminated with a deadly, infectious disease.

6.2.2 On-Disc Immunocapture

This dissertation thoroughly explained immunoassays along with their sensitivity and specificity, but this detection method has a downside: the antibodies. For example, antibodies are sensitive to temperature, pH, and ionic strength. The production of antibodies is labor intensive and expensive. Plus, if the antibodies are not stored or purified correctly, they can lose their binding ability which can result in a false-positive or a false-negative by cross reacting with another antigen or substrate. Additionally, they have a shelf-life and they must be maintained in a climate-controlled environment or container. There is an alternative

to antibodies, called aptamers; they are a synthetically-produced oligonucleotide which are stable in a wide range of conditions and can be made to be specific to a single target analyte.⁴ Additionally, they can be manufactured faster and cheaper than antibodies. Next, using gold-nanoparticle (AuNP) conjugated antibodies is an easy, inexpensive detection method for immunoassays but this method makes it difficult to quantify the amount of target analyte present in a sample. In future studies, replacing AuNPs with fluorescence labeled antibodies should be explored; this will allow for increased sensitivity as well as the quantification of the target analyte. In future work, replacement of the antibodies for aptamers and the gold-nanoparticles for fluorophores will make these PoN assays more sensitive, reliable, and accurate.

When testing complex sample matrixes, non-specific binding and false positives can be eliminated by removing the salts and electrolytes before analyzing a sample for *Y. pestis* or Ebola. The sample (e.g., artificial blood plasma or urine) could be run through a desalting column to remove the salts and small molecules to eliminate any potential non-specific binding to molecules in the solution. Once the sample is run through the column, the *Y. pestis* or Ebola gold-nanoparticle conjugated antibodies would be added to the sample to detect for the F1 antigen or eVLP, respectively. Additionally, the removal of the salts will most likely prevent the nitrocellulose membrane pores from swelling which has been known to slow or completely stop fluid discharge.

The *Y. pestis* reagents did not produce the results that were expected, most likely due to the reagents stability along with being used beyond their expiration

date. A lateral flow strip should be used or developed to determine if the reagents are still viable. An alternative method to an LFI strip is an indirect ELISA to determine if the *Y. pestis* capture and detection antibodies are binding to the F1 antigen. A microtiter plate could be coated with F1 antigen followed by the *Y. pestis* capture antibody. Next, a secondary horseradish peroxidase (HRP) labeled goat anti-mouse antibody is added, followed by tetramethylbenzidine (TMB); the colorimetric change in the well could be measured to determine how much, if any of the antibodies are binding to the F1 antigen.

6.2.3 Nitrocellulose Membrane Replacement

As previously mentioned in this dissertation, NC membranes are the preferred material for use in LFIs and paper-based immunoassay PoN devices because they are easy to use, robust, and cost-effective. Unfortunately, NC membranes are prone to swelling and de-swelling (**Chapter 4**); this can greatly affect fluid discharge through the membrane leading to membrane fouling or fluid stoppage. Cytiva Life Sciences developed an alternative proprietary glass microfiber membrane, called Fusion 5.⁵ This membrane was designed to replace NC membranes on LFI strips and is known to be immune to swelling. Additionally, Fusion 5 is hydrophilic and requires additional steps to immobilize antibodies onto the surface. In order to do so, antibodies will need to be conjugated to the latex beads first then blot the beads onto the Fusion 5 surface. The implementation of a new membrane, i.e., Fusion 5, will greatly maintain the rate of fluid discharge and eliminate membrane swelling or de-swelling, further improving the reliability of the cOFI device to analyze a variety of human bodily fluids (e.g., saliva and whole blood) at the PoN.

6.2.4 Hardware Improvements and Assay Automation

Beyond disc and assay optimization, development of a fully automated, ruggedized mechatronic spin system which can perform the assay steps (i.e., pre-wash, sample, post-wash), regulate fluid control, and perform image analysis all without needing the user to pipette additional reagents is a minimum requirement for PoN implementation. The semi-automated system described in **Chapter 4** could become fully automated with additional programming of the app. Additionally, all the necessary wash buffers could be stored on disc by designing a new 3D printed chamber; each solution could be released at the appropriate time through laser-valving. Another important improvement would be to automate image analysis of discs; with further programming of the app and using the integrated optical sensor, the cOFI disc could position each membrane under the camera phone for the app to perform the image analysis. These simple but significant changes will meet the requirements to deploy a portable, diagnostic device to the PoN and have tremendous impacts on providing the necessary care to infected personnel.

6.3 Summation

The increase in demand for PoN diagnostics, specifically during a pandemic, has led to the growth in capabilities of centrifugal microfluidics for use in forward operating locations and underdeveloped countries. Centrifugal microfluidic devices have the ability to perform complex bioassays with complete automation and increased portability while being cost-effective to produce and administer. The work described here focused on leveraging the many advantages of centrifugal microfluidics by increasing sensitivity of traditional immunoassays

and incorporating automation, which decreased the number of steps and reduced the sample-to-answer processing time. The initial studies included designing and characterizing fluid movement on a novel cOFI disc, to overcome the shortfalls of traditional LFIs. Next, the focus was on leveraging 3D-printed technology to increase the sample volume on disc to improve sensitivity. The cOFI device bridges the gap in PoN diagnostics with its increased sensitivity and automated sample analysis. With further research in disc manufacturing and assay development, the implementation of this device has the potential to have a profound impact on PoN diagnostics.

6.4 References

- (1) Thompson, B. L.; Ouyang, Y.; Duarte, G. R. M.; Carrilho, E.; Krauss, S.; Landers, J. P. Inexpensive, Rapid Prototyping of Microfluidic Devices Using Overhead Transparencies and a Laser Print, Cut, and Laminate Fabrication Method. *Nat. Protoc.* **2015**, *10* (6), 875–886. <https://doi.org/10.1038/nprot.2015.051>.
- (2) Woolf, M.; Dignan, L.; Karas, S.; Lewis, H.; Hadley, K.; Nauman, A.; Gates-Hollingsworth, M.; AuCoin, D.; Green, H.; Geise, G.; et al. Characterization of a Centrifugal Microfluidic Orthogonal Flow Platform. *Micromachines* **2022**, *13* (3), 487. <https://doi.org/10.3390/M13030487>.
- (3) Devadhasan, J. P.; Gu, J.; Chen, P.; Smith, S.; Thomas, B.; Gates-Hollingsworth, M.; Hau, D.; Pandit, S.; AuCoin, D.; Zenhausern, F. Critical Comparison between Large and Mini Vertical Flow Immunoassay Platforms for *Yersinia Pestis* Detection. *Anal. Chem.* **2021**, *acs.analchem.0c05278*. <https://doi.org/10.1021/acs.analchem.0c05278>.
- (4) Song, K.-M.; Lee, S.; Ban, C. Aptamers and Their Biological Applications. *Sensors* **2012**, *12*, 612–631. <https://doi.org/10.3390/s120100612>.
- (5) Wong, R. C.; Tse, H. Y. *Lateral Flow Immunoassay*; Humana Press, 1981; Vol. 53.